Behavioral and Physiological Studies of Visual Functions in Tree Shrews and Mice

Chuiwen Li (李垂文)

A dissertation presented to the graduate faculty of ***University of Virginia***

in candidacy of the requirements for the degree of

Doctor of Philosophy in Psychology

Department of Psychology

University of Virginia

June, 2025

Abstract

Vision is an important function that guides behaviors. However, our understanding of the visual system in the brain remains incomplete. In this dissertation, I combine behavioral, electrophysiological, and computational approaches in two model organisms — tree shrews and mice — to study the vision from two perspectives: visually guided behavior and its implicated neural mechanism, and motion processing on single neuron level and its implicated computational principle. For the former perspective, I studied visual decision-making in tree shrews; for the latter perspective, I studied motion representation in the superior colliculus (SC) of both tree shrews and mice.

In Chapter 1, I review the historical view of vision and visually guided behavior, summarize key anatomical and physiological properties of the SC as a subcortical visual structure, and highlight accumulating findings that link SC activities to cognitive processes. I conclude by proposing the tree shrew as an intermediate model for comparative vision research, lying between rodent and primate visual systems.

Chapter 2 presents our work on establishing and characterizing visual decision-making behaviors in freely moving tree shrews. Using a two alternative forced choice contrast-discrimination task with manipulations of trial-delay schemes, I demonstrate that tree shrews rely on a stimulus-independent process to guide their choice behaviors. The comparison between two forms of racing diffusion models fit to the choice and response time data further shows a potential mechanism for these task-dependent non-sensory decision signals can arise from a time accumulation process.

In Chapter 3, I shift focus to the mouse SC and ask how individual neurons represent “plaids”, a type of complex motion patterns. Using asymmetric plaid stimuli, I show that mouse SC neurons

do not implement the classic intersection-of-constraints (IOC) rule, which is followed by primate perception and cortex neurons to integrate the motion, but instead compute a probabilistically constrained vector sum (VS) of component directions. By examining optokinetic reflex (OKR) behaviors to plaids, I further demonstrate that this probabilistically constrained VS computation directly drives reflexive eye movements. The findings raise intriguing questions about subcortical visual motion processing and its functional significance.

Chapter 4 extends the motion-processing investigation to the tree shrew SC. Through in-vivo electrophysiological recordings and OKR behavioral measurements, I establish that tree shrew SC neurons are tuned to spatial frequency, temporal frequency, orientation, speed, and motion direction in a manner comparable to mouse SC, although the exact tuning ranges exhibit a priority on processing rapid motion stimuli. In response to symmetric and asymmetric plaids, tree shrew SC neurons also implement a VS-like representation of pattern direction, mirroring the mouse results. Conversely, tree shrew SC demonstrates a lower level of pattern selectivity compared to mice, and the VS computation is not limited by the probabilistic constraints observed in mice. The findings show both the conserved functionality and the specialized adaptation of the tree shrew SC.

Finally, Chapter 5 discusses these cross-species findings and explores their broader implications in light of the literature on other species. I first discuss the tree shrew's exceptionally fast behavioral responses and the implication of the underlying neural mechanisms and drive force. Next, I call attention to the importance of subcortical visual functions, with an emphasis on the SC. Comparative perspective highlights how subcortical processing supports rapid behaviors, while cortical circuits can augment precision under the requirement of behavioral context and species needs. Finally, I briefly discuss the SC function in a broader range of behaviors including abstract cognitive processes and urge for a integrative view on the SC.

In summary, this dissertation demonstrates a collection of my investigations of vision with a comparative perspective. These cross-species insights illuminate how evolution potentially shapes the trade-offs in visual processing, and they underscore the SC's pivotal role in bridging visual inputs with behavior.

Acknowledgements

I would first like to thank my advisors, Dr. Jianhua (JC) Cang and Dr. Per Sederberg. They have been great mentors throughout my PhD life.

I always feel lucky to have joined JC's lab. As my first stop in an academic (hopefully) career, JC's lab provided fantastic learning opportunities and a great environment. JC himself is knowledgeable and curious as a scientist, thoughtful and caring as a mentor. These characteristics in him create a wonderful, somewhat utopian small world, that encourages scientific exploration, personal development, and the expression of diversity. His perfectionism in writing also influenced me a lot. As a person who hates communicating and writing, he is a role model that made me realize the importance of precise and efficient communication. I am still working on these skills, as one can see in this thesis, and will keep working on it for life. I will certainly miss the lab retreat and the backyard parties where we had so much fun.

Per is also a splendid scholar with a broad scope of research interests. I am amazed every time he quickly catches critical questions/problems in my research, even when I only described to him briefly once or twice. When it comes to math and models, Per always has the solution. After working with him, I became more convinced that we need a mathematical model for the neural processes of interest, and we should try to use math as a universal language for communicating scientific findings. As a mentor, Per keeps trying his best to create an inclusive environment where lab members care for each other and research opportunities are provided to people with vastly different levels of training and background. I enjoy the joyful meals out and home parties all these years.

I would also like to thank my committee members, Dr. C. Daniel Meliza, for his wonderful course Computational Neuroscience, his advice when I was struggling with learning computational methods during the first two years, and his supportive and helpful suggestions on my research projects; Dr. Xin Cynthia Tong, for her inspiring perspective on my research and constructive discussions and support, and Dr. Michele Basso, for her critical input on my research paper and storytelling, as well as her warm encouragements for a young scientist like me.

I want to express my gratitude to our fabulous community in Cang and Liu labs, Sederberg lab, and in Gilmer Hall. I want to thank Dr. Seiji Tanabe, whose office door I kept knocking on way too much, for all the brilliant and patient discussions and encouragement. He is essentially my mentor as well for my PhD. I want to thank Dr. Elise Savier, who taught me mouse and tree shrew surgeries, ephys recordings, tree shrew perfusion, and so much more. Elise has also been a mentor figure during my PhD study, and will likely continue to be bugged by me in my future career. More thanks go to Mingna Liu, who has been the greatest lab manager ever. She has always been exceptionally meticulous at work, and super kind and caring in life, helping me in all kinds of scenarios. Thanks also go to Hui Chen, who helped with almost all the hardware and software issues I have in the lab. Mingna and Hui helped me when I first came to UVa for a summer internship in Cang lab. They took me to groceries and offered me furniture, making me feel like home. They, along with their children Emma, Sarah, and Patrick, also helped me look after my baby dog Catrina, which gives me so much relief when I had to be away from time to time. I want to thank Kara McHaney, for helping with all those tree shrew training sessions. We chatted a lot which I enjoyed so much. I want to thank Dr. Brandon (Beeg) Jacques, for patiently helping me with the SMILE programming for the decision-making study; and Dr. Ryan Kirkpatrick, for the guidance and discussions on the sequential sampling models. Beeg, Ryan, Dr. Adam Fenton, Dr. Emily Weichart and I spent many happy-hour dinners together. I cherish those times so much. I thank Yuanming Liu, my same-year lab cohort, for always being nice and supportive and the one to talk to when I have issues with work and life. I enjoy searching for restaurants with him during SfNs. I thank Jieming (Jenny) Fu, for a lot of help including but not limited to taking me to road tests for 3 whole times. Thanks to Yao Lu, who is a dear friend and a role model of mine at the same time, for sharing her love for life and science with me. Thanks to Sueyoung (Sue) Oh, who is another dear friend, for spending cheerful times together - I keep feeling fortunate that we did the New York trip right before the pandemic, and I miss it very much! Thanks to Dr. Jingyi Gao from Liu lab, for being my roommate for a while, showing me her passion for swimming, music, reading, and hotpot! She certainly influenced me enough that swimming becomes the only sport that I occasionally do currently. I thank Chen Chen, for our frequent casual chat on all kinds of topics, including the life philosophies and introspection, as well as teaching me perfusion and brain dissection with vibratome. I miss us being the social-anxiety group during conferences. Thanks to Dr. Victor DePiero, for our nice collaboration on the plaids paper. He has been very supportive and contributes to many constructive discussions in the lab, and I miss our group lunch outside of Gilmer. I thank Lu Yang, for saving me so many times during tree shrew surgeries and perfusions. She taught me tree shrew intubation, and also kindly offered her parking lot near the lab which absolutely made my last two years of PhD a lot easier. Many thanks to Dr. Xiaorong Liu, who showed ultra-kindness during my 2018 internship and the 6 years of PhD life. I love the parties held at her (also JC's) home. Thanks to Wenjin Xu and Shichu Chang, for all the good food recommendations, as well as all the nice gatherings along with Dr. Jiahui Wu and Weile Liu. Wenjin also took care of Catrina when I was away - I appreciate it very much. I want to also thank Dr. Adema Ribic for all the advice she gave me. I miss the holidays and weird hours we spent in the lab together. I want to thank Dr. Masashi Kawasaki, for teaching me how to use the laser cutter and make acrylic boxes and lending me all the tools, which made my first publication ever possible. Sadly he left us forever 1 month before my defense. He will be missed deeply. I want to thank Dr. Peter Brunjes for his wonderful Functional Neuroanatomy and literature discussion courses in my first year. I was struggling so much with language at that time, and he helped me with much patience and made me interested in broader neuroscience topics. I thank Dr. Rolf Skyberg, Dr. Manavu Tohmi, Ahmad Elsayed, and John McDaniel in Cang lab, Dr. Marta Grannonico in Liu lab, Dr. Kevin Darby, Rebecca (Becky) Waugh, Christopher Hall, Austin Greene, Bao Le in

Sederberg lab, Francesca Sciaccotta, Samantha Moseley, Minah Kim in Gilmer, and all the other members of this gorgeous community for creating a supportive academic environment.

I want to thank the support from my family and friends, especially my mother, who tries her best to always be there, and tries even harder to give me space when I need it. I appreciate her tolerance of those hour-long FaceTime calls. I appreciate my father and mother's financial support all these years. Choosing science as a career is still a privilege these days. Thanks for tolerating my financial independence. I thank my grandparents for trying their best to stay healthy. I want to also thank my PhD buddy Yuening Li who has been in the UK, but kept organizing journal clubs on Zoom/Teams which largely expanded my knowledge on in-vitro neuroscience work. I thank my friends for the love and support no matter whether I am abroad or home. I want to express my deep appreciation for Catrina, who came to me in 2022 and has stayed ever since with me. She is my pet, my daughter, my family. She has been sleeping right beside me throughout the thesis writing. I would not recommend getting a dog during PhD if someone asks but I never regret having her. I experienced an unexpected psychological crisis during the PhD (although mental meltdown in PhD has become a cliche nowadays), and if it were not for her, I would not have been able to hold myself together.

Contents

Chapter 1

Introduction

1.1 Vision and Behavior

Vision is a function that allows biological organisms to interact with light and form images within the nervous system. This critical function is broadly found in different evolutionary branches across animal kingdoms, including insects, fish, birds, and mammals. Compared to other sensations, vision enables high-resolution and long-distance information acquisition, which transcends the physical limits of the body and hugely expands the range where the animals can interact with their environment.

Across species, the organization and function of visual systems are remarkably conserved. Functional convergence can be found in multiple aspects. For example, the photoreceptors in the retina of vertebrates are nicely arranged spatially, with nearby photoreceptors representing neighboring locations in the visual fields. Such topographic organization is called retinotopic map and is preserved within the retina and in downstream visual structures (Hjorth et al., 2015; Spead et al., 2021; Li et al., 2022b; Chandrasekaran et al., 2005; Wandell and Winawer, 2011; Adams and Horton, 2003). Another example is optokinetic reflex (OKR), a highly conserved visuomotor reflexive behavior observed in all vertebrates studied so far (Masseck and Hoffmann, 2009). OKR presumably helps stabilize images on the retina during relative motion. Subcortical structures drives the

OKR in non-mammal vertebrates, while in mammals both subcortical and cortical brain areas exert control on this behavior. A further example of organizational and functional conservation is the orientation columns in primary visual cortex (V1), which have been observed across various higher mammals such as primates, cats, tree shrews, and ferrets, but not in rodents or squirrels (Ho et al., 2021; Humphrey and Norton, 1980; Bonhoeffer and Grinvald, 1991; Hubel et al., 1977; Chapman et al., 1996; Kaschube et al., 2010). Such map structure indicates the grouping of functional units is a common solution for efficient visual processing in the cortex of animals with more developed visual systems. Moreover, one of the studies has shown that despite primate species vary widely in brain sizes, the estimated neuron numbers within an orientation hypercolumn is only weakly correlated with the cortex size (Ho et al., 2021), suggesting the neural allocation for orientation representation is likely optimized early in evolution, and more advanced functions are developed and built upon this common basic computational unit. Together, these findings highlighted the value of studying vision as it is a foundational neural function that has the potential to reveal general principles of brain organization.

Vision is not just a passive process of receiving information. Its most evident and direct outputs are visually guided behaviors such as eye movements, orienting behaviors, predation, escape, navigation, and social interaction. Thus, by adopting a visual paradigm, one can study a complete input-output transformation. Many of these visuomotor transformations are innate and reflexive, enabling the study of the most naturalistic behaviors that require minimum amount of training. In the laboratory setup, artificial stimulus on the screen has been widely shown to effectively drive neuronal responses in various species, allowing for precise control and flexible manipulations of the visual inputs. In addition to innate behaviors, visual information can also guide cognitive processing such as perception, attention, decision-making and memory. Visually guided cognitive behaviors provide a great entry point to investigate the neural mechanisms underlying cognition, especially considering the extensive body of literature that informs our understanding of the visual system.

In mammals, the neural substrates for vision can be devided into two pathways, the primary visual pathway and the secondary visual pathway. The primary visual pathway refers to the visual information processing stream from retina, to the lateral geniculate nucleus (LGN) in the thalamus, then to V1 and the rest of the visual cortex. The secondary visual pathway refers to a different route starting from the retina to the superior colliculus (SC). The "primary" and "secondary" are mainly influenced by the primate anatomy, where retinal ganglion cells (RGC) project mainly to the LGN while only $\sim$10% to the SC (Perry and Cowey, 1984). However, this projection difference is reversed in mice where the majority of the retinal output goes to the SC (Hoy and Farrow, 2025). In this study, I focus on the visual function of the SC, a structure that remains underexplored given its functional importance.

1.2 The Superior Colliculus as a Visual Structure

The SC, despite sometimes classified as part of the "secondary" visual pathway, is a highly conserved midbrain structure that plays an important role in image-forming vision and visual behaviors. In evolution, the SC is phylogenetically older than the LGN; all vertebrates have an optic tectum (OT, the homologous structure of the SC in non-mammal vertebrates) or a superior colliculus (in mammals) (Ulinski et al., 1992). The SC receives input majorly from the retina, as well as V1 and other cortical and subcortical areas, and also projects widely to subcortical brain structures (Cang et al., 2024). Across species, the SC has been shown to respond to spatial locations of visual stimuli, specific visual features (on/off, motion direction, etc.), and visually guided behaviors (orienting, saccades, etc., Hoy and Farrow, 2025; Isa et al., 2021; Sprague and Meikle, 1965). Therefore, the SC is an essential brain structure to study for investigating the general principle of visual processing.

1.2.1 Visual Feature Tuning

The SC is a layered structure with the superficial layers mostly representing visual information. Just like other visual structures in the brain, the SC contains a retinotopic map to represent the visual spaces projected onto the 2 dimensional retina. In addition, the receptive field (RF) of the SC neurons are smaller for central visual fields and bigger for the peripheral visual fields across various species including mice with no fovea (Hafed et al., 2023; Drager and Hubel, 1976; Hafed and Chen, 2016). This indicate that the SC, like other visual areas, process the visual information with an emphasis on the central visual field in front of the animals. The SC visual neurons usually have overlapped circular on-off RFs, meaning that they respond to both bright and dark stimulus appearing in the same visual fields (Wang et al., 2010). This is different from the upstream RGC, which contain a lot of on-cells and off-cells. This is also different from the V1 neurons, which are another input source to the SC and contain many cells with gabor-like RFs. Thus, the prevalent on-off RFs in the SC indicate a high level of non-linearity during the visual processing there.

The SC is well known to be sensitive to visual motion. Researchers have found the superficial SC exhibits selectivity to motion direction/axis and spatial/temporal frequency, as well as performs surround suppression and motion integration (Wang et al., 2010; Lee et al., 2020; Gale and Murphy, 2016; Cang et al., 2024; De Franceschi and Solomon, 2018; Li and Meister, 2023; Barchini et al., 2018; DePiero et al., 2024; Li et al., 2025) . Among these properties, direction selectivity is the most well studied feature, which is observed in all the mammalian species that has been studied (Cang et al., 2024, 2018). Direction selective (DS) SC neurons were found to be most enriched in the very superficial lamina of SGS (stratum griseum superficiale) in mice (Inayat et al., 2015), while this nearly 80% DS proportion dropped to around 30% when measuring across all depth of the SGS (Wang et al., 2010). In mice, this strong direction selectivity found in the SC has been shown to be inherited from the retina (Shi et al., 2017). However, it should be noted that the SC neurons also showed advanced motion processing capabilities such as motion direction integration (DePiero et al., 2024) and direction contrast facilitation (Barchini et al., 2018) that were not observed in the retina. This indicates that these DS neurons do not simply relay the directional information from the retina; rather, they process motion information in a higher, more integrative level. This is also consistent with the findings in primates that while the direction selectivity in the retina is very limited (Kim et al., 2022), the SC still shows a substantial amount of visually DS neurons (Horwitz and Newsome, 2001; Cynader and Berman, 1972; Goldberg and Wurtz, 1972). Taken together, the SC is likely a critical structure that solves visual motion processing tasks in the subcortex.

1.2.2 Complex Visual Processing

In addition to low level feature selectivity, SC has also been found to represent higher order visual elements. For instance, a series of studies suggest the primate superficial SC might encode the saliency of visual scenes (White et al., 2017a,b, 2021; Heeman et al., 2025). Such saliency representation is independent of saccadic goals, emerging earlier and more robustly than the V1 signals. Given that V1 is the dominant input of the SC in primates, these findings suggest the SC pools and integrates a variety of visual features to perform a higher-level processing intermediate between purely passive sensory representation and fully top-down modulated processing.

In the past few years, more studies have revealed an interesting role of the SC in visual object representation (Bogadhi and Hafed, 2023; Yu et al., 2024; Mekhaiel et al., 2024; Nguyen et al., 2014). Object representation is traditionally studied in the cortex, especially the inferotemporal (IT) cortex of primates. By contrast, in subcortical structures, object representation is typically linked to valence or motivational significance. Researchers have found rapid preferential responses to extrafoveal real-life objects over spectral matched control images in primate SC (Bogadhi and Hafed, 2023). Moreover, SC neurons show a characteristic bimodal response to visual objects, consisting of an early, strong burst followed by a late, weaker response (Yu et al., 2024; Nguyen et al., 2014). These studies also consistently demonstrate SC neurons are sensitive to visual object categories, with a particular preference for the face stimuli. Interestingly, this object representation with ultra-short latency ($\sim$ 40 - 50 ms), together with the subsequent late response, was abolished completely by inactivating the LGN (Yu et al., 2024). LGN does not project to the SC in primates, while V1, the downstream of LGN, is a major input of the SC. Therefore, it was proposed that the SC signal representing visual objects depends on the LGN-VC (visual cortex) pathway.

1.2.3 The SC is Multi-sensory

Beyond the visual information, the SC, especially its intermediate and deep layers, is also known to represent other sensory modalities. For example, researchers have found auditory and somatosensory inputs are co-represented in the SC, and can interact with visual representation to induce enhancement and depression in neuronal responses (Meredith and Stein, 1986; Ito et al., 2021; Wallace et al., 1996; Knudsen, 1982). In non-mammalian species, the optic tectum has also been shown to encode other sensory modalities, including electrosensation and thermosensation (Isa et al., 2021; Kardamakis et al., 2016; Hartline et al., 1978; Newman and Hartline, 1981) . These multimodal representations are aligned topographically, allowing the integration of ethologically relevant cues in the surrounding environment and thus guiding animal behaviors (Isa et al., 2021; Jay and Sparks, 1984; Suzuki et al., 2019) . Notably, such multi-sensory organization is shown to exist during development and provide guidance to the segregation of sensory modalities in the cortex (Guillamón-Vivancos et al., 2022).

1.2.4 The SC is Involved in Orienting Behaviors

With the enriched representation across sensory modalities and an emphasis on visual responses, the SC appears well positioned to compute signals relevant for behavior. Indeed, a large body of literature has shown SC's role in guiding a wide range of behaviors. For example, the SC guides eye movements, especially saccades in primates (Basso and May, 2017). Neurons in the deeper layers of the SC can generate saccades in a certain direction and distance (i.e. saccade vectors) depending on the site of those neurons. This dependence is described as a map for eye movement in the SC, similar to the sensory maps described above. In addition, in head restrained mice, SC stimulation in its intermediate and deep layers can also trigger saccades (Zahler et al., 2023; Masullo et al., 2019). Interestingly, these neurons seem to encode saccadic end points instead of vectors in mouse SC (Zahler et al., 2023). Other than eye movements that are particularly prominent in primates, the SC is also found linked to a range of orienting behaviors including head movements, goal-directed arm/tongue reaching, or the reversed form of orienting - evasive responses Masullo et al. (2019);

Zahler et al. (2023); Campagner et al. (2023); Cang et al. (2024); Hoy and Farrow (2025); Isa et al. (2021, 2020). Predation can also be viewed as an orienting behavior, and the SC has been shown to play a critical role in driving this behavior in mice (Hoy et al., 2016, 2019; Shang et al., 2019). Curiously, one recent study showed narrow-field cells, a type of DS neurons in the SC essential for normal hunting behaviors, do not require their direction selectivity to guide predation (Krizan et al., 2024). These neurons inherit the direction selectivity from one specific type of RGC. When eliminating this source of direction selectivity, the narrow-field cells became non-DS, yet the hunting behavior remained unaffected. This is surprising given the direction selectivity is a major response property in the SC, and is generally assumed to be critical for predation - an activity that relies on rapid visual motion analysis. Therefore, how the SC and the rest of the brain utilize the visual processing outputs of SC neurons remains an open question to explore for future investigation.

1.3 Connecting the SC Neuronal Activity to Cognitive Behavior

1.3.1 Attention

Notably, the SC is involved in the behaviors that 1. require fast processing, 2. reminiscent to a behavioral product of attention, which guides the animal to "face" a field enriched of relevant information. This is supported by the findings that the SC is involved in both overt and covert attention (Ignashchenkova et al., 2004; Krauzlis et al., 2013). Researchers have shown the response facilitation phenomenon in the SC visual neurons during saccade preparation period (Li and Basso, 2008; Wurtz and Goldberg, 1972; Wurtz and Mohler, 1976). However, in these studies, the actual or planned saccade location is coupled with the attention target space cued by the experimenters, making the causal attribution ambiguous. Later studies using artful designs to disentangle the two variables illustrated the SC is really involved in the cognitive spatial attention rather than simply the motor preparation (Lovejoy and Krauzlis, 2010; Zénon and Krauzlis, 2012). Curiously, inactivation of the SC neurons impairs behavioral performance requiring attention to their receptive fields, but leaving the 'attention-related' effect in the cortex intact (Zénon and Krauzlis, 2012). Moreover, microstimulation of the SC facilitate the attention toward the corresponding receptive fields without eye movements (Müller et al., 2004; Cavanaugh and Wurtz, 2004). Such facilitation cannot be explained by the possible phosphene effect (Cavanaugh et al., 2006). Thus, the SC has a unique role that can directly affect spatial attention behaviorally and the underlying mechanism is independent from the cortex.

1.3.2 Perceptual Decision-making

Since the SC is involved in attention that seems to be distinct from the pure motor preparation or sensory processing, many studies have explored whether other cognitive processes depend on the SC as well. One prominent framework to study the SC's cognitive function is perceptual decision-making. Given that the SC is a sensory-motor hub, it is natural to speculate that it may encode signals of the intermediate states between sensory and motor transformation. Perceptual decision-making is the minimal form of such cognitive transformation, where decisions are made based on sensory evidence.

However, studying decision-making signals in the SC is challenging due to the contamination of co-existing sensory- and motor-related signals in SC neurons. In fact, this is a common issue to study perceptual decision-making in almost all brain areas. Yet, the SC literature explicitly demonstrated the prevalence of non-cognitive signals. Thus, researchers have been working on adopting various experimental designs that can dissociate the cognitive variables of interest.

One of the early and influential attempts was to use a semi-dissociative 2 alternative forced choice (2AFC) paradigm (so called "loose stimulus–response association task") to separate choice from motor (saccadic) signals in the primate SC (Horwitz et al., 2004). Monkeys can be very effectively trained to use saccades to report their choices. However, because SC neurons directly contribute to the initiation and targeting of saccades, and because saccadic vectors are mapped topographically in the SC, motor-related activity can easily contaminate neural representations of choices deployed spatially in the behavioral task. To overcome this, the researchers randomly presented the choice targets for 2 options at different visual field locations on each trial, while maintaining their relative spatial arrangement. With this design, the choice saccades of the same option could appear at different locations on the screen, decoupling from the SC motor map. This study illustrated that the a subpopulation of SC neurons encoded the abstract choice even before the choice targets were presented. Nevertheless, this paradigm represents only a partial dissociation, since the relative spatial arrangement of the two choice targets was still fixed during the experiment. As a result, it is still possible that a spatial motor plan could form before the target presentation, although being more abstract than planning the exact saccadic endpoint or vector. Later studies advanced this dissociation with designs that used the color instead of location to indicate the identity of choice targets (Crapse et al., 2018), or incorporating pure saccade tasks to enable a subtractive design (Jun et al., 2021; Cho et al., 2021).

Subsequent studies utilizing neural manipulation such as muscimol inactivation demonstrated that the SC plays a causal role in decision-making, particularly in generating decisions contralateral to the inactivation site (Stine et al., 2023; Jun et al., 2021; Peysakhovich et al., 2024). This effect has been observed not only in primates using saccade to report their choices, but also in rodents reporting their choices with licking or nose-poking behaviors (Wang et al., 2020b; Essig et al., 2021; Felsen and Mainen, 2008; Thomas et al., 2023). It is worth noting that these decision-reporting approaches, while differ in modality, are still spatial and fall within the orienting behavior categories, on which the SC neurons exert substantial influence as discussed above.

To further tease apart which step of the decision-making process the SC is involved in, the researchers manipulated various aspects of behavioral tasks to segregate the latent decision variables. For example, in signal detection theory (SDT) which is widely used to model decision behaviors, both the sensitivity and decision criterion can induce changes in the overall decision accuracy. Sensitivity is the distance between the signal and noise distribution, while criterion (or bias) is the threshold on which the decision/classification is based. One study developed a carefully crafted

Yes-No task with sensorimotor priming to independently manipulate these two variables (Crapse et al., 2018). Specifically, instead of two symmetric sensory decisions, the animals need to report whether or not they saw a coherent orientation structure emerging from a glass pattern. The frequency of orientation occurrence was manipulated, so to induce a bias in animals' behavior. This bias corresponded to the decision criterion change but the visual sensitivity could be viewed as stable throughout. This study illustrated that the SC neuronal responses, together with the behaviors, changed with priming. Interestingly, electrical stimulation in the SC that is intermittent on a trial-by-trial basis generated a criterion change in the whole block, suggesting a long-lasting and global effect of the stimulated neurons on decision-making. Other studies also found similar role of the SC in decision criterion instead of sensitivity (Jun et al., 2021; Sridharan et al., 2017). In a recent study, however, the researchers found SC visuomotor neurons encoded the perceptual sensitivity independent from the decision criterion or motor biases (Ghosh and Maunsell, 2025). This sensitivity encoding was related to attention modulation induced by their task instruction. In mice, both sensitivity and criterion changes were found when inactivating SC, although the Go-Nogo task design could not strictly isolate the two (Wang et al., 2020b).

The SDT models the choices in decision-making behaviors. Another behavioral output is response/reaction time (RT), which is very informative for the neural mechanisms underlying decisions. One type of models called sequential sampling models (SSM) has been successful in capturing the choice-RT data observed in humans and other animals (Ratcliff, 1978). SSM family has a lot of variants, but the shared core assumption is that evidence is accumulated through time. This process can be realized with several key decision variables: the drift rate of the accumulators, start point of the accumulation, and a threshold. Once the accumulated evidence crosses a threshold, a decision is generated. Many brain areas such as the lateral intraparietal cortex (LIP) were shown to have 'ramping' neuronal activities that resembled evidence accumulators (Roitman and Shadlen, 2002; Horwitz and Newsome, 1999; Ding and Gold, 2010; Mante et al., 2013), which provided the neural level support of the SSMs in explaining decision-making behaviors. The SC was suggested to have an influence on several decision variables in the SSM framework, such as drift rate (Ratcliff et al., 2007, 2003; Cho et al., 2021), drift rate offset (Jun et al., 2021), and threshold (Stine et al., 2023; Zhang et al., 2021). Further investigation revealed more details of the SC mechanisms. For example, Stine et al. (2023) found that despite the average responses of both SC and LIP showed ramping properties during decision-making, the SC neurons on single-trial level in fact showed bursting responses, in contrast to the LIP neurons which maintained a characteristic ramping activity. This finding provides clue to the previous mystery of why ramping response is so prevalent in the brain, and suggests different computations take place in the SC and LIP. Another study also demonstrated the SC response to random dot motion patterns was similar to accumulation, but the response to glass pattern resembled a stepping process more (Cho et al., 2021). Further comparison with a saccade task confirmed such accumulation or stepping response did not result from attention, reward, or motor planning.

Moreover, two studies (Odegaard et al., 2018; Grimaldi et al., 2018) addressed the question of whether SC represents the subjective confidence or the decision accuracy, which are two co-varying variables in decision tasks. To dissociate them, they adopted a clever design previously developed by Kiani and Shadlen (2009) where the monkeys were allowed to “opt-out” some trials to guarantee a moderate reward, as opposed to no reward for incorrect responses. Opt-out choices indicate low subjective confidence, but do not necessarily predict low accuracy on the task. Indeed, the behavioral data confirmed when the difference between the evidence for two options were similar, the decision accuracy was similar but monkeys were more prone to opt-out when the overall sensory evidence is weaker. They found SC responses on both single neuron and population level remained the same in this condition, thus encoding decision accuracy rather than subjective confidence.

In addition, several studies also implicated the SC’s role in representing abstract rule or context for decision-making (Thevarajah et al., 2009; Chu et al., 2025; Zhang et al., 2021; Peysakhovich et al., 2024). This is conceptually consistent with an early finding illustrating different levels of speed-accuracy tradeoff in the SC for pursuit and saccade tasks (Krauzlis and Dill, 2002), suggesting the SC contribute to flexible interpretation of the sensory stimuli in a manner that is aligned with the animal's current task demands.

Finally, the SC's involvement in perceptual decision-making is not only limited to the visual modality. Rodent studies have shown that in addition to visual decision, the SC also participates in decision-making based on auditory, somatosensory, and olfactory stimuli, and the SC neurons behaves similarly to that in primates (Duan et al., 2021; Chu et al., 2025; Felsen and Mainen, 2008; Essig et al., 2021). This suggests a broader impact of the SC on cognitive functions, pointing to its potential contribution to the integration and generalization of the task-relevant information. Researchers have also taken advantage of the transgenic rodent lines and optogenetic tools to examine cell type specific contributions to decision-making in the SC. Both excitatory and inhibitory neurons were found to be involved in generating contralateral choices, while interestingly, inhibitory neurons exihibited a reversal in lateralized preference during the late phase of the decision period (Duan et al., 2021; Essig et al., 2021). Subsequent work highlighted the importance of a delay epoch in the experiment design to isolate vision- and motor-related signals, which have opposite spatial preferences in mouse SC (Thomas et al., 2023).

In summary, the SC is a great brain area to study for its broad involvement in various visual functions including cognitive ones.

1.4 Tree Shrew As A Bridging Animal Model for Vision Study and Cross-Species Comparison

In most vertebrates, the major output target of the retina is the SC (Sanes and Zipursky, 2010). In mice and pigeons, nearly 85%-90% of the retinal output directly goes to the SC, while in primates and cats, the main projection region of the retina shifts to the LGN (Hoy and Farrow, 2025). This suggests a redistribution of the early visual processing pathways in evolution. Behind this redistribution, is it merely a migration of function, or could it reflect the emergence of completely new computations? In fact, the answer is likely at a middle point between the two extreme scenarios. This uncertainty calls for more studies on the nature of such anatomical transition. To disentangle the general evolutionary principle from the species specific specializations, it is ideal to adopt comparative approaches and introduce intermediate animal models.

Tree shrew, we propose, has its unique advantages when it comes to vision research. Tree shrews (*Tupaia*) comprise the entire order of *Scandentia*, and are evolutionarily close to primates. First of all, tree shrew are diurnal animals with good visual acuity (Petry et al., 1984; Petry and Bickford, 2019), roughly around 2 cpd This is higher than the acuity of nocturnal animals such as mice ($\sim$0.5 cpd) or rats ($\sim$ 1 cpd) (Prusky et al., 2000), but lower than primates ($\sim$ 25 cpd) (Ridder III et al., 2019). Notably, this visual acuity is similar to squirrels and one nocturnal primate species called mouse lemur (Ho et al., 2021).

Second, Tree shrews exhibit a strong reliance on vision for daily tasks in their wild environment as well as in the laboratory. These animals navigate through complex 3 dimensional space with rapid and frequent jumps, similar to squirrels, reflecting their need for precise visuomotor coordination. One piece of evidence is that compared to mice, tree shrew V1 shows very sharp neuronal tuning to binocular disparity (Tanabe et al., 2022). The binocular disparity is an important cue for depth perception. In addition, this study showed that tree shrew V1 responded to disparity in both random dot pattern and grating patterns, while mouse V1 was only responsive to grating phase disparity. This generalized representation of disparity across different types of visual stimuli suggests the tree shrew V1 might have more advantages in processing and generating depth information that is beneficial to the visually guided navigation in complex environment.

In addition to disparity representation, tree shrew visual system also anatomical and functional similarities to primate visual systems. For example, tree shrew LGN has been found to have 6-layer structure which resembles that in primates (Conway and Schiller, 1983). Moreover, orientation columns have been observed in tree shrew V1 (Humphrey and Norton, 1980), which is a feature found in primates, cats, and ferrets, but not in mice.

Tree shrews also have some unique characteristics in their visual system. These animals are dichromatic and have cone dominated retina, which is especially suitable for studying color vision (Müller and Peichl, 1989; Shriver and Noback, 2008; Jacobs and Neitz, 1986). Tree shrew retina contains roughly 15% of direction selective retinal ganglion cells (DSGC) (Roy et al., 2024). This proportion is less than the $\sim$35% in mice (Summers and Feller, 2022) but more than the $\sim$1.5% in monkeys (Detwiler et al., 2019). This intermediate level of direction selectivity positions the tree shrew as a useful model for linking retinal computations with motion processing strategies observed across species. Interestingly, a study found that tree shrew V2 contains an unexpected periodic retinotopic map, elucidating the general principle of visual circuit wiring under specific cortical spatial constraints (Sedigh-Sarvestani et al., 2021).

As an animal model for laboratory studies, tree shrews can be trained to perform visually guided detection, discrimination, and memory tasks, using a variety of visual cues such as contrast, color, orientation, etc(Ohl et al., 1998; Casagrande and Diamond, 1974; Petry et al., 1984; Petry and Kelly, 1991; Mustafar et al., 2018; Savier et al., 2021). In addition, the postnatal development of brain areas such as V1 is continuous and active until adulthood (Drenhaus et al., 2006), with eye-opening around 3 weeks postnatal (Guo et al., 2013), giving opportunities to study the formation and fine tuning of visual functions. Finally, the tree shrew user community has also been actively developing genetic and viral tools to support manipulations on a finer scale (Yao et al., 2024; Savier et al., 2021).

To summarize, the tree shrew can be a promising animal model for vision or broader research topics. Furthermore, introducing diverse animal models can accelerate our understanding of the general and fundamental principles of vision. In my studies, I used tree shrews as my main animal model, and mice as a comparison, to investigate the neural computation of visual motion in the SC as well as visual decision-making.

Chapter 2

Tree Shrews as an Animal Model for Studying Perceptual Decision-Making Reveal a Critical Role of Stimulus-Independent Processes in Guiding Behavior

This chapter has been published in eNeuro (Li et al., 2022a). The work was conducted in collaboration with the contributions with the following coauthors: Kara M. McHaney, Per B. Sederberg and Jianhua Cang.

Author List

Chuiwen Li[1], Kara M. McHaney[2], Per B. Sederberg[1], Jianhua Cang[1,2,3]

Author Affiliation 1. Department of Psychology, University of Virginia, Charlottesville, VA 22904, USA; 2. Department of Biology, University of Virginia, Charlottesville, VA 22904, USA. 3. Lead contact

Author Contributions PBS and JC Conceptualization; CL and PBS Designed Experiment; CL

and KMM Performed Research; CL and PBS Analyzed data; CL, JC, PBS and KMM Wrote the paper; JC and PBS Funding Acquisition

Acknowledgements

This work was supported by the National Institutes of Health (U01 NS122040 to J.C. and P.B.S.) and Jefferson Scholars Foundation (to J.C.). We thank Masashi Kawasaki for the help with making the behavior box; Seiji Tanabe for advice on building electronic circuits of the lick port system and animal training; Michele Basso and Vaibhav Thakur for the helpful discussion and suggestions; Alev Erisir for sharing and coordinating tree shrew usage; Brandon Jacques for technical assistance and feature addition of the SMILE library; and Ryan Kirkpatrick for advice on modeling procedure.

Conflict of Interest: No

2.1 Abstract

Decision-making is an essential cognitive process by which we interact with the external world. However, attempts to understand the neural mechanisms of decision-making are limited by the current available animal models and the technologies that can be applied to them. Here, we build on the renewed interest in using tree shrews (*Tupaia Belangeri*) in vision research and provide strong support for them as a model for studying visual perceptual decision-making. Tree shrews learned very quickly to perform a two-alternative forced choice contrast discrimination task, and they exhibited differences in response time distributions depending on the reward and punishment structure of the task. Specifically, they made occasional fast guesses when incorrect responses are punished by a constant increase in the interval between trials. This behavior was suppressed when faster incorrect responses were discouraged by longer inter-trial intervals. By fitting the behavioral data with two variants of racing diffusion decision models, we found that the between-trial delay affected decision-making by modulating the drift rate of a time accumulator. Our results thus provide support for the existence of an internal process that is independent of the evidence

accumulation in decision-making and lay a foundation for future mechanistic studies of perceptual decision-making using tree shrews.

2.2 Introduction

Decision-making is a vital cognitive process, playing an important role in many brain functions such as categorization, learning, memory, and reasoning. Among different forms of decision-making, perceptual decision-making, where decisions are based on sensory stimuli, is a simple yet informative task that is particularly amenable to experimental studies. Visual stimuli are often used because the visual system is arguably the best studied sensory system, thus advantageous for understanding perceptual decision-making from sensation to action.

Considering decision-making is a dynamic process with complex combinations of distinct underlying variables, researchers have frequently applied Sequential Sampling Models (SSMs) to interpret and decompose decision behaviors. These models assume that the evidence (i.e., a variable depending on the sensory stimulus strength) is accumulated through time, and a corresponding choice is made when the accumulated evidence passes a threshold. By defining these stochastic accumulation processes, SSMs can simulate decisions and response times (RTs) with the stimulus as the input. The discovery of "ramping neurons" during decisions in many brain regions provides neural evidence for these models (Horwitz and Newsome, 1999; Roitman and Shadlen, 2002; Mante et al., 2013; Ding and Gold, 2010). Despite the models' effectiveness in a wide range of applications, variants of the SSM make different predictions regarding what decision variables (bias, threshold, time perception, etc.) are involved and how they interact with each other (Ratcliff, 1978; Usher and McClelland, 2001; Brown and Heathcote, 2005; Cisek et al., 2009). More importantly, the neural mechanisms of these variables and their interactions remain largely unknown, which typically require studies in animal models.

Monkeys and rodents (mostly rats and mice) are commonly used in decision-making studies, with respective advantages and drawbacks. Monkeys are closely related to humans, but they are expensive and limited in availability, thus difficult to study or control individual differences. Furthermore, most modern ”circuit-busting” opto- and chemo-genetic techniques are not yet routinely used in primates. On the other hand, recent use of rodents, especially mice, has significantly advanced our understanding of decision-making (e.g., Odoemene et al., 2018; Aguillon-Rodriguez et al., 2021; Ashwood et al., 2022). However, mice and rats are nocturnal animals with poor eyesight, making them less than ideal for visual tasks. In addition, rodents often learn visual tasks slowly (Urai et al., 2021; Aoki et al., 2017), costing both time and effort to obtain high quality data. Here, we use a different animal model - tree shrews (*Tupaia Belangeri*, Fig. 2.1A) for visual decision studies. Under the order of *Scandentia*, tree shrews are evolutionarily closer to primates than rodents are (Yao, 2017). They are diurnal, have an excellent acuity, and display visual system complexity similar to primates (Petry and Bickford, 2019). Earlier studies have shown that they could be reliably trained to perform visual (color, orientation, spatial frequency, temporal frequency, etc...) discrimation tasks (Casagrande and Diamond, 1974; Petry et al., 1984; Petry and Kelly, 1991; Callahan and Petry, 2000; Mustafar et al., 2018). In addition, tree shrews are of lower cost, smaller, and have a faster reproduction cycle than monkeys, making them more accessible. Finally, modern viral, genetic, and imaging techniques are being applied in tree shrews with much better success than in primates (Lee et al., 2016; Sedigh-Sarvestani et al., 2021; Li et al., 2017; Savier et al., 2021). Taken together, tree shrews have the potential to advance the understanding of neural mechanisms underlying perceptual decision-making. In this study, we seek to establish a rigorous perceptual decision-making paradigm for tree shrews, and to characterize the decision-making features, including both response accuracy and response time, in this animal model quantitatively with both summary statistics and trial-level computational modeling.

2.3 Methods

2.3.1 Contrast Discrimination Task

We trained in total of 9 (male = 7, female = 2) freely moving tree shrews to perform a two-alternative forced choice (2AFC) contrast discrimination task (Fig. 2.1C). At the beginning of each trial, a visual stimulus of two orthogonal overlapping alpha-transparent gabors appeared at the screen center to indicate that the tree shrew could lick the center port to initiate the trial. After initiation, the center stimulus disappeared, and two side gabor patches were presented immediately on the left and right of the screen. Tree shrews needed to choose the side with a higher contrast by licking the corresponding lick port. This self-initiation design helped to ensure that the animals were focused from the beginning of each trial and allowed us to record accurate RTs, which were calculated as the duration between the stimulus (2 side gabors) appearance and the side-port lick detection. Once a choice lick was detected, the stimulus would disappear from the screen. We adopted a free-response structure that if no choice was detected, the stimulus would be on for an infinite amount of time.

Inter-Trial Intervals (ITIs) were randomly drawn from a truncated normal distribution with a mean of 0.6, a standard deviation of 1, a lower bound of 0.5, and an upper bound of 0.7 (unit: sec). For correct responses, liquid reward (50% grape juice) was given right after the animals reported their choices. The reward volume was determined by the duration of the valve opening, which was randomly drawn from a truncated normal distribution with a mean of 0.1, a standard deviation of 0.06, a lower bound of 0.2, and an upper bound of 0.4 (unit: sec). The speed of liquid flow was 150 $\mu L/s$. The average reward volume in one correct trial was 33 μL (0.22 s). The random ITI and random reward duration helped the animals to stay engaged in the task.

For incorrect responses, 2 protocols were used to generate a delay as a punishment. (1) A fixed delay of 4 s was used in the first group of tree shrews for all incorrect responses. If the animal licked the center port during the delay (i.e. blank screen licks; detected in 0.8 s periods), a penalty of 0.8 s was then added to the delay, with a maximum of 8 sec for the total delay. (2)

An exponential decay function (Eq.2.1) was applied in the second group of animals to generate a between-trial delay based on the trial-level RT:

$$T = \frac{1}{s} e^{-\frac{RT-l}{s}}, \tag{2.1}$$

where T is the between-trial delay, RT is the response time of the current incorrect trial, and l and s are the location and scale parameters, which shift and scale the function in the stimulus generation code. For all animals, we used $l = 0.1$, $s = 1.7$. For the blank screen lick penalty, 1.5 s was added for every center-port-lick, with the total delay being $Max(T, t_{passed} + penalty)$, and no upper limit. To determine the potential effect of these two delay paradigms, we calculated the reward rate using the data of a representative animal from the first group of tree shrews (Eq.2.2): the response accuracy of each RT bin was fitted with a sigmoid function, which was then used to calculate the theoretical reward per unit time (pulse/s).

$$RR(t) = \frac{Acc(t)}{Acc(t) \times t + (1 - Acc(t)) \times (t + Delay(t))}, \tag{2.2}$$

where $RR(t)$ is the reward rate for a response time of t, $Acc(t)$ is the response accuracy (i.e., ratio of correct choices) under this response time t obtained from the observed data, $Delay(t)$ is the inter-trial delay for incorrect responses, which is 4 for the fixed-delay rule or follows the exponential decay function defined above (Eq.2.1) for the exponential-delay rule.

2.3.2 Animal Training And Data Collection

Tree shrews were first acclimated to the behavior box for 1-2 days. For most animals (7 out of 9), water restriction started at this stage of training (stage 1). For the other two animals, water restriction started a couple of days before acclimation. Two approaches of water restriction were used: 1) we gradually reduced their water intake from baseline (20 - 40 mL/day) to 5-10 mL/day by limiting the availability of drinking water; 2) we used citric acid (CA, Urai et al., 2021) water in their home cage to reduce water intake and gradually increased its concentration from 2% to 4%.

The progress of water restriction depended on the animals' weight loss, water-intake baseline, and tolerance, to make sure that they were motivated to stay focused on the task for at least 25 minutes per day, and at the same time, not experiencing any health issue (Weight $\geq 90\% \times$ Baseline). Depending on the animals' acclimation and learning speed, the water restriction progress (2-7 days) could extend to stage 2 and even 3 before reaching a stable restriction level.

During stage 1, a single gabor stimulus would be shown right above the center lick port. After the gabor appeared, the animals could lick the center port at any time to trigger a liquid reward (grape juice diluted with water in a 1:1 ratio). Each tree shrew was left in the behavior box to learn to use the center port for no more than 20 minutes every day for acclimation, but this stage usually took only 1 day ($\sim$20-40 trials per day). Having learnt to get liquid reward from the center port, the animals progressed to the next stage. At stage 2, the contrast discrimination task was set up with contrast pairs of 1.0 (full contrast) vs 0.0 (zero contrast), i.e., a single side stimulus was shown. The goal of stage 2 was to train the animals to use the left and right lick ports. Liquid reward from the center port was gradually reduced to zero within about 50 trials. Animals usually perform 100-300 trials per day at this stage. Once they learned and had a stable correct rate of more than 75%, they progressed to stage 3. Note that most animals learned very fast and graduated both stages 1 and 2 within 2 days.

At stage 3, we first gave the animals an easy condition by using contrast pairs of 1.0 vs 0.1, and gradually mixed in other pairs of smaller contrast differences, finally achieving the stimulus set we use in the formal data collection. During this stage of training, we also adjusted the ratio of easy (e.g., comparing the highest and lowest contrast) and difficult (same or similar contrast) trials for each animal. By including sufficient easy trials and limiting the number of equal-contrast trials, we were able to keep the animals motivated to keep doing the task. For equal contrast trials, the correct answer was randomly assigned to left or right, so that the animals still had 50% chance to get a reward in these trials. At this stage, the animals performed 500-600 trials per day. Some animals could finish it within 30 minutes, while some of the others needed as long as 1 hour, especially when they produced large numbers of incorrect choices (giving rise to more penalty time) or they started to lose patience and focus (giving rise to more idling time). To control the frustration level, we would stop the training when the duration was over 1 hour. At this time, some animals ($\sim$50%) also developed biased behavior by making most choices to the same side. We discouraged this behavior by automatically adjusting the probability of left/right trials depending on their real-time performance. For example, we calculated the proportion of choosing rightward in the previous 10 trials, denoted as Pr. The probability of the next trial being rightward was $1-Pr$. This real-time bias correction quickly discouraged the biased behavior in the tree shrews.

After the animals achieved a stable (3-5 consecutive days) overall accuracy $\geq 60\%$ (at this time, the accuracy is expected to be lower because of the existence of equal contrast trials and other difficult trials), we collected data for consecutive days (500-600 trials per day) to reach at least 100 repeats for each condition of contrast discrimination. The data were first culled by applying a 3 standard deviation outlier removal on the Box-Cox transformed response time distribution in preprocessing. The remaining trials were used in further analysis.

All animal procedures were performed in accordance with the University of Virginia animal care committee's regulations.

2.3.3 Stimulus and Apparatus

The experiment program was written in Python and the stimuli were generated and presented with the State Machine Interface Library for Experiments (SMILE, `https://github.com/compmem/smile`). The Gabor patch size was 28°, and the spatial frequency was 0.2 cpd. The stimulus screen had a 1280×1024 resolution and 60Hz refresh rate, and was gamma-corrected. It was set at a distance of 15 cm from the animal. There were 6 levels of stimulus contrasts ranging from 0.08 to 0.99, which were evenly-spaced. All combinations of left and right contrasts are presented in a randomized order.

The lick-detector circuit (adapted from: Marbach and Zador, 2017), and reward-valve control circuit (adapted from: `https://bc-robotics.com/tutorials/controlling-a-solenoid-valve-with-arduino/`) were controlled with an NI USB-6001 multifunction I/O device (`https:`

`//www.ni.com/en-us/support/model.usb-6001.html`). The Plexiglass behavior box was L: 40 cm×W: 22 cm×H: 20 cm with a transparent window on the front side to allow the animals to watch the screen.

2.3.4 Data Analysis and Models

To test the relationship between RT and contrast difference, we fitted a mixed effect linear regression model with RT as the dependent variable, the absolute contrast difference between left and right stimuli as the independent variable, and individual animal as the group variable, using the statsmodels library in Python.

We fitted the behavioral data with two sequential sampling decision-making models, the Timed Racing Diffusion Model (TRDM) and the Racing Diffusion Model (RDM), and compared their performance using a Bayesian approach. TRDM contains 3 independent accumulation processes, namely two evidence accumulators and one time accumulator (or "timer"), whereas RDM only has the two evidence accumulators (Fig. 2.3A& B). The probability density function ($f(t)$) and cumulative distribution function ($F(t)$) for each evidence or time accumulation process are defined by the inverse Gaussian (Wald) distribution in Eq.2.3:

$$\begin{aligned}
f(t|\rho,\sigma,\alpha,t_0) &= \frac{\alpha}{\sigma\sqrt{2\pi(t-t_0)^3}} exp\left(-\frac{[\alpha-\rho(t-t_0)]^2}{2\sigma^2(t-t_0)}\right) \\
F(t|\rho,\sigma,\alpha,t_0) &= \Phi\left(\frac{\rho(t-t_0)-\alpha}{\sigma\sqrt{t-t_0}}\right) + exp\left(\frac{2\alpha\rho}{\sigma^2}\right)\cdot\Phi\left(-\frac{\rho(t-t_0)+\alpha}{\sigma\sqrt{t-t_0}}\right),
\end{aligned} \tag{2.3}$$

where t is the response time, ρ is the mean drift rate, σ is the within-trial variability of the drift rate, α is the threshold (which was fixed to 1.0), t_0 is the non-decision time, Φ is the cumulative distribution function of a standard normal distribution(Heathcote, 2004; Hawkins and Heathcote, 2021).

The mean drift rate (ρ) of each evidence accumulator was calculated using the following equation (Eq.2.4), taking into consideration both the stimulus difference and their total strength.

$$\begin{aligned} \rho_l &= v_0 + v_d * (s_l - s_r) + v_s * (s_l + s_r) \\ \rho_r &= v_0 + v_d * (s_r - s_l) + v_s * (s_l + s_r), \end{aligned} \tag{2.4}$$

where ρ_l and ρ_r are the mean drift rate of the left and right evidence accumulators, v_0 is the baseline drift rate, s_l and s_r are the contrasts of left and right stimuli, v_d is the coefficient of the contrast difference term, v_s is the coefficient of the contrast summation term (van Ravenzwaaij et al., 2020).

The accumulators race against each other. If one of the evidence accumulators first reaches the threshold, a corresponding choice is made. If the time accumulator reaches the threshold first, one of the options will be chosen randomly with a partial dependence on which evidence is greater at that time point. This is done through a process controlled by a parameter γ, ranging from 0 to 1, with 1 being fully dependent on the evidence accumulated up until that point, and 0 being completely random regardless of the accumulated evidence. Other parameters of the model include ρ_t, ω and t_0, as described in Table 1.

To apply Bayesian inference, we first defined the “priors” - the belief of the true parameter values before data observation - by assigning a probability distribution for each of the parameters based on previous experience (Table 1; Kirkpatrick et al., 2021). We then used the observed data to update the prior distributions, in order to achieve a more constrained posterior distribution of what parameters could have generated the observed data for each model. Posterior samples were generated with the differential evolution Markov chain Monte Carlo (DE-MCMC, Ter Braak, 2006; Turner and Sederberg, 2012; Turner et al., 2013) algorithm, which was shown to be computationally efficient. This was implemented by the RunDEMC library (`https://github.com/compmem/RunDEMC`). We set $10k$ (k is the number of parameters) parallel chains for 200 iterations in the burn-in stage and 500 iterations to sample the posterior.

Specifically, we apply a standard Metropolis–Hastings algorithm to accept or reject proposed samples from the posterior. Here, a new parameter proposal is evaluated by comparing its posterior probability with that of the current proposal, with the probability of accepting a new proposal:

$$P(accept) = \frac{P(D|\theta')P(\theta')}{P(D|\theta)P(\theta)}, \tag{2.5}$$

where D represents the observed data, θ' is the new proposal, θ is the current proposal, $P(D|\theta')$ and $P(D|\theta)$ are the likelihoods calculated with Eq.2.6, and $P(\theta')$ and $P(\theta)$ are the priors.

To calculate the likelihood $P(D|\theta)$ of observing the data D given the parameters θ, we multiply the likelihoods of observing each choice and RT as determined by the model probability density function (PDF) defined by the parameters θ. For example, the PDF for observing a $left$ response with a decision time t is defined by the following equation (Heathcote, 2004; Hawkins and Heathcote, 2021):

$$\begin{aligned} PDF_{left}(t) &= f_{E,left}(t)\left(1 - F_{E,right}(t)\right)(1 - F_T(t)) + P_T f_T(t)\left(1 - F_{E,left}(t)\right)\left(1 - F_{E,right}(t)\right) \\ P_T &= \gamma F_X(0) + \frac{1}{2}(1-\gamma) \\ X &\sim N\left(\rho_r t - \rho_l t, \sqrt{2\left(\eta_c \sqrt{t}\right)^2}\right), \end{aligned} \tag{2.6}$$

where $f(t)$ and $F(t)$ are the density and distribution functions defined above, f_E and F_E are for the evidence accumulators, while f_T and F_T are for the time accumulator. F_X is the cumulative distribution function for the random variable X, and X follows a normal distribution defined by the difference in evidence accumulator distributions. ρ_l and ρ_r are the mean drift rate for left and right evidence accumulators, η_c is the within-trial variability of the drift rate for the evidence accumulators.

Finally, to compare the performance of the two models, we first calculated the Bayesian Information Criterion (BIC) values (Eq.2.7) of each model fitting result:

$$BIC = k\ln(n) - 2\ln\left(L(\hat{\theta})\right), \tag{2.7}$$

where k is the number of parameters, n is the number of data points, $L(\hat{\theta})$ is the maximum likelihood of the model's fit to the data. Then we approximated the Bayes factor with BIC as in Eq.2.8 (Kass and Raftery, 1995):

$$BF_{ij} \approx \exp\left(-\frac{1}{2}(BIC_i - BIC_j)\right), \tag{2.8}$$

where BIC_i and BIC_j are BIC values for Model i (in this case the TRDM) and Model j (the RDM)) respectively. $BF_{i,j} > 1$ means evidence is in favor of Model i over Model j. $BF_{i,j} > 3, 20, 150$, correspondingly $\ln(BF_{i,j}) > 1, 3, 5$, indicates positive, strong, very strong evidence for Model i over Model j, respectively (Lodewyckx et al., 2011).

2.4 Results

2.4.1 Tree shrews quickly learned to perform a contrast discrimination 2AFC task.

We trained a total of 9 (male = 7, female = 2) tree shrews to perform a 2AFC contrast discrimination task (Fig. 2.1). The 2AFC design was chosen over other classic paradigms such as "Go/no-Go" tasks because it eliminates the asymmetry between responses for different options. Also, we designed the trials to be self-initiated and self-paced by the animals, in order to obtain precise response time (RT) data for comprehensive behavioral analysis. During training, freely moving tree shrews were first acclimated in the behavioral box with a single gabor stimulus appearing at the center or either side of the screen (Fig. 2.1B). After the animals learned the association between the stimulus and liquid reward, often within 1-2 days, two gabors of different contrasts were introduced with the higher contrast one indicating the location of the reward (Fig. 2.1C). All the tree shrews were able to learn the task and reach an accuracy greater than 75% for the easiest condition within 1 week (Fig. 2.1D). In fact, most of them reached 75% accuracy within 2 days. It is worth noting that, once the animals reached a good performance, the overall difficulty was increased progressively. In other words, the "easiest" condition often became more difficult in successive days. Yet, the animals' performance was stably above 75%, indicating that they had learned the rule of the task, instead of the specific stimuli, within a very short period. These observations thus highlight the impressive learning capability of tree shrews and indicate that they can be a promising animal model in cognitive neuroscience research.

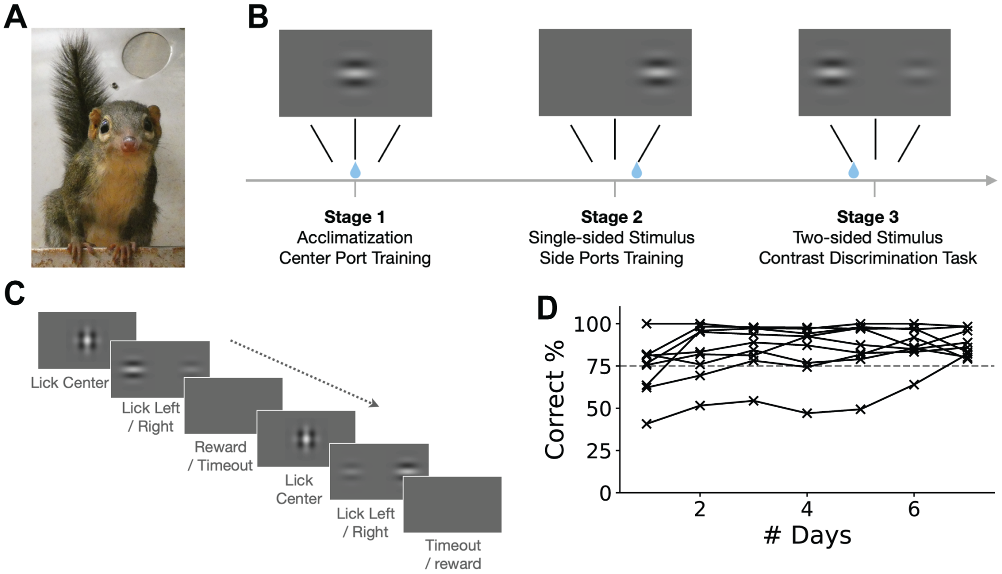

Figure 2.1: Experimental design. A A photo of a tree shrew in the home cage. **B** A schematic of the training procedure. **C** The contrast discrimination task. The animal needs to choose the side that has a higher contrast gabor and report the choice by licking the corresponding port. **D** Learning curve of individual animals. The y axis is the response accuracy for the easiest condition on each day. Day 1 refers to the first day of training with two-sided gabor stimulus. Dashed gray line: 75% accuracy. Most animals reached this level by day 2 and all by day 7.

2.4.2 Tree shrews showed different behaviors under two training schemes.

In the first group of animals (n = 5; male = 4, female = 1), a fixed trial delay of 4 seconds was used to punish incorrect responses (Fig. 2.2A). All animals were able to learn the task. An increase in difficulty (i.e., a decrease of contrast difference between the two stimuli) induced an expected drop of response accuracy (Fig. 2.2B). However, task difficulty did not have a significant effect on the response time (RT) in correct trials (mixed effect linear regression, $\beta = .008^a$, $p = .125$, Table 1-1), whereas the RT in incorrect trials increased with task difficulty (Fig. 2.2C, mixed effect linear regression, $\beta = -.075^b$, $p < .001$). This result is different from previously reported

RT trend in humans, monkeys, and mice (Philiastides et al., 2011; Dmochowski and Norcia, 2015; Roitman and Shadlen, 2002; Palmer et al., 2005; Jun et al., 2021; Orsolic et al., 2021), where increasing task difficulty usually resulted in an increase in RT in correct trials. We examined the RT distribution of individual animals and saw a bimodal-like shape in most animals (n = 4 out of 5) in this group (e.g., Fig. 2.2D, Fig. 2.5), instead of the more common log-normal distribution (Ratcliff, 1978; Smith and Ratcliff, 2004). Furthermore, the first small peak of the RT distribution contained a similar proportion of correct and incorrect trials, while the second peak had many more correct than incorrect trials. This bimodal distribution suggested 2 possible modes in the behavioral responses, a "fast-guessing" mode of random performance and a slower mode where an animal was more "engaged" in the task.

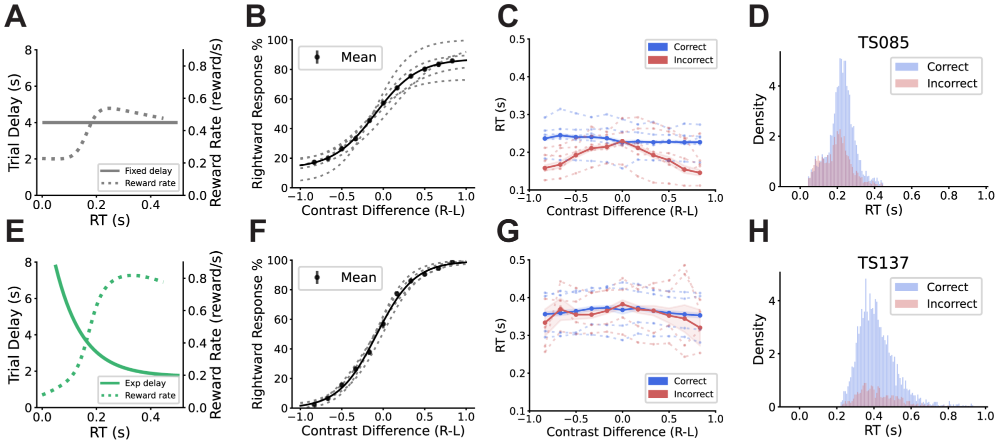

Figure 2.2: Tree shrews show different behaviors under two training schemes. A A fixed delay of 4 seconds (solid line) was used in training 1 group of animals. The dashed line shows the theoretical reward rate under this fixed delay. **B** Psychometric curve of animals from this training scheme. Contrast difference: right contrast(R) - left contrast(L). Grey dashed line: individual animals. Black solid line: average across animals. **C** response time (RT) as a function of contrast difference. Dashed line: individual animals. Solid line: average across animals. The shaded area is 95% confidence interval. **D** RT density histogram from a representative animal. Correct and incorrect trials are separately plotted. **E** An exponential decay delay scheme (solid line) was applied in another group. The dashed line shows the theoretical reward rate under this scheme. **F**, **G**, **H**: Same as **C**, **D** and **E**, but for the second group.

To discourage the animals from "fast guessing", we employed an exponential decay trial delay for incorrect responses in the second group (n = 4; male = 3, female = 1) (Fig. 2.2E). The exponential decay delay would punish fast incorrect responses more than slow incorrect ones, at a more aggressive level than the fixed trial delay procedure (Fig. 2.2A & E). All animals in this group were again able to learn the task quickly (Fig. 2.2F & G). Notably, the overall RT was substantially slower compared to the fixed-delay group, indicating the effectiveness of the new trial delay paradigm. Furthermore, the RTs in correct trials showed a slightly increasing trend with task difficulty (mixed effect linear regression, β = -.021[c], p = .001), while the effect on the incorrect RT became less prominent than for the fixed-delay group (mixed effect linear regression, β = -.046[d], p = .014). When examining the RT distribution of individual animals, we saw one-peak log-normal distributions, similar to what was reported in other species, and a clear above-chance accuracy across the entire range (e.g., Fig. 2.2H, Fig. 2.6).These behavioral data thus demonstrate that the tree shrews responded to the two trial delay schemes with different behaviors.

2.4.3 Non-evidence accumulation mechanism is crucial to interpreting tree shrew behaviors.

The above behavioral data suggest the involvement of a process in addition to evidence collection during decision-making. One possibility is a time accumulation process where the animals had an internal time threshold on the task, and they would rush into a more or less random choice if the time threshold was reached before accumulating enough evidence to guide the choice. This time limit would be different under the two trial delay paradigms: shorter under fixed delay, thus leading to many fast guesses. To test the plausibility of this explanation, we turned to cognitive models of decision-making.

We fitted two models, Racing Diffusion Model (RDM) and Timed Racing Diffusion Model (TRDM, Hawkins and Heathcote, 2021), to the data obtained from individual animals. In a 2AFC task, the RDM describes 2 independent evidence accumulators racing against each other. When one of the accumulators first reaches the threshold, a corresponding choice is made (Fig. 2.3A).The TRDM has one additional accumulator that tracks time (Fig. 2.3B). If the time accumulator reaches the threshold before the evidence accumulators, a decision is made based on the current accumulated evidence with a certain probability γ. We fixed all the accumulation thresholds to be 1. A fast time accumulator was thus effectively equal to a short time limit as described above. The two models allowed us to test if an additional timing mechanism can better explain tree shrew decision behaviors.

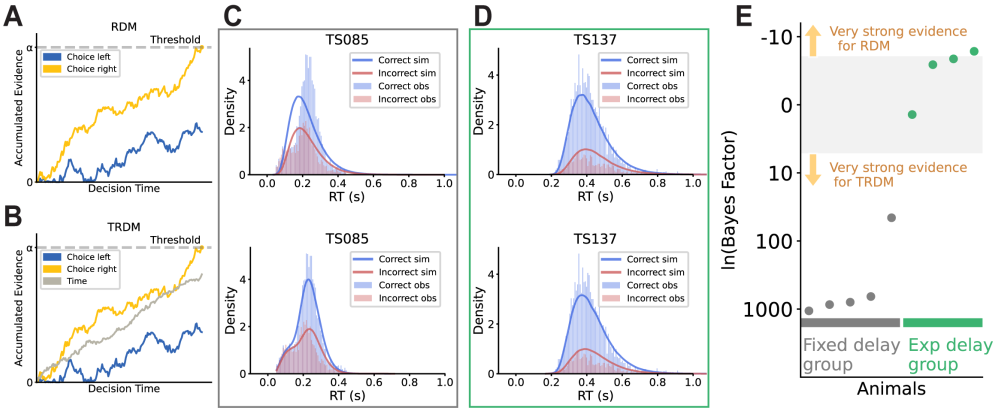

Figure 2.3: Modeling results suggest that evidence accumulation combined with a timing mechanism better fits tree shrew decision-making behavior. A and **B** Racing Diffusion Model (RDM, **A**) and Timed Racing Diffusion Model (TRDM, **B**). Blue trace: the evidence accumulator for left choice. Yellow trace: the evidence accumulator for right choice. Grey trace: the time accumulator. The 2 evidence accumulation processes race against each other. In these schematics, the accumulator for right stimuli (yellow) reaches the threshold first, resulting in a rightward choice. **C** Observed (histograms) and simulated (lines) RT distribution for the representative animal from the fixed-delay group. *Top*: RDM simulation. *Bottom*: TRDM simulation. **D** Observed and simulated RT distribution for the representative animal from the exponential-delay group. *Top*: RDM simulation. *Bottom*: TRDM simulation. **E** Estimated log Bayes Factor comparing the two models' performance. Positive values favor TRDM, while negative values favor RDM. Grey dots represent the animals from the fixed-delay training, and green dots represent the exponential-delay group. The upper and lower edges of the gray shaded area represent the lower limit for "very strong" evidence ($ln(BF) = 5$).

We used a Bayesian approach for model fitting (Ter Braak, 2006; Turner and Sederberg, 2012; Turner et al., 2013), and then simulated choice and RT data with the best fitting parameters to visualize the goodness of fit. We found that the RDM captured the RT distribution of the exponential-delay group well, but failed to fit the fixed-delay group (Fig. 2.3C & D, top panels). On the other hand, the TRDM fitted well to both groups (Fig. 2.3C & D, bottom panels). To quantify their performance difference, we estimated the Bayes Factor (BF) of the two models for each animal (Fig. 2.3E). For animals in the fixed-delay group, the values of ln(BF) were extremely high, ranging from 45 to 1062, providing overwhelming support for the TRDM. These values were much higher than 5, which is a conventional threshold for "very strong" evidence for one model over the other in Bayesian modeling (Lodewyckx et al., 2011). For the exponential-delay group, the evidence favored the RDM for 3 out of the 4 tree shrews, although the magnitude of evidence was not nearly as strong ($ln(BF)$ ranging from -6 to 1). It should be noted that Bayes Factor in our estimation punishes complex models that have more parameters. As a result, despite the similar performance of the two models in fitting the exponential-delay group data, the RDM had the advantage of simplicity, thus leading to the winning BF.

We then simulated choice and RT data with the best fitting parameters (Table 1-2 and 1-3) for each animal using the winning model, to visually check the goodness of fit. Fig. 2.4 illustrates that the TRDM fit the data of the fixed-delay group well (Fig. 2.4A), and the RDM was able to reproduce the behavior of the exponential-delay group (Fig. 2.4D), for both the psychometric curves and the RT-contrast relationship. Consistent with the result in Fig. 2.3, the TRDM was also able to fit the psychometric curves and the RT-contrast relationship for the exponential-delay group (Fig. 2.4C), similarly to the RDM, while the RDM failed to capture the RT-contrast relationship for the fixed-delay group (Fig. 2.4B). The fact that the behavior of both groups could be explained by the TRDM supported the involvement of the non-evidence-accumulation process during tree shrew visual decision making, and this process can be manipulated by applying different trial delay rules.

The models allowed us to track down the generating mechanism of the simulated data, i.e., whether each decision was initiated by an evidence accumulator or the timer crossing the threshold. We separated the TRDM-simulated data for each animal according to the generating mechanism, and found the timer and evidence accumulators contributed to two separate RT peaks. Fig. 2.7 shows the comparison between simulated data and observed data for an example tree shrew from the fixed-delay group (Fig. 2.2D). The results indicated that the fast RTs were largely generated by the timer (Fig. 2.7A). In addition, when examining the simulated RTs for correct choices generated by evidence accumulators only, they increased with the task difficulty (Fig. 2.7D), similar to what has been previously reported in humans, monkeys, and mice (Philiastides et al., 2011; Dmochowski and Norcia, 2015; Roitman and Shadlen, 2002; Palmer et al., 2005; Jun et al., 2021;

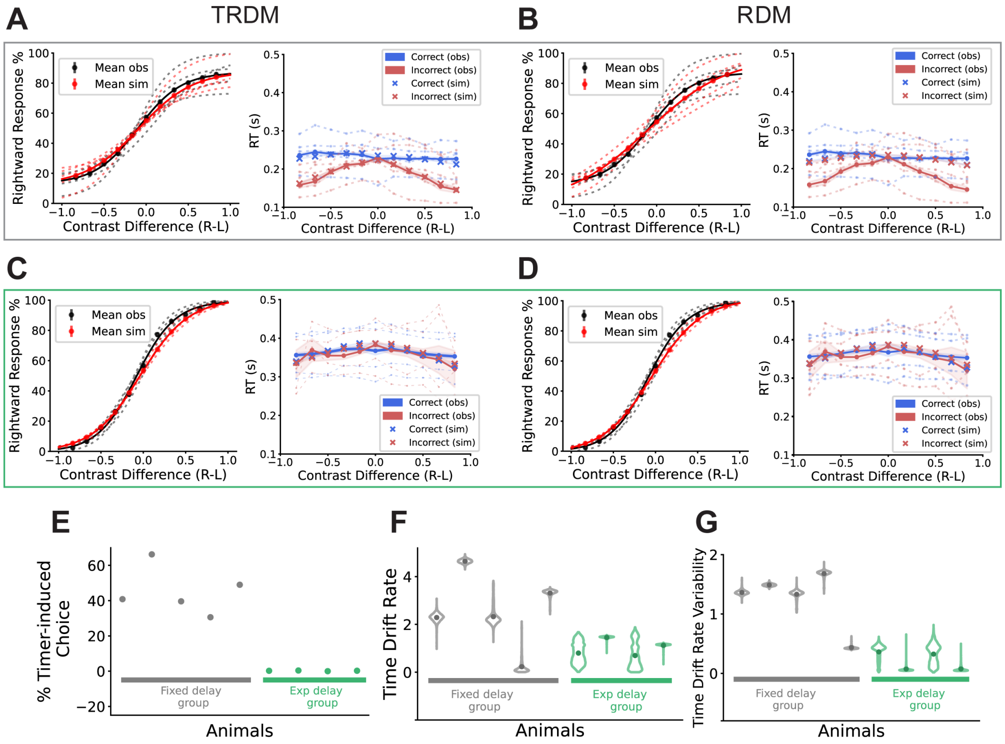

Figure 2.4: Model simulation of the psychometric curves and associated response time, and the posterior of the timer-related parameters. **A** TRDM simulation for the fixed-delay group. *Left*: Observed (black) and simulated (red) psychometric curves for individual animals (dotted lines) and the group average (solid lines). The simulations were done with the best fitting parameters of the TRDM. *Right*: Observed (dots, solid lines, and dotted lines) and simulated RT function (“x”). Dotted lines: individual animals. Solid lines: group average. **B** RDM simulation for the fixed-delay group. **C** TRDM simulation for the exponential-delay group. **D** RDM simulation for the exponential-delay group. **E** Percentage of timer-induced choice calculated from the TRDM-simulated data for each animal. **F** The posterior distribution of the time accumulator mean drift rate (ρ_t) for individual animals from the TRDM fitting. The dot in each distribution indicates the mean value. **G** Same as **F**, but for the drift rate variability of the time accumulator (η_t).

Orsolic et al., 2021). These model results suggest that the tree shrews learned the visual decision-making task, and they had similar behaviors as other animals when "engaged" in the task. Moreover, the timer-driven random choices explained the plateau of a non-perfect accuracy, even in the easiest conditions (Fig. 2.7C).

Next, for each tree shrew, we quantified the percentage of timer-induced choices from the TRDM-simulated data (Fig. 2.4E). As expected from the above analysis, all of the animals from the fixed-delay group showed many timer induced choices (ranging from 30% to 66%), while the value was near zero for every animal in the exponential-delay group. To understand what decision variables were altered by the change of delay rule, we examined the posterior distribution of the parameters in the TRDM. The posteriors of the timer-related parameters showed a general trend of higher mean drift rate for the time accumulator (ρ_t) and higher time drift rate variability (η_t) in the fixed-delay group than in the exponential-delay group (Fig. 2.4F & G). The two parameters work together to determine the accumulation speed of time during decision-making, with the fixed-delay group having faster timers. The model results therefore proposed a possible mechanism that the exponential delay worked by slowing down the time accumulation process in the tree shrews, which resulted in far fewer "timer-induced" fast responses with compromised accuracy, and more correct responses guided by the evidence accumulation process.

2.5 Discussion

In this study, we aimed to and succeeded in establishing a response-time paradigm of perceptual decision-making for tree shrews. The behavioral results showed that tree shrews are able to perform a contrast-discrimination perceptual decision task and generate informative choice and response time data. Model-based analyses suggest that, other than the choice-related evidence accumulation process, additional mechanisms, presumably mechanisms that keep track of time, are involved in the decision-making process depending on the specific design of trial delay due to incorrect responses. This new animal model will facilitate future decision-making studies with fast learning, reliable behaviors, increased availability, and more modern techniques.

We carefully considered two points when designing the behavioral paradigm. First, we adopted a 2AFC framework, where two alternative options match symmetrically with two response targets. In other widely used tasks, there often exists asymmetry in either responses or stimulus categories, which can be problematic when interpreting different behaviors. For example, Go/no-Go tasks involve an action (“go”) and a suppression of action (“no-go”) as two responses, which are likely driven by different neural circuits. Such tasks have thus become more suitable for studying impulsion and inhibition (Dong et al., 2010; Ding et al., 2014; Eagle et al., 2008). On the other hand, yes/no tasks offer two asymmetric stimulus categories as options, which are likely represented differently at the neural level (Wentura, 2000; Donner et al., 2009). In comparison, a multiple alternative forced choice framework is better in perceptual decision-making studies. Second, we designed the task to be self-initiated and self-paced by the animals. Self-initiation ensures that the animals are focused during the stimulus presentation, and self-pacing encourages them to respond without delay once they reach a decision. Compared to the commonly-used design where the stimuli show up automatically and animals can respond at any time point within a fixed response window, our design allowed us to collect precise response times in addition to choice data. Response times are particularly useful because they are continuous (whereas choice data are discrete) and are more informative when characterizing decision behaviors. For example, fast correct responses have potentially different mechanisms from slow correct responses, which would be impossible to study without the RT information.

We used models under the SSM family to fit tree shrew decision behaviors on the trial level. SSMs predict the choice and RT distribution with a mathematically defined dynamic decision-making process controlled by cognitively meaningful parameters and offer testable hypotheses about the underlying mechanisms. Signal detection models have also been used to explain perceptual decision-making behaviors (Newsome et al., 1989), but they only predict the choices made by subjects in a decision process, ignoring the information contained in the response time. Furthermore, the choice data are usually averaged over trials, further reducing the information present in the raw data. By comparison, SSMs have the advantage of maximizing the efficiency of the animal experiments and data analysis (Ratcliff et al., 2003).

Despite the RDM showing a slightly better Bayes Factor than the TRDM in the exponential-delay group due to simplicity, the TRDM had the same ability to reproduce the observed choice and RT pattern. Together with its overwhelmingly better performance in the fixed-delay group, the TRDM was overall the better model for this dataset. By examining the source of the simulated data (Fig. 2.7), we found that timer-induced random choices largely contribute to the plateau of a non-perfect accuracy in the easiest conditions. Canonically, this non-perfect accuracy is modeled by "lapse rate" under the Signal Detection framework (Wichmann and Hill, 2001; Aguillon-Rodriguez et al., 2021; Wang et al., 2020a; Prins, 2012). The lapses are usually assumed to happen via a Bernoulli process, i.e., the animals simply make guesses at some random rate independently from trial to trial, while providing no detailed process of choice generation. In comparison, the TRDM utilizes a time accumulator that is highly similar to evidence accumulation to generate random choices. It offers a more integrative solution to the interaction between evidence-based and stimulus independent mechanisms. This can be more plausible on the neuronal level than two separate processes that involve very different calculations. In addition, the TRDM provides the extra ability to explain why we rarely see extremely long RTs in the difficult conditions, especially in the equal-evidence conditions. The time accumulator can limit the RT so that the decision-makers do not waste too much time on a single decision when the evidence is obscure. Thus, we think that the TRDM has more explanatory power than models that include a "lapse rate". Furthermore, a recent study showed that mice alternate between states, such as lapse or biased decisions, during a perceptual decision-making task, and they have a higher probability to stay in the same state for consecutive trials (Ashwood et al., 2022). Therefore, Bernoulli "lapses" would be an oversimplified explanation of how non-perfect choices happen. In future studies, the temporal sequence of choices and RTs should also be analyzed to further investigate the mechanism of decision state switching.

Finally, it is intriguing that the tree shrews in this study showed a fair amount of premature choices under fixed trial-delay even though this strategy was suboptimal, in that it did not maximize the reward rate. The TRDM suggested that the animals actively applied a fast timer (or a short time limit) on the task without being trained to perform the task speedily. Interestingly, this tendency of rushing into choices was discouraged by the exponential trial-delay design that specifically punished fast incorrect responses more. The baseline suboptimal behavior could partly be due to 1) the characteristics of this animal model and/or 2) the stimulus design. The tree shrews showed much faster responses compared to humans on similar tasks (Kirkpatrick et al., 2021) . They were very nimble and showed swift movements and reactions in various environments (behavior rig, home cage, nature, etc...). Given their motor capabilities, fast responses could be a survival strategy to guarantee the total amount of reward via high sampling frequency with slightly compromised accuracy, and could be broadly used in most scenarios to facilitate “exploration” behaviors - unless specifically discouraged. Additionally, in previous perceptual decision-making studies, stochastic stimuli with motion such as random dot kinematogram were usually used (Roitman and Shadlen, 2002; Resulaj et al., 2009; Ditterich, 2006). These stimuli require temporal integration to acquire evidence for choices. In our study, we used the static feature (contrast) as evidence. Although studies showed support for evidence accumulation even using the static stimuli in other species (Kirkpatrick et al., 2021), temporal integration might not be needed as strongly to generate a choice under this situation. This could result in short response times, leading the animals to a faster RT regime (more prone to make premature choices) and masking the effect of task difficulty on the RT (Fig. 2.2G, minor effect, although significant). Nevertheless, the tree shrew data emphasized the natural existence of f evidence-independent mechanisms in decision-making and offered an opportunity to examine their effects. These behavioral patterns also suggest that we should consider the involvement of processes in addition to the evidence accumulation process in other animal/human models when interpreting both behavioral and neural data from decision-making tasks. Here, we included an independent time accumulator to implement this additional process in our decision-making models (Hawkins and Heathcote, 2021). However, it should be noted that mechanisms other than the time accumulator could also generate the fast guessing responses and our results do not rule out these possible mechanisms. In other words, the time accumulator was not necessarily the true underlying mechanism, but rather a piece of evidence for the involvement of multiple generative processes for decision instead of one single process. Other studies have indeed applied alternative approaches to account for decisions not entirely based on evidence accumulation, such as combining the decision process with a probabilistic fast-guess mode that generates a normally distributed guessing time (Ratcliff and Kang, 2021). Future studies that incorporate neural data will be needed to reveal exactly how response times in perceptual decision tasks are affected by information other than the sensory strength.

Main Tables

Table 1: Priors of Free Parameters in Tested Models.

Parameter	Description	Prior
ω	Bias	$IL(0,1.4)$
$t_{0,c}$	Non-decision time of choice	$IL(0,1.4)$
v_0, v_s, v_d	Drift rate coefficients of choice	$LN(1.56,1.5)$
ρ_t^*	Mean drift rate of timer	$LN(1.56,1.5)$
η_c, η_t^*	Within-trial variability	$LN(1.56,1.5)$
γ^*	Mixture between random and evidence-based timer-induced decision	$IL(-1,1.0)$

^{IL} inverse logit distribution

^{LN} log normal distribution

* parameters only exist in TRDM

The best fitting parameters of the two models for each animal is shown in Table 1-2 and 1-3. We also tested the relationship between RT and contrast difference using non-model statistics described in Table 1-1.

Extended Data

Tables

Table 1-1: Statistical Table

Line	Data Structure	Type of Test	Power
a	Non-parametric	Mixed effect linear regression	(-.002, .019)
b	Non-parametric	Mixed effect linear regression	(-.103, -.046)
c	Non-parametric	Mixed effect linear regression	(-.034, -.009)
d	Non-parametric	Mixed effect linear regression	(-.084, -.009)

Table 1-2: TRDM Best Fitting Parameters of Each Animal

Animal	v_0	v_d	v_s	ρ_t	η_c	η_t	γ	ω	$t_{0,c}$	Log likelihood
085	3.388	1.524	0.254	2.306	0.600	1.358	0.194	0.516	0.048	3541.048
087	2.825	2.532	0.809	4.672	0.753	1.486	0.343	0.562	0.049	5162.741
101	3.037	1.768	0.636	2.154	0.603	1.362	0.374	0.519	0.055	5363.755
123	2.383	1.556	0.162	0.100	0.703	1.702	0.459	0.501	0.047	943.074
125	2.253	3.933	0.948	3.394	1.074	0.422	0.978	0.573	0.110	7309.722
130	2.790	2.633	0.185	1.155	0.946	0.042	0.577	0.513	0.195	3070.600
131	2.856	3.476	0.806	1.485	1.161	0.053	0.611	0.505	0.125	3782.443
137	1.612	2.608	0.465	1.572	0.865	0.440	0.969	0.528	0.167	2445.965
138	2.327	4.142	0.979	1.155	1.294	0.043	0.223	0.518	0.151	3190.957

Table 1-3: RDM Best Fitting Parameters of Each Animal

Animal	v_0	v_d	v_s	η_c	ω	$t_{0,c}$	Log likelihood
085	3.122	1.243	0.161	0.904	0.498	0.000	2668.097
087	3.724	1.577	0.352	1.235	0.485	0.001	4494.682
101	2.877	1.436	0.329	0.865	0.540	0.000	4287.514
123	2.041	1.713	0.160	1.054	0.515	0.000	137.629
125	4.362	2.969	0.333	0.893	0.543	0.098	7251.003
130	2.730	2.602	0.228	0.924	0.511	0.192	3063.955
131	2.820	3.370	0.812	1.133	0.505	0.123	3773.603
137	2.114	2.196	0.330	0.759	0.523	0.149	2431.973
138	2.398	4.043	0.946	1.282	0.518	0.150	3183.084

Figures

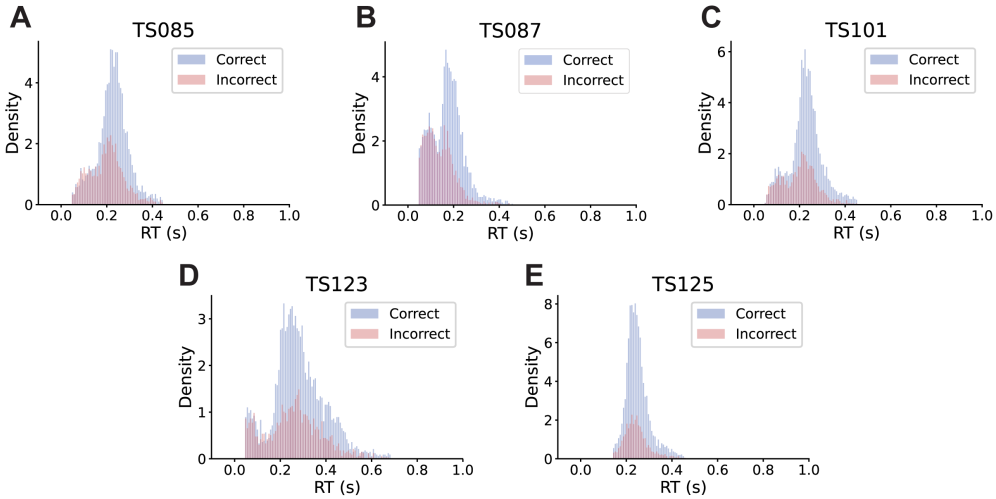

Figure 2.5: Response time distributions of the individual animals from the fixed-delay group.

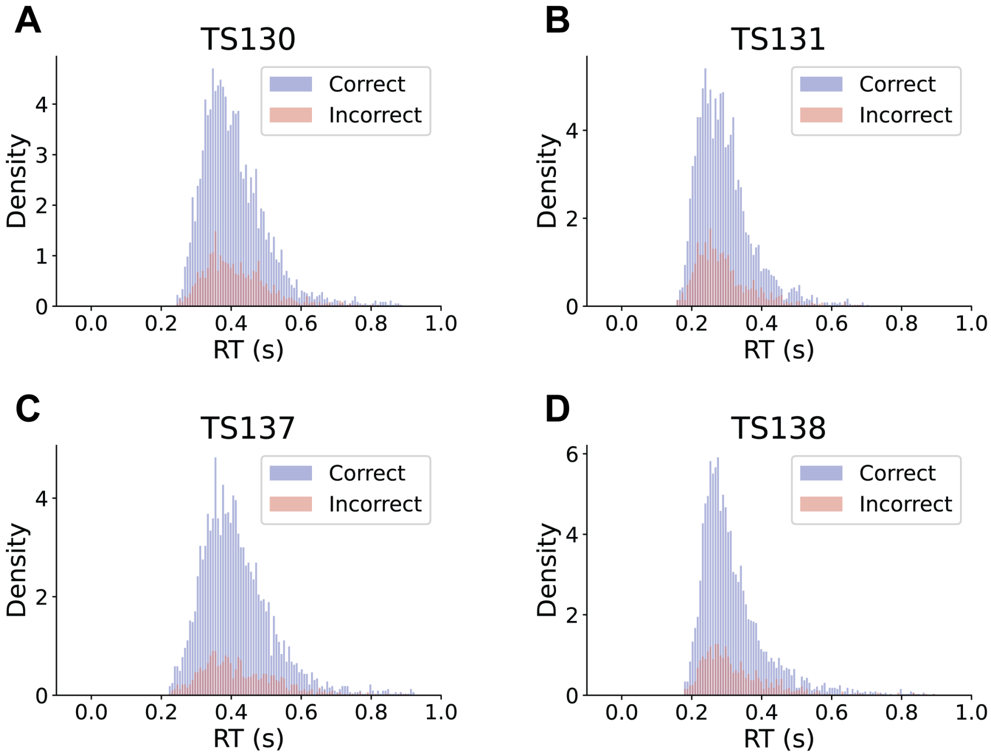

Figure 2.6: Response time distributions of the individual animals from the exponential-delay group.

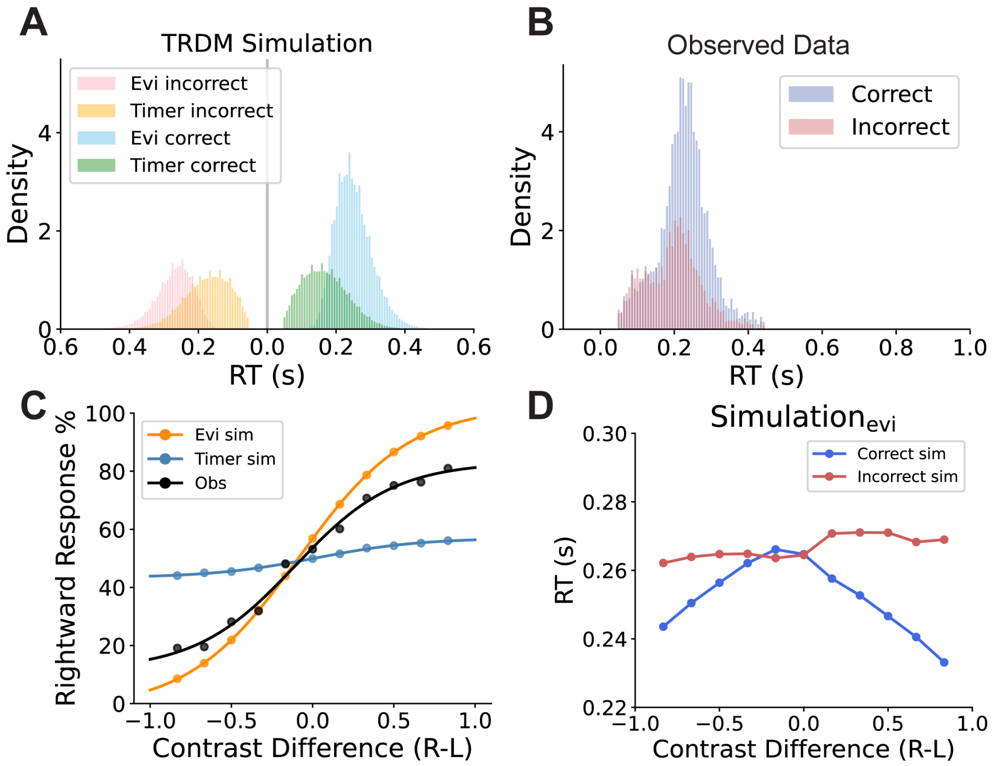

Figure 2.7: Decomposition of an example animal's simulated RT distribution by the TRDM.A The simulated RTs for one example animal (TS085) from the first group are divided into four groups: evidence accumulator generated RT for correct (blue) and incorrect (pink) responses, and time accumulator generated RT for correct (green) and incorrect (yellow) choices. Compared with the observed data (**B**), the plots show that the TRDM interprets the first peak (fast RT) in the RT distribution as generated by the time accumulator. **C** Simulated psychometric curves generated by the evidence accumulators and the time accumulator. **D** Evidence accumulator simulated RT as a function of contrast difference.

Chapter 3

Probabilistically Constrained Vector Summation of Motion Direction in The Mouse Superior Colliculus

This chapter has been published in eNeuro (Li et al., 2025). The work was conducted in collaboration with the contributions with the following coauthors: Victor J. DePiero, Hui Chen, Seiji Tanabe, and Jianhua Cang.

Author List Chuiwen Li[1], Victor J. DePiero[2], Hui Chen[2], Seiji Tanabe[1], Jianhua Cang[1,2,3]

Author Contact Correspondence and requests for materials should be addressed to Jianhua 'JC' Cang, at cang@virginia.edu

Author Affiliation 1. Department of Psychology, University of Virginia, Charlottesville, VA 22904, USA; 2. Department of Biology, University of Virginia, Charlottesville, VA 22904, USA; 3. Lead contact

Acknowledgements We thank Michele A. Basso, Elise L. Savier, Per B. Sederberg for discussions and comments on the manuscript. This work was supported by US NIH grants (EY026286 and EY020950) and Jefferson Scholars Foundation.

Author Contributions C.L., and J.C. designed the experiments; C.L. performed electrophysiology

and OKR and data analysis with assistance from H.C. and S.T.; V.J.P. performed 2-photon imaging and data analysis with assistance from H.C. and C.L.; C.L. and J.C. wrote the manuscript with input from all authors.

Declaration of interests The authors declare no competing interests.

3.1 Abstract

Visual motion is a crucial cue for the brain to track objects and take appropriate actions, enabling effective interactions with the environment. Here, we study how the superior colliculus (SC) integrates motion information using asymmetric plaids composed of drifting gratings of different directions and speeds. With both in vivo electrophysiology and two-photon calcium imaging, we find that mouse SC neurons integrate motion direction by performing vector summation of the component gratings. The computation is constrained probabilistically by the possible physical motions consistent with each grating. Excitatory and inhibitory SC neurons respond similarly to the plaid stimuli. Finally, the probabilistically constrained vector summation also guides optokinetic eye movements. Such a computation is fundamentally different from that in the visual cortex where motion integration follows the intersection of the constraints. Our studies thus demonstrate a novel neural computation in motion processing and raise intriguing questions regarding its neuronal implementation and functional significance.

3.2 Introduction

How the nervous system processes visual motion information in the environment is critical for the animal's survival, such as in capturing running prey and escaping from looming predators. Using simple stimuli such as bars, dots, and gratings, past studies have discovered that many neurons in the early visual system respond selectively to motion stimuli, especially to motion direction. In natural scenes, processing motion can be challenging because the signals are numerous and complex across the visual field. Proper integration of the motion signals is necessary for effectively interpreting visual stimuli and taking corresponding actions.

Researchers have used the so-called “plaids” to study motion integration, where two gratings of different orientations are superimposed and drifting along their respective axis. Perceptually, human subjects usually see such stimuli as a rigid plaid pattern with a coherent motion, instead of gratings sliding through each other, especially when two gratings are close in their contrasts and spatial frequencies (Adelson and Movshon, 1982). Physiological studies showed that plaids are represented in a hierarchical manner in the primate visual cortex, with V1 neurons first decomposing the plaids into grating components and the downstream area MT subsequently integrating V1 input to encode pattern motion (Movshon, 1985). Consistent with perception, the integration of motion direction of MT neurons was found to follow the intersection of constraints (IOC) (Khawaja et al., 2013; Wallisch and Movshon, 2019), where all the possible motions given a component grating’s motion form a constraint line (Figure 3.1A-C, green dashed lines), and the intersection of the constraints becomes the pattern motion of the plaid (Figure 3.1A-C, yellow arrows).

In addition to perception, which guides our understanding and interpretation of the world, motion processing is also important for “action” – the motor output that allows animals to interact with the environment (Goodale, 2011, 2014; Goodale and Wolf, 2009; Goodale and Milner, 1992; Milner and Goodale, 2008). The dynamic environment that is constantly changing requires an enormous amount of real-time processing that gets updated based on the relationship between the organism and its surroundings. The question is then whether visual processing for perception and action shares the same principle. On the one hand, consistent perception and action would be beneficial for a coordinated biological system. On the other hand, the two functions have different focuses, and a dissociation has been found between them (Dewar and Carey, 2006; Goodale et al., 1986; Schenk, 2006). Specifically, certain illusory visual stimuli were shown to only affect subjects’ perception but not their motor action in response to those stimuli (Aglioti et al., 1995; Zivotofsky, 2005; Platkiewicz and Hayward, 2014; Grandy and Westwood, 2006; Flanagan and Beltzner, 2000; Buckingham and Goodale, 2010; Ganel et al., 2008).

The superior colliculus (SC) is an evolutionarily conserved midbrain structure critical for ac-

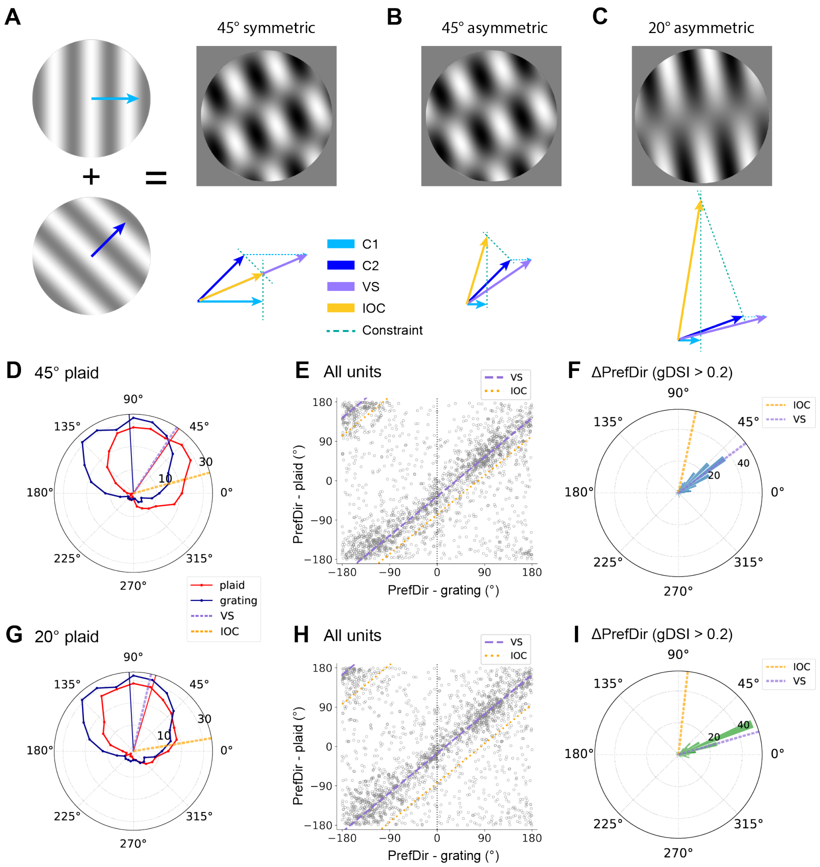

Figure 3.1: SC performs vector sum for 45° and 20° asymmetric plaids. (A) Schematic of a symmetric plaid with a 45° cross angle. The two component gratings (C1 and C2, light and dark blue respectively) have the same drifting speed (indicated by the length of the vector). Intersection of constraints (IOC, yellow arrow; intersection of the green dashed lines) and vector sum (VS, purple arrow) have the same direction. (B) Schematic of an asymmetric plaid with a 45° cross angle. C1 and C2 have a speed ratio of 1:4 and C2 is 45° counter-clockwise to C1. IOC predicts an integrated motion towards the yellow arrow (77.9° counter-clockwise to C1), while VS predicts an integrated motion towards the purple arrow (36.5° counter-clockwise to C1). (C) Same as (B) but the cross angle is 20°. The IOC direction is 83.6° counter-clockwise to C1. The VS direction is 16.0° counter-clockwise to C1. (D) An example neuron's tuning to drifting grating (dark blue curve, with preferred direction of 93.1°). Purple and yellow dashed lines are the VS and IOC prediction of the preferred direction to the 45° asymmetric plaid when the tuning curve is plotted in reference to C1's direction. This example neuron's tuning to 45° plaid follows VS (red curve, with preferred direction of 55.0°). (E) The preferred direction to grating (x axis) versus to 45° plaid (y axis) of all recorded clusters (n=1941, including both single- and multi-units). Purple and yellow dashed lines are the VS and IOC prediction. (F) Difference of the preferred direction between responses to grating and 45° plaid (grating - plaid) for highly selective clusters (gDSI > 0.2 for both grating and plaid responses). Purple and yellow dashed lines are the VS and IOC prediction. The distribution has a mean of 35.6° and a standard deviation of 42.6°. (G-I) same as (D-F), but for the 20° asymmetric plaid. The example neuron is the same as in (D). The mean of the distribution in panel (I) is 17.9° with a standard deviation of 40.7°. See also Figure 3.6

tion generation (Cang et al., 2024; Basso and May, 2017; Basso et al., 2021). The SC contains visual neurons that are motion direction selective across various mammalian species, and it plays important roles in guiding eye and head movements (Cang et al., 2024; Dorris et al., 1997; Munoz and Wurtz, 1995; Zahler et al., 2021), as well as innate behaviors such as orienting, escaping, and predatory hunting (Isa et al., 2020; Hoy et al., 2019; Yilmaz and Meister, 2013; Huang et al., 2021; Shang et al., 2019). Recently, direction selective neurons in the mouse SC were found to respond to the pattern motion rather than component motion of symmetric plaids (DePiero et al., 2024). However, this result is consistent with multiple interpretations. For example, other than IOC, vector sum (VS), which is simply the summation of two component motion vectors, predicts the same integrated direction (Figure 3.1A, purple arrow).

In the current study, we aim to investigate the rule of motion integration in the SC by studying its response to asymmetric plaids with unequal component motion strength (e.g. Figure 3.1B, right panel). The IOC and VS lead to contrasting predictions when asymmetric plaids are used, thus providing an opportunity to test which computation the SC performs. Surprisingly, we find a clear VS representation in the mouse SC, which is strikingly different from the integration rule in the primate visual cortex. Interestingly, the VS computation in the SC is constrained probabilistically by the possible physical motions consistent with each individual grating. Further, we show that the excitatory and inhibitory SC neurons respond similarly to the plaid stimuli. Finally, by examining optokinetic reflex (OKR), a behavior guided by subcortical circuits, we show that the optokinetic eye movement follows the probabilistically constrained VS computation in response to asymmetric plaids. Therefore, this computation is likely a general principle of motion integration that is shared across visual action pathways.

3.3 Results

3.3.1 SC neurons perform vector sum in response to asymmetric plaids

We recorded visual responses from the superficial layers of the SC in awake mice (n=8) with 64-channel silicon microprobes. Many neurons showed direction selective responses to single drifting gratings (e.g. Figure 3.6), as previously reported (DePiero et al., 2024; Cang et al., 2018; Wang et al., 2010; Inayat et al., 2015). To investigate how SC neurons integrate visual motion, we studied their responses to asymmetric plaids. We set the speed of the two component gratings (C1 and C2) to be 6.25 and 25 deg/s, respectively (i.e., ratio of 1:4), and displayed the tuning curves relative to the direction of C1. When C1 and C2 have a cross angle of 45°, their vector sum is 36.5° away from C1's direction (counter-clockwise in Figure 3.1B), whereas the IOC direction is 77.9° from C1 (Figure 3.1B). For the example neuron, which prefers direction of 93.1° to gratings (Figure S1 and 3.1D, dark blue trace), it would prefer 56.6° (i.e., 93.1°-36.5°) direction in response to the 45° cross angle asymmetric plaid if it follows the VS rule to integrate plaid motion; and 15.2° (i.e., 93.1°-77.9°) if it follows the IOC rule. Amazingly, this neuron's preferred direction to the 45° plaid became 55.0°, almost perfectly aligned to the VS (Figure 3.6 and 3.1D, red trace). The same finding was seen at the population level, including both single units and multi-unit clusters (Figure 3.1E). We then calculated the difference between the preferred direction to gratings and plaids for all the highly direction selective units (gDSI > 0.2). The distribution (mean = 35.6°, std = 42.6°, n = 185, Figure 3.1F) centered at the VS prediction (i.e., 36.5°), instead of IOC (i.e., 77.9°).

We next used asymmetric plaid with a 20° cross angle, where VS prediction would have a shift of 16.0° and IOC a shift of 83.6° (Figure 3.1C). The VS and IOC predictions are more separated for the 20° plaid than for 45° plaid, providing an even clearer test of how SC neurons integrate motion. The example neuron was tuned to the VS direction of the 20° plaid rather than IOC (Figure 3.1G, a shift of preference from 93.1° to 73.5°, i.e., a 19.6° difference), and the same observation was seen at the population level (Figure 3.1H). The distribution of preferred direction difference for gratings and plaids for highly selective units was again found to be centered at the VS prediction

(Figure 3.1I, mean = 17.9°, std = 40.7°, n = 174). These results thus demonstrate that SC neurons perform VS computation, rather than IOC, in response to the asymmetric plaids with 20° and 45° cross angles.

3.3.2 SC neurons represent motion direction as joint probability function in response to asymmetric plaids

The plaids with 20° and 45° cross angles fall into the category of "type II" plaids, where both component directions are at the same side of the IOC direction. We next expanded the cross angle to 135°, which no longer meets the "type II" definition, but still has different VS (shift of 122.9°) and IOC (shift of 81.5°) predictions (Figure 2A). The spatial pattern of a 135° plaid is a mirrored version of 45° plaid (see stimulus video in Supplemental Information). Surprisingly, in response to the 135° plaid, the same example neuron preferred a direction closer to the IOC prediction than VS (Figure 2B, a shift of preferred direction from 93.1° to 359.8°, i.e., a 93.3° difference). This was also true for the population data (Figure 2C). For highly direction selective units, the distribution of preferred direction difference between grating and plaids was centered near the IOC prediction (mean = 86.7°, std = 53.1°, n = 132) and showed a wider spread than the distribution for 20° and 45° plaids (Figure 2D).

To understand this puzzling result, we note an important difference between 135° plaid and the other plaids we tested: the VS direction of 135° plaids exceeds the ±90° range of C1 direction (Figure 3.2A & E). The ±90° range is critical because it is the limit of possible directions of 1-dimensional motion stimuli such as drifting gratings. In other words, a grating drifting along its perpendicular direction could have a "true" motion direction anywhere within the ±90° range, but not beyond, because any motion parallel to the grating is invisible when shown in a limited patch (Figure 3.2E, yellow shade and grey arrows).

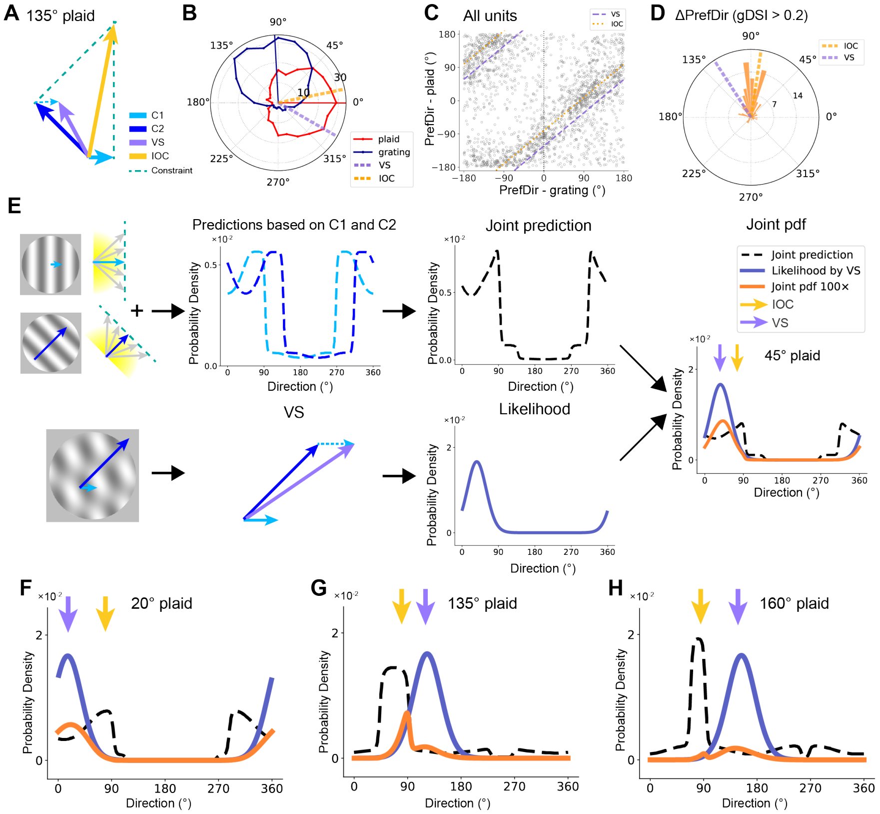

Figure 3.2: SC response deviates from VS for 135° plaids and can be explained by a probabilistically constrained vector sum computation. (A) Schematic of the 135° asymmetric plaid. IOC predicts an integrated motion towards the yellow arrow (81.5° counter-clockwise to C1), while VS predicts an integrated motion towards the purple arrow (122.9° counter-clockwise to C1). (B) The tuning curve of the same example neuron as in Figure 3.1D&G to grating (dark blue curve) and the 135° plaid (red curve). Purple and yellow dashed lines are the VS and IOC predictions, respectively. The neuron's preferred direction to the plaid (359.8°) is closer to IOC than to VS. (C) The preferred direction to grating versus to 135° plaid of all recorded clusters (n=1941). Purple and yellow dashed lines are the VS and IOC predictions, respectively. (D) Difference of the preferred direction between responses to grating and 135° plaid for highly selective clusters (gDSI ¿ 0.2). The distribution has a mean of 86.7° and standard deviation of 53.1°. (E) Top, given the motion of a single grating, the possible true motion lies within its ±90° range (yellow shades). Grey arrows indicate some example motion vectors that are compatible with the grating. The possible true motion of each grating is modeled as a probability density function (pdf) as illustrated by the light and dark blue dashed lines, respectively. The normalized product of the two functions is the joint prediction function (black dashed line). Bottom, vector summation (VS) is modeled with a likelihood distribution (von Mises function) centered at the VS direction (purple line). Multiplication of the joint prediction and the likelihood function returns the final joint probability function (orange). Purple and yellow arrows are the VS and IOC predicted motion direction for the 45° plaid.

(F) Same as the joint probability density function as in (E) but for 20° plaid. (G) Same as (F) but for 135° plaid. In contrast to the 45° and 20° plaids, the peak of the likelihood distribution (purple curve) for the 135° plaid falls near the prediction decay region (cliff of the black dashed line). The VS peak is attenuated after multiplication with the prediction distribution, resulting in a joint pdf peak away from VS but closer to IOC (orange curve, peak closer to the yellow arrow than purple). (H) Same as (F) but the prediction of SC response for 160° plaid. The likelihood (purple curve) of 160° plaid falls completely out of the prediction transition region. The resulting joint pdf (orange) maintains its peak at the VS direction (purple arrow). Due to the multiplication with low prediction values, the likelihood turns into a joint pdf distribution with a much lower amplitude. See also Figure 3.7

Given this property of 1-dimensional motion stimuli, we hypothesized the following computational process. When integrating two gratings of a plaid, the ±90° constraints from each component are also combined, thus forming a joint prediction of the shared motion direction in the form of a probability distribution (Figure 3.2E-H, “joint prediction”, see Methods for detailed explanation for the shape of the curve). At the same time, vector summation of the two components results in a likelihood distribution centered at the VS direction (Figure 3.2E-H, “likelihood by VS”). The joint prediction and likelihood distribution are then multiplied to achieve an unnormalized joint probability density distribution of the stimulus direction (Figure 3.2E-H, “joint pdf”). We propose that SC neurons’ direction tuning in response to plaids are generated following a stochastic process, probabilistically sampling from this joint pdf distribution. When the cross angles are smaller than 90°, the multiplication only has a scaling effect on the direction representation (Figure 3.2E-F & 3.7B). For the 135° plaid, however, the peak of the likelihood falls outside of the range of high prediction probability (Figure 3.2G & 3.7C). The peak is hence attenuated, while the likelihood within the high prediction region is amplified, resulting in the joint pdf peak away from the VS and closer to the IOC.

Such a multiplicative operation of pdfs makes a specific prediction: if the cross angle is expanded further, to 160° for example, where the likelihood by VS falls in the low but flat prediction region, the SC responses would again become closer to the VS prediction, but weaker in strength (Figure 3.2H & 3.7D). We tested this prediction by investigating SC responses to 160° plaids, where VS predicts a shift of 153.6° and IOC predicts a shift of 86.0°. Indeed, in response to these plaids, the direction representation was closer to the VS than IOC (Figure 3.3A-D, example neuron tuning shifted 147.0°; Figure 3.3D: mean = 139.7°, std = 71.3°, n = 110). We next compared responses of the same units that were highly selective across all 4 plaid conditions. Their response shifted from VS for 20° and 45° plaids, to IOC-like for 135° plaids, then back to VS for 160° plaids (Figure 3.3E). Remarkably, as predicted by the joint pdf, fewer units showed highly selective response for plaids with larger cross angles (n = 174, 185, 132, and 110, for 20°, 45°, 135°, 160° plaids, gDSI $>$ 0.2). Consistently, the direction selectivity across population also became weaker with increasing cross angles (Figure 3.3F, n = 261, gDSI $>$ 0.2 to gratings). Moreover, the preferred direction estimated from each repeat of stimuli showed a higher variability for plaids with larger cross angles (Figure 3.3G), also consistent with the probabilistically constrained vector sum model.

3.3.3 Excitatory and inhibitory SC neurons respond similarly to asymmetric plaids

We next performed 2-photon calcium imaging to target direction selective neurons that are enriched in the superficial SC (Inayat et al., 2015; Barchini et al., 2018), which also allowed us to study specific neuron types (Figure 3.4A-B). First, we injected AAV to express GCaMP6s in both excitatory and inhibitory neurons in similar locations as in the electrophysiological recording experiments (n=3 mice). Overlaying cortical tissues were removed to expose the SC surface for imaging (DePiero et al., 2024). In response to the same 4 types of plaid stimuli, the imaged neurons shifted their direction preference exactly like what was observed with electrophysiology – VS for 20°, 45°, and 160° plaids and closer to IOC for 135° plaid (Figure 3.4C-D). The same results held true for neurons that were highly selective across all 4 plaid conditions (n = 191, Figure 3.4E).

Next, we injected AAV to express Cre-dependent GCaMP6s in Vgat-Cre mice, resulting in GCaMP6s expression only in inhibitory neurons (n=3 mice). A VS representation was again observed for 20°, 45°, and 160° plaids, whereas IOC-like representation was seen for 135° plaids, suggesting that inhibitory and excitatory neurons respond similarly to these plaids (Figure 3.4F).

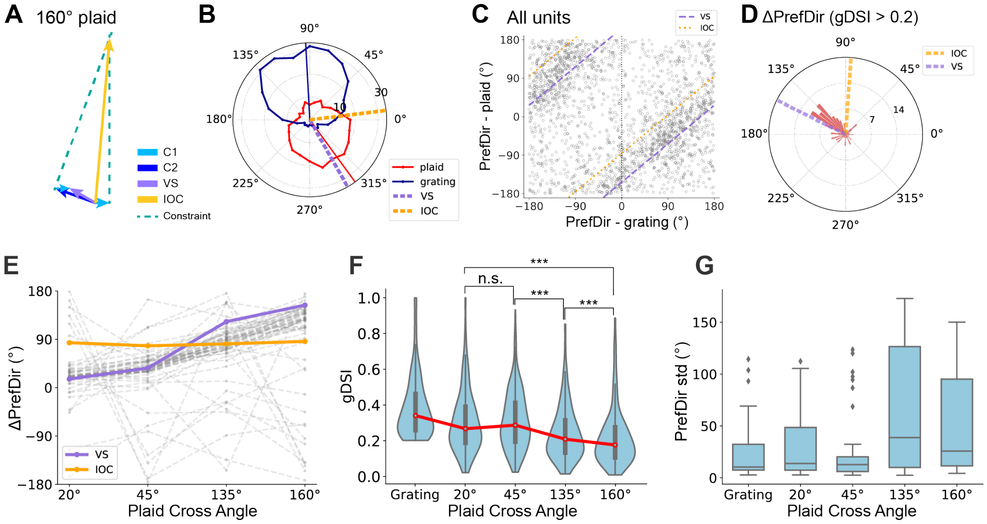

Figure 3.3: SC performs probabilistically constrained vector sum to represent the direction of asymmetric plaids. (A) Schematic of the 160° asymmetric plaid. IOC predicts an integrated motion towards the yellow arrow (86.0° counter-clockwise to C1), while VS predicts towards the purple arrow (153.6° counter-clockwise to C1). (B) The tuning curve of the same example neuron as in Figure 3.1D&G & Figure 3.2B to grating (dark blue curve) and the 160° plaid (red curve). The neuron's preferred direction to the 160° plaid (306.1°) is closer to VS (purple dashed line) than to IOC (yellow dashed lines). (C) The preferred direction to the grating versus to 160° plaid of all recorded clusters (n=1941). Purple and yellow dashed lines are the VS and IOC prediction. (D) Difference of the preferred direction between responses to the grating and 160° plaid for highly selective clusters (gDSI ¿ 0.2). Purple and yellow dashed lines are the VS and IOC prediction. The distribution has a mean of 139.7° and standard deviation of 71.3°. (E) Difference of the preferred direction between responses to the grating and plaids for clusters that are highly selective (gDSI ¿ 0.2) for all 4 plaid conditions (n=61). Gray dashed lines connect responses of individual units. Purple and yellow lines are the VS and IOC prediction. (F) The gDSI of clusters that are highly direction selective (gDSI $>$ 0.2) to grating (n = 261) under all 5 stimulus conditions. (Friedman test, p ¡ 0.001. Post-hoc Wilcoxon tests are performed between adjacent plaid conditions, p = 0.76 for 20° and 45° plaids, p ¡ 0.001 for 45° and 135° plaids and for 135° and 160° plaids). The connected points represent median. The thick vertical bars within each column represent the range from the first to the third quartiles. The whiskers represent the data range excluding the outliers. (G) The standard deviation of the preferred direction estimation across 10 stimulus repeats for individual neurons. In response to the 20° (std median = 13.80°) and 45° (std median = 12.81°) plaids, the preferred direction estimate are comparably reliable as to gratings (std median = 10.49°). For plaids with larger cross angles, the variability increases (std median = 38.86° for 135° plaid; std median = 25.77° for 160° plaid). The horizontal lines in each box represent median. The boxes represent the range from the first to the third quartiles. The whiskers represent the data range excluding the outliers. The diamond points are outliers.

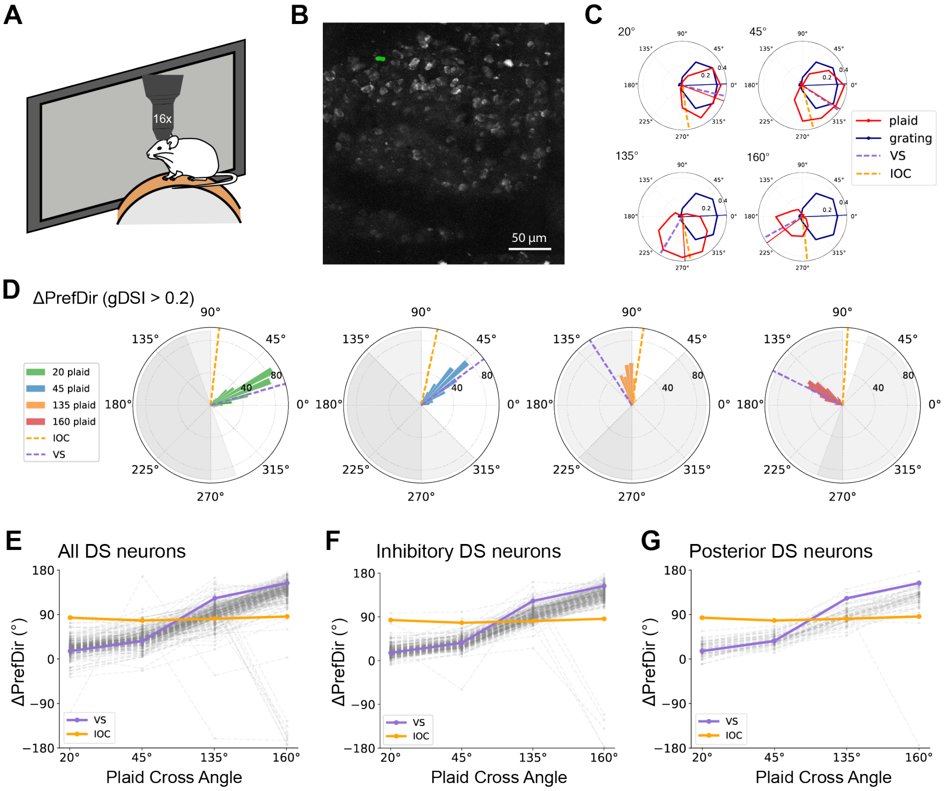

Figure 3.4: Excitatory and inhibitory SC neurons respond similarly to asymmetric plaids. (A) Schematic of two-photon imaging experiment. Head fixed mice were allowed to freely run on a wheel while passively viewing the visual stimulus. (B) An example field of view imaged from the anterior SC. Both excitatory and inhibitory neurons were included. Green marks an example neuron. (C) The example neuron's tuning curve to grating and plaids of 4 different cross angles. This neuron's preferred direction was 2.2° for grating; and 339.7°, 327.9°, 273.6°, and 216.2° for 20°, 45°, 135°, and 160° plaids, respectively (i.e., a shift of 22.5°, 34.3°, 88.6°, and 146.0°). (D) Distributions of the difference between preferred directions of responses to the grating and plaids for all direction selective (DS, gDSI > 0.2) neurons imaged from the anterior SC. (E) The preferred direction difference between responses to the grating and plaids for all direction selective neurons imaged from the anterior SC (gDSI > 0.2). Gray dashed lines connect individual neurons. Purple and yellow solid lines are VS and IOC predictions respectively. (F) Same as (E), but for inhibitory neurons only. (G) Same as (E), but for DS neurons imaged from the posterior SC. See also Figure 3.8

Finally, to determine if this newly discovered response property displayed any regional specificity, we imaged the posterior and medial corner of the SC that has receptive fields more lateral and dorsal in visual field (n=2 mice). Notably, no tissue was lesioned in this experiment, leaving cortical input intact (Savier et al., 2019). The same response pattern to plaids was also observed for direction selective neurons in this region of the SC (Figure 3.4G). Additionally, in all three sets of imaging experiments, the direction selectivity showed a decreasing trend with larger cross angles of plaids (Figure 3.8), which further confirmed the findings obtained with electrophysiology (Figure 3.3F).

Together, the robustness of our findings, seen with both physiology and imaging and across SC regions and cell types, indicates that the probabilistically constrained vector summation is a fundamental computation performed by the mouse SC when integrating motion information.

3.3.4 Probabilistically constrained VS computation guides optokinetic eye movement

Our results demonstrate that the motion integration principle in the SC is strikingly different from that in the cortical pathway. Given the SC's role in reflexive behavior and controlling eye movements, we tested whether there is any behavioral relevance of the subcortical VS representation of motion direction. We turned to optokinetic reflex (OKR). OKR is an important subcortical reflexive behavior where the eye movements follow the stimulus involuntarily and presumably helps stabilize images on the retina. Although the SC is not directly involved in generating the slow and smooth movement in OKR37, we aimed to test whether the VS computation is utilized in this subcortical behavior, without implicating a driving role of the SC.

Full-field drifting gratings (9.375 deg/s with spatial frequency of 0.16 cyc/deg and temporal frequency of 1.5 Hz) and plaids (approximately 8 deg/s in VS direction, see STAR Methods) were shown on a 3-screen setup surrounding the animal (n=7, Figure 3.5A). We recorded the right eye through the reflection by a dichroic mirror and measured the speed of its movement along the horizontal axis. As expected, horizontally drifting gratings elicited the largest horizontal OKR response (Figure 3.5B, top panel), with 0° grating (drifting leftward) and 180° grating (rightward) evoking eye movements in the corresponding directions (quantified as negative and positive OKR gain, respectively).

We then investigated OKR in response to asymmetric plaids of the 4 cross angles tested in physiological and imaging experiments. If OKR follows the VS direction of the plaid, the stimulus that evokes the largest rightward eye movements (i.e. the peak of the tuning curve) would shift from near-180° to the VS prediction line (Figure 3.5B, purple dashed lines); whereas if it follows the IOC direction of the plaid, the peak would shift to the IOC prediction line (Figure 3.4B, yellow dashed lines). Remarkably, the OKR was closer to the VS prediction for 20°, 45° and 160° plaids, but to the IOC prediction for 135° plaid (Figure 3.5B & C), just like the SC responses. In addition, the strength of OKR responses (OKR gain) became weaker for the 135° and 160° plaids (Figure 3.5D), consistent with the finding at the neuronal level (Figure 3.3F & 3.8B, D, & F). These results thus suggest that the probabilistically constrained vector summation is an essential motion processing computation used in the mouse brain to guide behavior.

3.4 Discussion

In this study, we found that neurons in the mouse SC integrate plaid motion by computing the vector sum of the component gratings. This representation is probabilistically constrained by predictions based on individual components of the plaid. These findings reveal a novel computation of motion transformation that is fundamentally different from what has been found in the primate cortical pathway, where a computation that generates IOC-like results is the dominant principle (Khawaja et al., 2013; Wallisch and Movshon, 2019).

Plaids have been used to study motion integration along visual pathways. Perceptually, plaids are coherently moving "blobs". On the neuronal level, studies have found V1 represents moving plaids as a linear summation of two gratings (i.e., responding to individual components), while the downstream MT area represents plaids as single patterns in motion (Movshon, 1985). In other

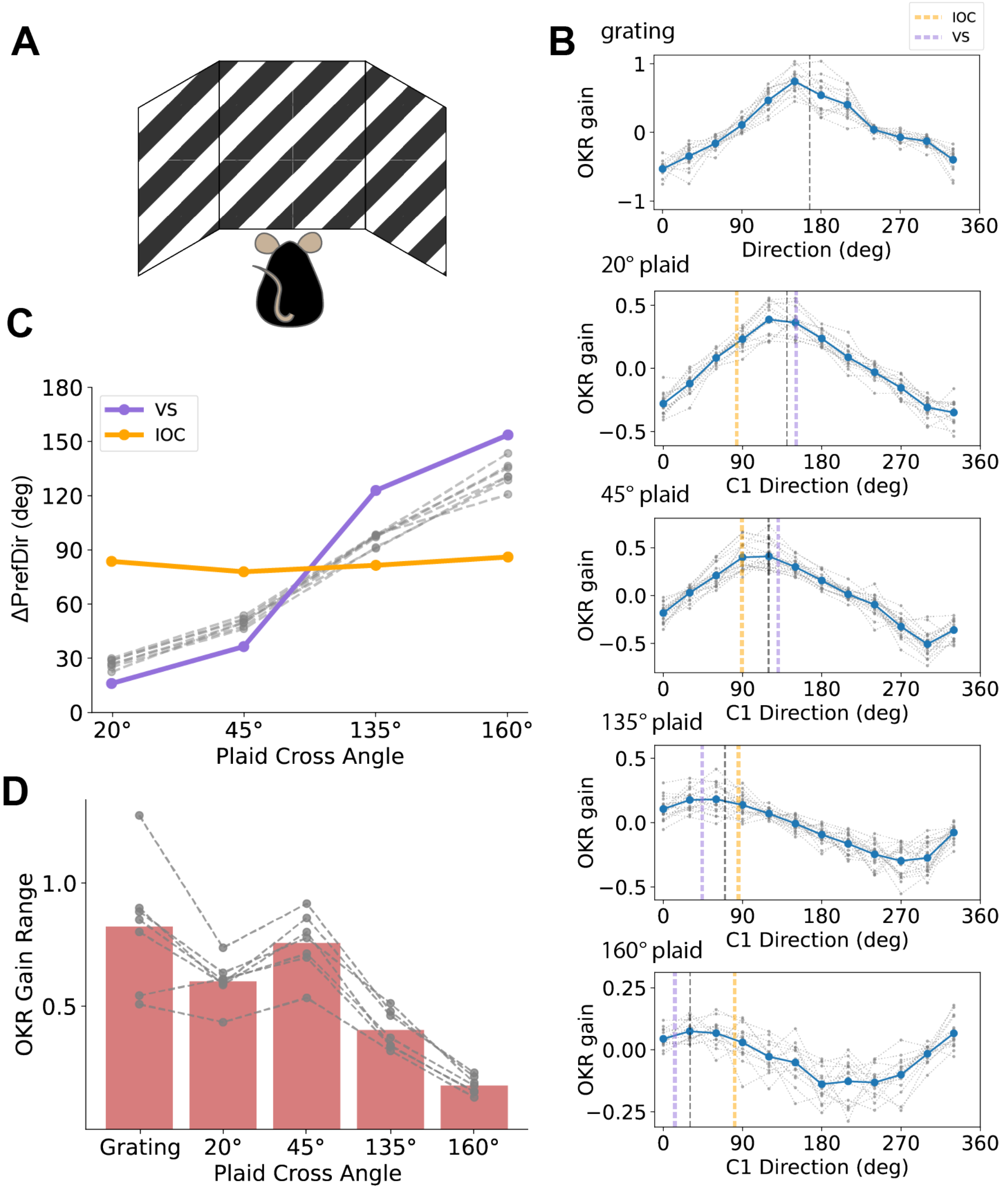

Figure 3.5: Probabilistically constrained VS computation guides optokinetic eye movement. (A) A schematic of the full field stimulus delivered by a 3-screen setup. (B) Optokinetic response (OKR) to grating and all 4 plaids of an example mouse. The x axis is the grating direction (top panels) or component 1 direction in plaids. Gray dashed lines are individual repeats (15 total for each condition) of the stimulus. Yellow and purple dashed lines in the plaid panels are IOC and VS prediction based on the OKR tuning to grating.(C) The difference between preferred directions to grating and plaids for all animals (n = 7). Gray dashed lines connect data from individual animals. Purple and yellow solid lines are VS and IOC predictions, respectively. (D) The OKR gain range, calculated as the difference of maximum and minimum OKR gain, for grating and all 4 plaid conditions.

words, the MT signals resemble more of the perceptual end product. Moreover, using unikinetic plaids (a type of asymmetric plaids with one of the components being static), researchers found that the motion represented by MT neurons followed the IOC direction (Khawaja et al., 2013; Wallisch and Movshon, 2019), which is also consistent with perception (Adelson and Movshon, 1982; Movshon, 1985; Kreyenmeier et al., 2024; Barthélemy et al., 2010; Pattadkal et al., 2023). Interestingly, behavioral responses along the VS direction have also been reported in response to certain asymmetric plaids in humans and nonhuman primates, which was sometimes characterized as “misperception”39,41–45. For example, in a direction matching task where human subjects reported the plaid direction with a pointer, the perceived direction was found to depend on the duration of the asymmetric plaids (Yo and Wilson, 1992a). A response along the VS direction was more likely to happen if the plaids were presented for a short duration (60 ms). With longer durations, the perception (measured by direction matching or eye tracking) were found to change from the VS back to IOC (Barthélemy et al., 2010; Yo and Wilson, 1992b; Masson et al., 2000). In addition, it was found that pigeons followed the VS direction when performing a direction discrimination task in response to asymmetric plaids, measured by pecking between two choices (Hataji et al., 2020). Here we show, for the first time, a VS computation at the neuronal level in response to asymmetric plaids. The VS responses of SC direction selective neurons may be the neural basis underlying the VS guided behavioral responses in the direction discrimination tasks. The potential role of the SC in such perceptual responses is supported by its short response latency (Yu et al., 2024; Boehnke and Munoz, 2008) and involvement in many cognitive functions (Basso and May, 2017; Basso et al., 2021; Jun et al., 2021; Stine et al., 2023; Peysakhovich et al., 2024).

Importantly, our data further demonstrate that not only does the SC represent the VS direction of plaid patterns, but also the optokinetic eye movement follows the VS direction. Together, these suggest that VS may be a behaviorally relevant computational principle shared across multiple subcortical areas, and it may be used for tasks that are fundamental to these areas. The SC is known for its role in driving actions like head and eye movements across species (Cang et al., 2024; Dorris et al., 1997; Munoz and Wurtz, 1995; Zahler et al., 2021). When presented with two possible visual targets, eye movements typically follow a vector average of the stimuli, before the winner-take-all selection of a single target (Becker and Jürgens, 1979; Coren and Hoenig, 1972; Ottes et al., 1984; Findlay, 1982; Coëffé and O'regan, 1987; Chou et al., 1999). The SC was shown to contribute to both phases of eye movements (Vokoun et al., 2014; Nummela and Krauzlis, 2011; Glimcher and Sparks, 1993; van Opstal and van Gisbergen, 1990; Edelman and Keller, 1998). This vector averaging, which is a form of weighted VS, shares a very similar computation as VS, and it is beneficial for bringing the subject's view to the most information-dense area in the visual space. In addition, recent studies in monkeys and mice indicate that the SC is also involved in spatial attention (Zénon and Krauzlis, 2012; Wang et al., 2022). Together with its role in driving eye and head movements, the SC must compute signals to guide fast orienting behaviors to maximize information gain. This process is closely related to action generation rather than visual perception; thus it requires a high speed but can tolerate a low precision, which may benefit from a simple operation like VS. Interestingly, previous studies in humans showed that unikinetic plaids elicited ocular following (the open-loop phase of OKR in primates), with the direction shifting from component direction (the same as VS direction in this case) in ultra-short latency to the 2D pattern direction (consistent with IOC direction) later in time (Masson and Castet, 2002). Another study compared human closed-loop phase OKR with that of cats in response to plaids, and showed that both species follow a direction between the component and pattern directions, but human OKR is biased toward the pattern direction while cat OKR is biased toward the component direction (Harris et al., 1993). In the current study, we found that mouse OKR is also not perfectly VS, but deviates slightly towards the IOC direction. These results thus suggest that OKR is likely mediated by the competing signals of component (likely a VS) and pattern representations. The relative contribution of the two signals varies on a spectrum across species. OKR is largely controlled by subcortical circuits for afoveate animals, while the control shifts to the cortex in foveate animals (Harris et al., 1993; Cahill and Nathans, 2008; Ambrad Giovannetti and Rancz, 2024). Thus, the position of each species on such component-pattern spectrum might be determined by the subcortical-cortical balance involved in the behavior.

In this study, we also show that the VS computation in the SC is under an additional constraint. VS by itself is a straightforward linear operation that does not depend on any assumptions or constraints. Yet, the constraint as illustrated in our model (joint prediction, Figure 3.2 & 3.7) relies on two assumptions that are closely related to IOC and the perception of object motion. First, to generate the predictions based on individual gratings (Figure 3.2E, yellow shades and "predictions"), an underlying assumption must be met, which is that a 1D grating pattern is a part of a larger moving pattern viewed through an aperture. Without additional information, the computation does not reject other possible motion directions that are compatible with this 1D moving pattern. On top of that, the combination of the two predictions from component gratings (i.e. the joint prediction) indicates a second assumption, which is that the two gratings come from the same rigid, coherently moving pattern. Only under this assumption does it matter to search for a shared motion that is compatible with both constraints. These two assumptions are the same ones behind IOC, which are also consistent with the perception of plaids. These assumptions suggest an existing knowledge ("prior" in the Bayesian framework) about motion information in the brain. More specifically, the underlying neural network must have mechanisms to deal with the information ambiguity caused by spatially limited receptive fields. Further, the network seems to prioritize processing visual information superimposed spatially as coming from the same entity with locally rigid motion, rather than independent transparent motion.

What neuronal mechanism can give rise to this newly discovered computation in the SC? We recently showed that mouse SC neurons display pattern motion selective responses to symmetric plaids and such responses can arise from a nonlinear transformation of converging retinal inputs, which are more diverse in their pattern versus component motion selectivity (DePiero et al., 2024). How retinal ganglion cells respond to asymmetric plaids as we used here needs to be studied. A VS computation, and maybe even the constraint, may already exist in the retina, which is then further transformed in the retinocollicular convergence. Additionally, or alternatively, local circuits in the SC may perform VS computation or direction-specific constraint through weighted connections among cells with different preferred directions. For example, to represent the probable and improbable motions given a single grating, direction selective neurons may form stronger excitatory connections with similarly tuned neurons, and weak excitatory connections (and/or stronger inhibitory connections) with oppositely tuned neurons. It should be noted that the constraint representation should only depend on the stimulus direction, not the motion speed, while VS computation needs to take the speed into account. Consequently, to implement this computation may require the multiplication of two separate streams of stimulus representation. Future studies are needed to understand the underlying circuitry for plaid motion integration in the SC.

Finally, we did not test how changes of other stimulus parameters, such as spatial frequency and contrast, could influence the neural and behavioral response, and whether the influence could be explained by the model. In addition, we focused on predicting the direction selective responses of SC neurons, without considering their tuning to speeds. Thus, our model cannot distinguish vector sum and vector average, since they predict the exact same direction. Further studies to address this issue will benefit especially from studying neuron populations that have well-characterized speed tuning function. It is important to note that vector average and vector sum are not mutually exclusive, as vector average is a special form of weighted vector sum. A generalized investigation to measure the weights of VS will be ideal in the future.

3.5 Methods

3.5.1 Experimental Model and Study Participant Details

We used 8 adult wild type C57BL/6 mice for electrophysiology recording of SC visual responses (female=4, male=4, 4-7 months old. The Jackson Laboratory, RRIC, IMSR_JAX:000664). For two-photon calcium imaging, 8 adult Vgat-Cre mice (all male, 5-7 months old. The Jackson Laboratory, stock #028862, RRID, IMSR_JAX:028862) were used. For OKR behavior test, 7 adult C57BL/6 mice (female=5, male=2, 3-4 months old for 3 females and all males, 9 months old for 2 females. The Jackson Laboratory, RRIC, IMSR_JAX:000664) were used. All experimental procedures in this and following sections were approved by the University of Virginia Institutional

Animal Care and Use Committee and in conformance with the National Institutes of Health Guide for the Care and Use of Laboratory Animals and the Public Health Service Policy.

3.5.2 Method Details

Electrophysiology

Animals were first prepared for head plate implantation and craniotomy. A 2mm diameter cranial window was made 1mm lateral (right side) and 0.5mm anterior to the lambda point. We used 2.5% agarose and Kwik-Cast sealant to cover and seal the craniotomy. A titanium head plate was cemented with C&B Metabond onto the skull. Isoflurane was used for anesthesia during the surgery (2-3%), and carprofen (5mg/kg) was given as analgesic. Eye ointment was applied to the eyes for protection during surgery.

1-4 days after the surgery, electrical signals from the SC of head-fixed awake mice were recorded using 64 channel silicon microprobes (Yang et al., 2020) via a multichannel amplifier from Intan Technologies at 20 kHz. The mice were allowed to freely run on a cylindrical wheel. The receptive field location of each recording session was estimated using flashing dark squares ($5^\circ \times 5^\circ$) across the screen. The grating and plaid stimuli were then centered on the approximate receptive field location. Spikes were bandpass filtered with 300–6000 Hz range. Spike waveforms were sorted offline into single- and multi-units using MountainSort (Chung et al., 2017).

Visual stimuli were generated by customized script in MATLAB based on Psychtoolbox-3 and shown on an LCD monitor (59.7 × 33.6 cm, 60 Hz refresh rate, gamma corrected). Gratings and plaids (100% contrast) were shown within a circular patch (diameter = 40°) against a grey background. The screen was placed 25 cm away from the eye contralateral to the recording site. The grating had 0.08 cpd spatial frequency (SF) and 2 Hz temporal frequency (TF), thus resulting in a speed of 25 deg/s. We used 24 directions evenly spaced from 0° to 345° with a 15° increment. The 0° direction represents leftward motion of vertically oriented grating. For plaid, both grating components had a SF of 0.08 cpd. Component 1 (C1) was always the slower component with a TF of 0.5 Hz (speed of 6.25 deg/sec), while component 2 (C2)'s TF was 2 Hz (25 deg/s). We varied

C1's direction across 24 directions evenly spaced from 0° to 345°. C2 direction was always C1 direction plus cross angle. Four different cross angles were tested: 20°, 45°, 135°, and 160°. The stimulus was presented for 2s with a 0.5s inter-stimulus grey screen. Each condition was repeated 10 times in a pseudorandom order. Movies of the example visual stimuli are provided in Video S1.

Two-photon Calcium Imaging

The surgical and imaging procedures were as described in the previous studies (DePiero et al., 2024; Savier et al., 2019). To image the anterior portion of the SC, a 3.2 mm craniotomy was made on the left hemisphere centered 1.5-2 mm lateral and anterior to the lambda point. The cortex above the SC was aspirated to expose the SC. To image the posterior SC, a 2.5 mm craniotomy was centered over the lambda point. The dura over the colliculus was cut with a sharp needle (30 gauge) to expose the SC surface without lesioning the cortex or the overlaying blood vessels. $\sim$50 nL of AAV solution was pressure injected via a glass pipette fitted to an injector (Drummond Scientific Nanoject II) at 500 μm and 250 μm below the pia surface of SC.

AAV1-hsyn-GCaMP6s (Addgene #10084372) was injected for imaging all neurons (i.e. excitatory and inhibitory; n=2 mice for anterior SC and n=2 for posterior SC). In another mouse, AAV.PHP.eB-hsyn-RiboL1-jGCaMP8s (gift from Kristian Lensjø Lab (Grødem et al., 2023)) was used for imaging the anterior SC. No significant difference was seen in direction selectivity between using the two viruses (Mann-Whitney U test, Z = -1.19, p = 0.23 for grating; Z = -1.16, p = 0.24 for 20° plaids; Z = 0.86, p = 0.39 for 45° plaids; Z = 0.41, p = 0.68 for 135° plaids; Z = -0.89, p = 0.37 for 160° plaids). We thus combined them in further analysis (i.e. n=3 for recording all neurons from the anterior SC). For imaging specifically the inhibitory neurons in the anterior SC, AAV9-hsyn-Flex-GCAMP6s (Addgene #10084572) was injected (n=3).

Mice were imaged 15-21 days post-surgery with a two-photon scanning microscope (Ultima Investigator or Ultima 2Pplus, Bruker Nano Surface Division) with a Ti:sapphire laser (Chameleon Discovery with TPC, Coherent) tuned to a wavelength of 920 nm through a 16×, 0.8 NA Nikon objective. Imaging data were acquired at 30Hz rate with the PrairieView software 5.4 with a resonant scanner at 2.25× optical zoom, resulting in a 412.2 × 412.2 μm field of view (at 512 × 512 pixel resolution). Images averaged over 4 frames were then used for later analysis.

Regions of interest (ROIs) were manually drawn on the motion-corrected average image of a population of neurons over the collected time-series. The raw Ca2+ signal of each ROI was calculated by averaging all pixels within that ROI in each frame. Neuronal response was calculated as $\Delta F/F_0 = (F - F_0)/F_0$, where F0 was the mean of the baseline signal over 0.8s period before stimulus onset, and F was the average fluorescence signal over the 2s stimulus presentation. The mean value of $\Delta F/F_0$ for each stimulus condition was then used for subsequent data analysis for all the neurons.

The visual stimulus used for imaging was similar as in electrophysiology, except for a longer inter-stimulus interval of 3s due to the slow Ca2+ dynamics. In addition, 12 directions (0-330º with 30º spacing) were used for each type of stimulus and each condition was repeated 5 times in a pseudorandom order.

Optokinetic reflex (OKR)

Mice were first implanted with titanium head plates cemented with C&B Metabond onto the skull. Isoflurane was used for anesthesia, and carprofen was given as analgesic. Each animal was head-fixed during the OKR test and allowed to run freely on a wheel.

Three computer screens (52.1 × 29.2 cm for each) were aligned vertically in portrait mode surrounding the animal. The angle between two neighboring screens was ∼120°. The distance between the eyes of the animal and the center of the screens was 25 cm. We recorded the mice in the dark with an infrared light source. A dichroic mirror was placed in front of the right eye, and a video camera captured the eye from the back of the animal through the reflection in the mirror, thus minimizing visual occlusion. The camera was model FL3-U3-13Y3M-C (FLIR), combined with an Edmund VZM 200i zoom imaging lens. Videos were recorded at 60Hz rate. We used Facemap (Syeda et al., 2024) to track the pupil location with the centroids coordinates. Only horizontal coordinates were used in our analysis to avoid the issue of direction-dependent gain difference in OKR behavior. Saccade-like eye movements were detected by their rapid speed and replaced by linear interpolation so that only slow eye movements were used to quantify OKR (Liu et al., 2023a). We represented eye movements towards the left of the animal as negative speed, and rightward movements as positive.

Full field drifting gratings were shown on the 3-screen setup. To effectively elicit OKR in mice, we used a slightly different set of parameters for drifting gratings and plaids. Specifically, for gratings, we used SF = 0.16 cpd and TF = 1.5Hz. For 45° and 20° plaids, we used SF = 0.16 cpd, TF_1 = 0.3 Hz, TF_2 = 1.2 Hz for component gratings. For 135° and 160° plaids, we used the same SF = 0.16 cpd, TF_1 = 0.4 Hz, TF_2 = 1.6 Hz for component gratings. These parameters made the VS motion speed for plaid and grating stimulus to be close, with 9.28, 8.92, 8.42, 7.70, 9.38 deg/s for 20°, 45°, 135°,160° plaids and single gratings, respectively. Each stimulus was presented for 10 seconds with a 3s inter-stimulus-interval and repeated for 15 times in a pseudorandom order.

3.5.3 Quantification and Statistical Analysis

Direction selectivity. We quantified the direction selectivity for each neuron/multi-unit cluster with global direction selectivity index (gDSI) as $gDSI = |\frac{\Sigma R_\theta e^i \theta}{\Sigma R_\theta}|$, where R_θ is the response magnitude to stimulus direction θ in radians. The preferred direction was calculated as the angle of the vector summation (i.e., $\theta_p ref = arg(\Sigma R_\theta e^i \theta)$).

OKR gain. Because the stimulus speed was different across gratings and plaids, we calculated the OKR gain to compare between the responses to different stimuli, $OKR\ Gain = speed_{eye}/speed_{stim,VS}$. Here, we used the stimulus speed at the VS direction as the denominator because we observed that the OKR direction was generally consistent with the VS direction. The preferred direction of OKR was calculated as the angle of the vector summation of the OKR Gain tuning curve. OKR gain range was calculated by the maximum OKR gain minus the minimum.

Probabilistically Constrained Vector Sum Model. The individual grating's prediction function was a probability density function (pdf, $w(x)$) approximated as a normalized product of two functions as follows:

$$
\begin{aligned}
v(x) &= t \cdot \tanh\left(\tfrac{s \cdot \sec^2(x)}{t}\right) \\
u(x) &= \frac{1-\alpha}{360} + \frac{\alpha}{b-a} \cdot \frac{1}{1+\exp\left(-\frac{g(x)}{c}\right)} \cdot \frac{1-\exp\left(-\frac{1}{c}\right)}{1+\exp\left(\frac{g(x)-1}{c}\right)} \\
w(x) &= \frac{v(x) \cdot u(x)}{\displaystyle\int v(x) \cdot u(x)\, dx}
\end{aligned}
\tag{3.1}
$$

where x is the direction; $v(x)$ applies a soft threshold on the $sec^2(x)$ function, with s controlling the softness and t being the threshold; $sec^2(x)$ is the squared secant function; $u(x)$ is a mollified uniform distribution (Weiß, 2024), where a and b are the lower and upper bounds of the probable direction range given a single grating (i.e. 0°+δ and 180°-δ for a grating moving towards 90° direction, δ being a small offset of two bounds); c is the parameter controlling the slope of the transition between high and low values; α controls the height of the mollified uniform distribution. $g(x)$ is defined as: $g(x) = \frac{x-a}{b-a}$. The normalization is done so that the function properly represents probability. The joint prediction was also a pdf obtained by normalizing the product of two pdfs of individual gratings so that its area-under-curve is 1.

We chose the above functions to estimate the joint prediction for the following reasons. First, given a drifting grating, one half of the full range of directions (covering 180° of the full 360° cycle) is compatible while the other half is not (Figure 3.2E, yellow shades). Thus, mollified uniform distribution was used to approximate it so that the joint prediction is of high probability for half of the directions but low for the other half. Second, the end point of all the compatible motion vectors of a drifting grating can be represented by its constraint line as in IOC (Figure 3.7A). In theory, every motion along the constraint line is equally probable (Figure 3.2E, grey arrows; Figure 3.7A). If one randomly samples on the constraint line and finds the corresponding motion directions, directions that are away from the grating direction are more likely to be sampled. This relationship between motion directions (x) and their corresponding positions on the constraint line (y) can be described by $y = c \cdot tan(x)$, where c is the speed of the grating (Figure 3.7A). The probability of each direction can be approximated by the derivative of y, which is a squared secant function as in $v(x)$. The squared secant function is further applied a soft threshold so that the probability does not go to infinite. This $v(x)$ function contributes to the ‘M’ shape in the prediction curves (Figure 3.2E & 3.7). Note that our main conclusions do not depend on the ‘M’ shape in the function. If $v(x)$ is substituted with a constant (i.e. making the ‘M’ flat), the model generates similar predictions that can still explain our data. Here, we use the full form of the function for theoretical accuracy.

The likelihood by VS is modeled with von Mises distribution:

$$L(x) = \frac{exp(\kappa \cdot cos(x - \mu_{VS})}{2\pi I_0(\kappa)} \tag{3.2}$$

where x is the direction; κ is the shape parameter; μ_{VS} is the VS direction; I_0 is the modified Bessel function of order zero.

The final joint pdf, which we propose is what SC neurons represents, is the product of the joint prediction and the likelihood. We kept the joint pdf unnormalized because we found weaker SC responses to plaids with larger cross angles (Figure 3.2-3.4, example neurons). For these plaids where the VS falls far outside the “likely” range given by the joint prediction, neuronal responses may resemble those elicited by non-directional stimuli.

Extended Data

Figures

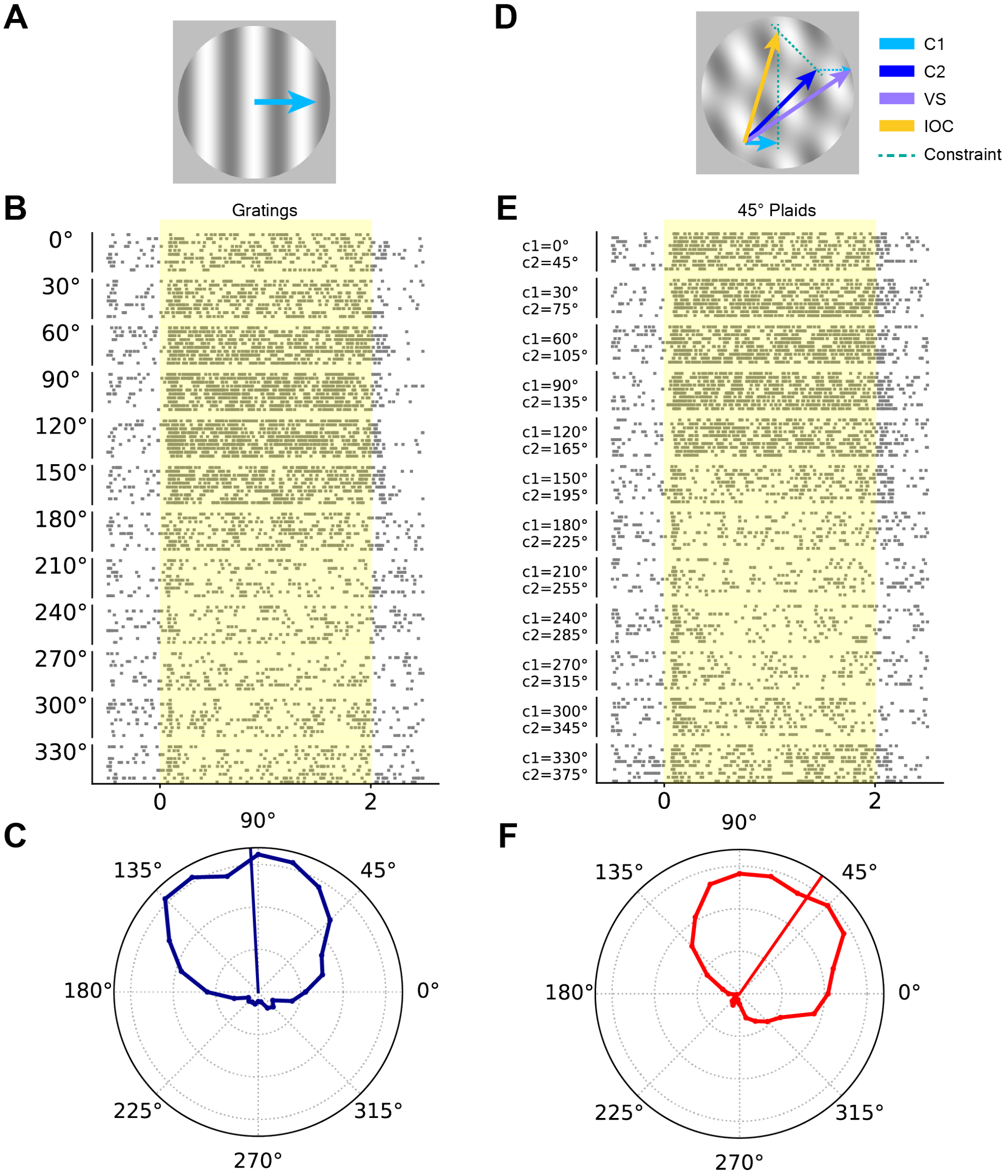

Figure 3.6: An example neuron's response to grating and 45° asymmetric plaid. (A-C) In response to a drifting grating (A), an example neuron's spike raster plot at different directions (B), and the resulting tuning curve (C). Yellow shade in is the window of stimulus presentation (2 seconds). Its preferred direction is 93.1°. (D-F) Same as (C), but for the 45° asymmetric plaid. The preferred direction is 55.0°, thus a shift of 38.1° compared to the grating tuning.

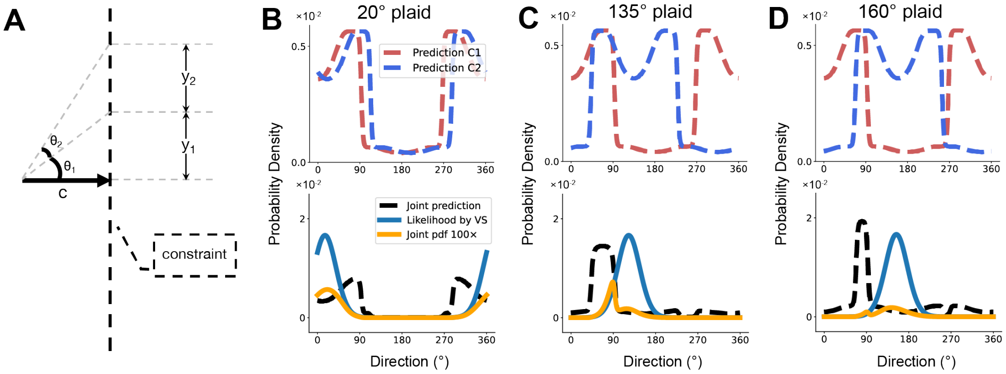

Figure 3.7: Schematics of the probabilistically constrained VS computation. (A) A diagram of the prediction function approximation. A drifting grating's motion is represented by the thick arrow. Its constraint is represented by the black dashed line. Every dot on the constraint line represents a possible motion vector's end point, and is equally probable. However, the relationship between motion direction and end point position is not linear. For example, y1 and y2 are of equal length on the constraint, but represent different ranges of directions θ_1 and θ_2. If one randomly samples points on the constraint, directions away from the grating direction are more likely to selected. Thus we used the "M"-shaped function (squared secant function) as in B-D to approximate such relationship. Note that our main conclusions do not depend on this specific shape of prediction curves. As long as the prediction functions have the cliff (approximated here with a uniform function), the conclusions hold. (B) The predictions (top) and joint pdfs (bottom) for the 20° plaid. (C) Same as (B), but for the 135° plaid. (D) Same as (B), but for the 160° plaid.

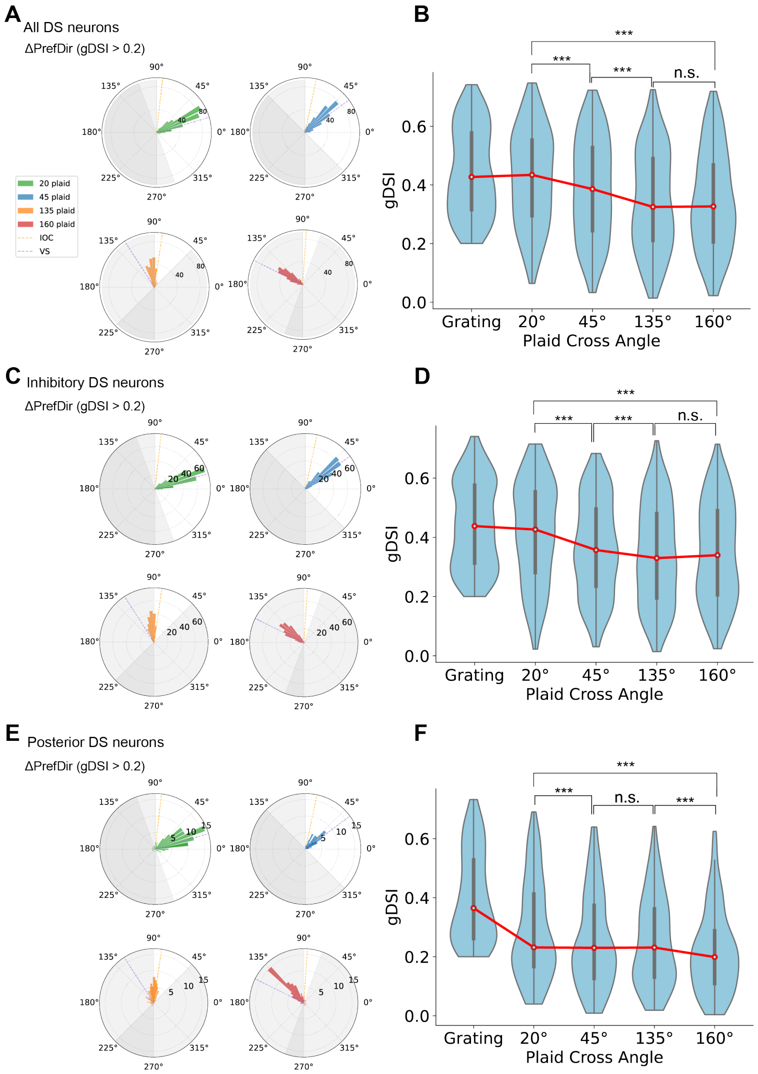

Figure 3.8: Additional quantification of direction selectivity of neurons recorded by two-photon calcium imaging. (A) The distribution of the difference between preferred directions to grating and all 4 conditions of plaids for direction selective neurons (gDSI > 0.2) imaged from the anterior SC. The mean ± std of the distributions are 21.3 ± 22.7° (n = 280, 20° plaid), 40.5 ± 23.7° (n = 255, 45° plaid), 92.6 ± 29.7° (n = 235, 135° plaid), and 144.9 ± 27.9° (n = 233, 160° plaid). (B) The gDSI of neurons imaged from the anterior SC that are highly selective to grating (gDSI > 0.2 for grating). Friedman test, $p < 0.001$. Post-hoc Wilcoxon tests are performed between adjacent plaid conditions, $p < 0.001$ for 20° and 45° plaids and for 45° and 135° plaids, $p = 1.00$ for 135° and 160° plaids. (C-D) same as (A-B), but for inhibitory DS neurons only. The mean ± std of the distributions in (C) are 18.7 ± 19.2° (n = 286, 20° plaid), 39.4 ± 19.0° (n = 265, 45° plaid), 97.5 ± 27.9° (n = 244, 135° plaid), and 141.1 ± 31.3° (n = 254, 160° plaid). (D) Friedman test, $p < 0.001$. Post-hoc Wilcoxon tests are performed between adjacent plaid conditions, $p < 0.001$ for 20° and 45° plaids and for 45° and 135° plaids, $p = 1.00$ for 135° and 160° plaids. (E-F) same as (A-B), but for DS neurons from the posterior SC. (E) The mean ± std of the distributions are 22.6 ± 36.9° (n = 92, 20° plaid), 41.6 ± 16.1° (n = 81, 45° plaid), 99.8 ± 37.0° (n = 79, 135° plaid), and 126.1 ± 34.5° (n = 71, 160° plaid). (F) Friedman test, $p < 0.001$. Post-hoc Wilcoxon tests are performed between adjacent plaid conditions, $p < 0.001$ for 20° and 45° plaids, $p = 0.94$ for 45° and 135° plaids, $p < 0.001$ for 135° and 160° plaids.

Chapter 4

Visual Motion Processing in The Tree Shrew Superior Colliculus.

4.1 Abstract

Over the past few decades, research has established that the superior colliculus (SC) plays a key role in visual motion processing and visually guided behaviors. However, detailed functional differences across mainstream animal models have made it difficult to integrate findings to form a general model of the SC. Here we used tree shrew - a species evolutionarily intermediate between rodents and primates - as an animal model to help bridge our understanding of this highly conserved brain structure. In this study, we recorded visual motion responses from the tree shrew SC neurons in vivo using a set of motion stimuli, including drifting gratings, random dots kinematograms, symmetric and asymmetric plaids. We were able to characterize a series of response properties from the tuning to motion direction, spatiotemporal frequency, and speed, to motion integration and its underlying rules. Our study thus provides fundamental insights into the visual motion representation in the tree shrew SC and establishes a basis for future studies on comparative studies on SC visual processing.

4.2 Introduction

Visual motion processing is a fundamental function of visual systems that supports survival-critical behaviors such as prey capture and predator avoidance. Accurate and rapid perception, as well as effective motor coordination, depends on how visual motion is represented in the brain.

The superior colliculus (SC, or optic tectum in non-mammals) is a highly conserved midbrain structure that is known to preferentially represent visual motion in various species (Basso et al., 2021; Cang et al., 2024; Isa et al., 2021; Lu et al., 2024; Duchemin et al., 2022; Huang et al., 2022). For example, neurons that are selective to motion directions were found in fish (Damjanović et al., 2023), hamsters (Mooney et al., 1985), mice (Cang et al., 2024; Gale and Murphy, 2014; Wang et al., 2010), and primates (Hafed et al., 2023). As a sensory-motion integration hub, the SC was also found to integrate vision with other sensory modalities in its deeper layers, as well as to guide eye and head movements (Isa et al., 2021; Basso and May, 2017; Cang et al., 2024). In mice, the SC's role is broadly studied in mediating innate behaviors such as hunting and escaping (Huang et al., 2021; Shang et al., 2019; Isa et al., 2020; Yilmaz and Meister, 2013; Hoy et al., 2019). Recently, studies using plaids have shown a motion integration taking place in the mouse SC, which was traditionally attributed to primate cortex (DePiero et al., 2024; Li et al., 2025). Taken together, these findings highlight that the SC plays an important role in visual motion processing, influencing fast behaviors essential for environmental interactions.

However, despite the overall evolutionary conservation, the function of the visual SC also shows divergence across species. For example, the superficial visual layer of the mouse SC was found to contain large proportions of direction selective neurons (Inayat et al., 2015), whereas in primates these neurons are much less prevalent (Hafed et al., 2023). In addition, more than 80% of the retinal output directly innervate with the SC in mice and pigeons, yet only 10% was reported in primates (Hoy and Farrow, 2025). A transition and specialization of the SC seems to happen evolutionarily at a point between rodents and primates. Thus, to gain a better understanding of the function of this ancient subcortical structure, we turned to tree shrew models to facilitate the cross-species comparison. Tree shrews (*Tupaia*), constituting the entire order of *Scandentia*, are primitive higher mammals close to primates. They are diurnal animals with excellent visual acuity, and display visual system complexity comparable to primates (Petry and Bickford, 2019; Savier et al., 2021; Sedigh-Sarvestani et al., 2021). These animals can be readily trained to utilize various visual cues for cognitive tasks (Lam et al., 2025; Li et al., 2022a; Petry et al., 1984; Petry and Kelly, 1991; Callahan and Petry, 2000; Mustafar et al., 2018; Li et al., 2023; Pan et al., 2022).

In this study, we used a series of motion stimuli including drifting gratings, random dot kinematogram, symmetric and asymmetric plaids to characterize the response properties of tree shrew SC neurons to various stimulus features, with an emphasis on motion direction. Drifting gratings are conventionally used for characterizing direction and orientation tuning in the mouse SC (Inayat et al., 2015; Liu et al., 2023b; Relota et al., 2025). Random dots are another type of traditional motion stimuli that are more often used in the primate SC and middle temporal cortex (MT) to characterize the direction tuning properties and sometimes cognitive variable representation in the neurons (Snowden et al., 1992; Odegaard et al., 2018; Horwitz and Newsome, 2001; Chaplin et al., 2017). Drifting gratings approximate visual stimuli containing a single dominant spatiotemporal Fourier component, corresponding to one direction and spatial frequency. In contrast, random dot kinematograms have a broader range of spatial frequencies and orientations. Therefore, we measured neuronal responses to both stimuli to compare their motion representation under 2 distinct types of spatial texture composition. Additionally, we also measured neuronal responses to symmetric and asymmetric plaids, aiming to study motion integration and make direct comparison with the recent findings in the mouse SC (DePiero et al., 2024; Li et al., 2025). Our results will provide a foundation for investigating visual processing in the tree shrew SC and will facilitate future studies on SC function and cross-species comparison.

4.3 Results

4.3.1 SC neurons are tuned to the spatial frequency, temporal frequency, and direction of drifting gratings.

We recorded the visual responses from superficial and intermediate layers of the SC in awake head-fixed tree shrews (n=3) with 64-channel silicon microprobes while the animals were passively viewing the stimulus on the screen. Firstly, we characterized the spatial and temporal frequency (SF and TF) preferences of the SC neuron population, as they are two major features of the drifting grating stimulus. We tested 6 SFs × 6 TFs × 4 cardinal directions. Out of 380 single units recorded, 185 neurons were visually responsive to this grating stimulus with a responsive rate of 48.68%). After min-max normalization, we averaged the responses across all responsive neurons (Fig. 4.1A). As a population, the neurons responded stronger to a medium level of TF tested and very low SF in all 4 directions. The SF and TF tuning curves obtained by averaging across the other two variables further showed SC neurons prefer an SF of 0.03 cpd and a TF of 8 Hz (Fig. 4.1B).

To characterize more detailed SF preference and direction selectivity in the SC neurons, we fixed the TF to 8 Hz and measured the neuronal responses to 6 SFs and 12 directions of the drifting gratings. Here, we maintained the lowest SF tested to be 0.03 cpd to ensure the 40° stimulus patch contained more than one cycle of the spatial pattern. 39.20% (205 out of 523) single units were responsive to the new grating stimulus. The normalized average response showed an overall preference to low SFs, consistent with the previous grating stimulus (Fig. 4.1C). Interestingly, the SF responses showed clear bimodal distribution in the neural population for the highest and lowest SFs tested (Fig. 4.1D). To classify neurons based on their SF response profiles, we applied K-means clustering to the normalized response curves across SFs (Fig. 4.1E). Using K-means clustering (k=2, average silhouette score = 0.55) on normalized SF tuning curves, neurons were divided into two groups. The first group showed decreasing responses with SF (Fig. 4.1E, blue), while the second group responded strongest to high SF (Fig. 4.1E, red). This can also be illustrated

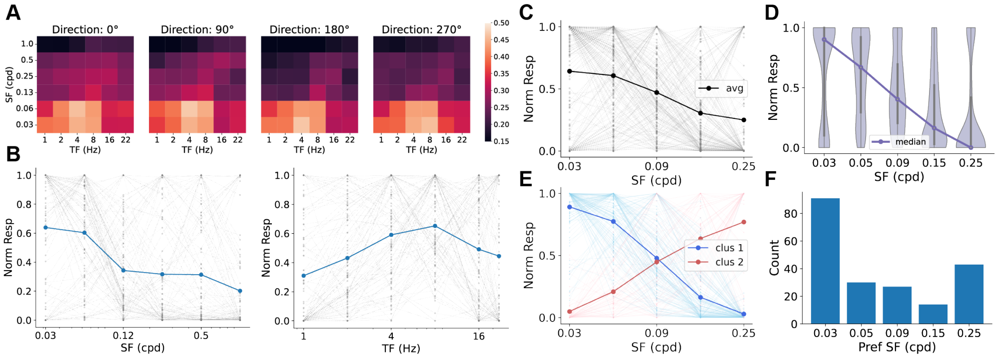

Figure 4.1: Spatiotemporal frequency tuning of SC neurons to drifting gratings. (A) The spatiotemporal frequency tuning map to drifting gratings moving in 4 directions (0°, 90°, 180°, 270°). Responses are normalized to a range from 0 to 1. Only single, responsive units were included in this and the following analysis unless otherwise specified. $n = 185$. (B) Normalized tuning curves to SFs averaged across all directions and TFs (left) and to TFs averaged across all directions and SFs (right). Blue solid lines: population average. Gray dotted lines: tuning curves of individual neurons. X axis was plotted on log scale.(C) Normalized tuning curves to SFs averaged across all 12 directions of a new grating stimulus. $n = 192$ (93.65%, out of all 205 single responsive neurons. Neurons with purely suppressive responses to all conditions were excluded). Black solid line: population average. Gray dotted lines: tuning curves of individual neurons. (D) Normalized responses distribution to 5 SFs showed bimodal shape to high and low SFs. Solid line: median. $n = 192$. (E) Normalized tuning curves of 2 clusters found by K-means method (k = 2, average silhouette score = 0.55). Blue: average of the first cluster showing a preference to lower SFs ($n = 135$). Red: average of the second cluster showing a high SF preference ($n = 57$). Light blue and red: tuning curves of individual neurons. (F) The distribution of the preferred SF across the single and responsive neuron population. $n = 205$.

by the histogram of the preferred SF in the population - more neurons preferred either the lowest or the highest SF, but fewer neurons preferred the SFs between them.

Next, we investigated the motion direction and orientation selectivity of the SC neurons. Fig. 4.2A showed an example direction selective (DS) neuron. This neuron exhibited consistent direction preference across different SFs, with a preference of high SF. Fig. 4.2B showed an example orientation selective (OS) neuron exhibiting consistent orientation preference across different SFs, with a preference of intermediate SF. In the responsive neuron population, direction response profiles were on average positively correlated across different SFs, with higher correlation in adjacent SFs (Fig. 4.2C), suggesting the direction tuning was stable across SFs. Therefore in the following analysis, we quantified the direction tuning of each neuron based on the responses under its preferred SF. We measured the direction and orientation selectivity by global direction/orientation selectivity index (gDSI and gOSI respectively, see Methods). We defined highly selective neurons as having an index value greater than 0.2. 30.24% of all responsive neurons were highly DS, and 27.31% were highly OS in response to drifting gratings (Fig. 4.2D). For highly DS neurons, the population showed a preference of vertical upward motion (Fig. 4.2E). On the other hand, the highly OS neurons showed a population preference of horizontal and vertical orientations (Fig. 4.2F). Notably, when examining the Z-score normalized responses, highly and weakly DS neurons showed similar tuning width and magnitude to directions, with slightly flatter and more OS-like tuning curves for weakly DS neurons (Fig. 4.2G). Similarly, highly and weakly OS neurons also had similar levels of tuning, only with flatter and more DS-like tuning curves for weakly OS neurons (Fig. 4.2H). The observation held true when more radical thresholding was applied (Fig. 4.6). This suggested DS and OS response property were more pervasive in the SC neurons than the selectivity index threshold indicated. Highly DS neurons showed a population preference of the lowest and highest SFs, while the highly OS neurons preferred the lowest SF (Fig. 4.2I&J). gDSI and gOSI showed a moderate correlation within the responsive neuron population (Fig. 4.2K, Spearman's $\rho = 0.32$, $p < 10^{-5}$).

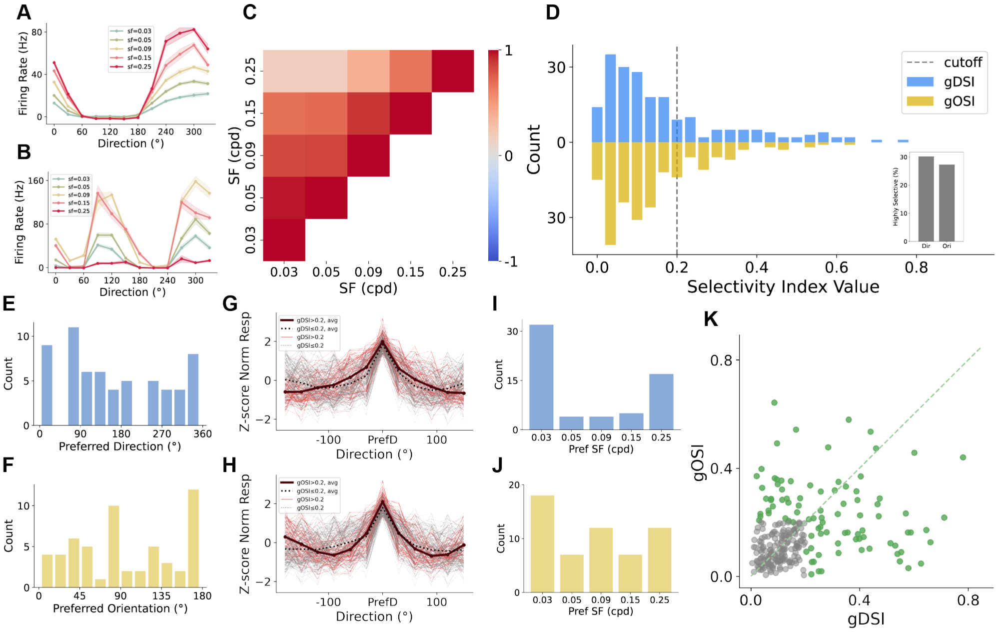

Figure 4.2: Direction and orientation tuning to drifting gratings. (A) Firing rate (baseline subtracted) of an example direction selective (DS) neuron. This neuron was tuned to 293.99° direction with a gDSI of 0.66 (calculated based on the response to the preferred SF, i.e. 0.25 cpd). (B) Firing rate (baseline subtracted) of an example orientation selective (OS) neuron. This neuron was tuned to two directions that were 180° apart, which corresponded to the grating orientation of 29.65° with a gOSI of 0.54 (based on the responses to SF = 0.09 cpd). (C) Pearson correlation coefficient between the direction tuning curves to each SF, averaged across the neuron population. Red and blue indicates positive and negative correlations. $n = 205$. (D) The distribution of gDSI and gOSI across the population ($n = 205$). Blue: gDSI. Yellow: gOSI. Vertical dashed line: the 0.2 cutoff used in this study to determine highly selective neurons. Inset: the proportion of highly DS ($n = 62$, 30.24%) and OS ($n = 56$, 27.31%) neurons. (E-F) The distribution of preferred direction of highly DS neurons ($n = 62$) and preferred orientation of highly OS neurons ($n = 56$). (G) Tuning curves of highly ($gDSI > 0.2$) and weakly ($gDSI \leq 0.2$) DS neurons aligned to their preferred directions. Thick lines: population average. Thin lines: individual neurons. (H) Same as G, but for highly and weakly OS neurons. (I-J) The distribution of preferred SF in the highly DS (I) and OS (J) population. (K) The gDSI and gOSI relationship of the same neurons. Gray: neurons that were neither highly DS or OS. Green: neurons that were highly DS or OS. Spearman's $\rho = 0.32$, $p < 10^{-5}$.

4.3.2 Motion direction and speed tuning of random dot kinematogram.

Next, we examined SC neuronal responses to another widely used motion stimulus: random dot kinematogram (RDK). We varied 100% coherence random dot pattern in 5 speeds and 12 directions. 47.20% (270 out of 572) single units were responsive to RDK stimulus. Neurons responded with a preference to the highest speed tested on average (Fig. 4.3A). Similarly to the population SF tuning to the grating stimulus, RDK with high and low speeds also elicited bimodal response magnitude in neurons (Fig. 4.3B). K-means clustering method found 2 clusters (average silhouette score = 0.51), with the first cluster showed high speed preference (Fig. 4.3C, blue), while the second group showed low speed preference (Fig. 4.3C, red). It is worth noting that in drifting gratings, the preference of lower SF with fixed TF also means higher speed. Thus we observed a consistency that SC neurons prefer lower SF of gratings as well as higher speed of random dots.

We also examined the motion direction preference to RDK stimulus. Overall, the direction tuning curves were correlated across speeds, with higher correlation value between adjacent speeds (Fig. 4.3E). Hence, the following analysis was based on the direction tuning profile under the preferred speed of each neuron. In RDK stimulus, there is no orientation. As a result, neurons tuned to 2 opposite directions were defined as 'axis selective' (AS, see Methods). Fig. 4.3F showed the direction tuning curve of an example DS neuron. Its direction preference was consistent across speeds, with stronger response to lower speeds. Fig. 4.3G showed an example AS neurons preferring lower speeds. Notably, the AS responses were noisier compared to OS responses to gratings (Fig. 4.2B). Indeed, 18.52% of the neurons were DS in response to RDK stimulus, and only 10.74% were AS (Fig. 4.3H), both are much lower compared to the DS and OS rate to gratings. This suggested that despite a similar or larger number of neurons were responsive to RDK than drifting gratings, the RDK was not very effective in driving direction selective responses. Chi-square test and post-hoc Z-test confirmed that DS and AS proportion to RDK were both significantly lower than DS and OS to gratings ($\chi^2 = 36.68$, $p < 10^{-7}$. two-proportion Z-test, $p = .006$ for $DS_{grating}$ and DS_{RDK}; $p < 10^{-5}$ for $OS_{grating}$ and AS_{RDK}, Benjamini-Hochberg FDR corrected). Moreover, the AS proportion was significantly lower than DS in RDK but such dif-

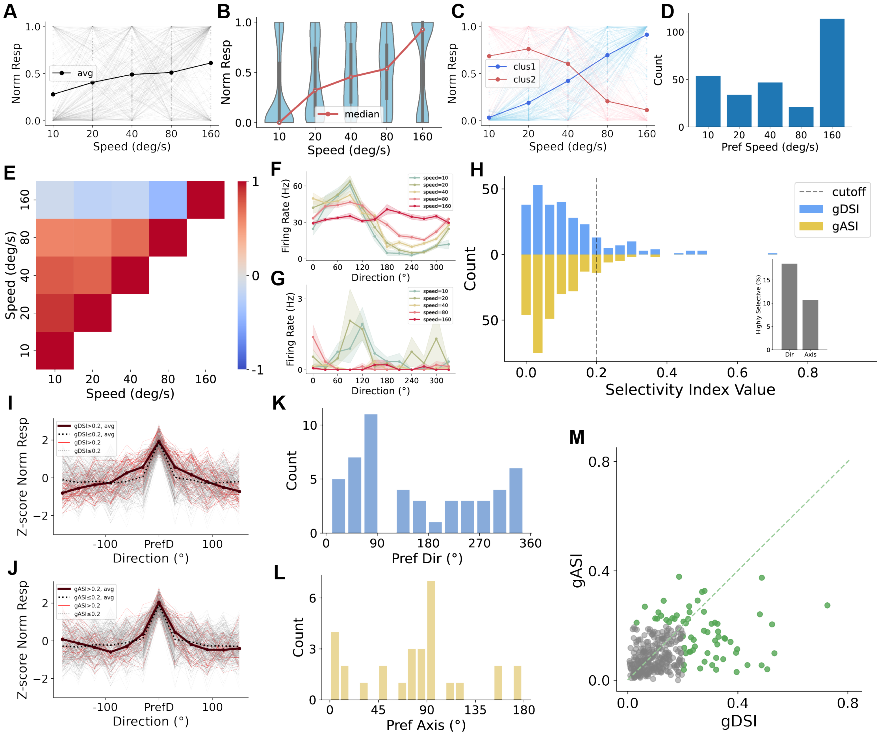

Figure 4.3: Direction, axis, and speed tuning to random dot motion. (A) Normalized response to speeds averaged across 12 directions tested ($n = 234$). Black solid line: population average. Gray dotted lines: responses of individual neurons. Neurons with suppressive responses to all conditions were excluded. (B) Normalized responses distribution to 5 speeds showed bimodal shape to high and low speeds. Solid line: median. $n = 234$. (C) Normalized tuning curves of 2 clusters found by K-means method (k = 2, average silhouette score = 0.51). Blue: average of the first cluster showing a preference to high speeds ($n = 146$). Red: average of the second cluster showing a low speed preference ($n = 88$). Light blue and red: tuning curves of individual neurons. (D) The distribution of the preferred speed across the neuron population ($n = 270$, all single, responsive neurons)(E) Pearson correlation coefficient between the direction tuning curves to each speed, averaged across the neuron population. Red and blue indicates positive and negative correlations. $n = 270$.(F) Firing rate (baseline subtracted) of an example direction selective (DS) neuron. This neuron was tuned to 64.71° direction with a gDSI of 0.48 (calculated based on the response to the preferred speed, i.e. 20 deg/s).(G) Firing rate (baseline subtracted) of an example axis selective (AS) neuron. This neuron was tuned to two directions that were 180° apart, which corresponded to the motion axis of 103.22° with a gASI of 0.50 (based on the responses to speed = 20 deg/s). (H) gDSI and gASI distribution of the population ($n = 270$). Blue: gDSI. Yellow: gASI. Vertical dashed line: the 0.2 cutoff for highly selective neurons. Inset: the proportion of highly DS ($n = 50$, 18.52%) and AS ($n = 29$, 10.74%) neurons. (I) Tuning curves of highly ($gDSI > 0.2$) and weakly ($gDSI \leq 0.2$) DS neurons aligned to their preferred directions. Thick lines: population average. Thin lines: individual neurons. (J) Same as G, but for highly and weakly AS neurons. (K-L) The distribution of preferred direction of highly DS neurons ($n = 50$) and preferred motion axis of highly AS neurons ($n = 29$). (M) The gDSI and gASI relationship of the same neurons. Gray: neurons that were neither highly DS or AS. Green: neurons that were highly DS or AS. Spearman's $\rho = 0.44$, $p < 10^{-13}$.

ference was absent between DS and OS proportions in gratings (two-proportion Z-test, $p = .016$ for DS_{RDK} and AS_{RDK}; $p = .513$ for $DS_{grating}$ and $OS_{grating}$, Benjamini-Hochberg FDR corrected). These results indicate that OS measured by drifting gratings is likely resulted from an interaction between spatial pattern (i.e. orientation) and motion axis preference. Similar to the findings in gratings, the z-score normalized responses showed similar level of direction selectivity between highly and weakly selective population (Fig. 4.3I&J). Highly DS neurons preferred upward motion direction as a population, and highly AS neurons preferred vertical and horizontal motion axis (Fig. 4.3K&L). Finally, gDSI and gASI showed a moderate correlation (Fig. 4.3M, Spearman's $\rho = 0.44$, $p < 10^{-13}$), consistent with the observation of grating responses. Taken together, the results indicate with gratings and RDK, we probed the same DS response properties in the SC.

4.3.3 Motion integration of symmetric plaids

Visual neurons in the SC was previously found to integrate motion direction of plaid patterns in mice (DePiero et al., 2024). Plaids are patterns created by overlapping two drifting gratings on each other. Studies have shown the neural representation of plaid motion direction follows a component to pattern transformation from the V1 (component dominant) to higher visual areas (e.g. MT and MST, pattern emerging) in primates (Adelson and Movshon, 1982; Movshon, 1985; Wallisch and Movshon, 2019; Khawaja et al., 2013). This motion integration function has thus long been studied in the cortical structures. However, a component-pattern transformation was recently observed in the mouse retina - SC pathway (DePiero et al., 2024), suggesting subcortical structures also integrate motion, potentially in a more conserved and widespread manner across species. In this study, we investigated the neural responses to plaids in the tree shrew SC. To make the results comparable to previous mouse studies (DePiero et al., 2024; Palagina et al., 2017; Muir et al., 2015; Juavinett and Callaway, 2015), we adopted a similar stimulus namely symmetric plaids (or so called "type I" plaids). In symmetric plaids, the two grating components have the same spatial and temporal frequencies, but only differ in their motion direction. Thus the pattern motion direction lies exactly at the average of the two component directions. Here, we used symmetric plaids with SF = 0.1 cpd and TF = 8 Hz. We varied the cross angle between the two gratings (60°, 90°, 120°) and compared the neurons' preferred direction of plaids and gratings.

Out of 621 single units, 242 neurons (38.97%) were responsive. 46.69% of these responsive neurons (113 out of 242) were highly DS to gratings. Compared to grating elicited responses, plaids evoked significantly higher maximum responses (Fig. 4.4A-C, Wilcoxon signed rank test, $p < 10^{-4}$ for 60° plaid, $p < .001$ for 90° plaid, $p < 10^{-5}$ for 120° plaid), yet significantly lower gDSI (Fig. D-F, Wilcoxon test, $p < 10^{-9}$ for 60° plaid, $p < 10^{-10}$ for 90° plaid, $p < 10^{-12}$ for 120° plaid). The preferred direction to grating and plaids closely correlated with each other, indicating the direction tuning is shared between the two stimulus types (Fig. G-H, circular correlation, $\rho = 0.76$ for grating and 60° plaid; $\rho = 0.51$ for grating and 90° plaid; $\rho = 0.56$ for grating and 120° plaid). Predictions of pattern and component selective responses were made based on the direction tuning curves to gratings (see Methods). By comparing the observed plaid responses to the predictions, neurons were classified to 3 types: pattern-motion selective (PM), component-motion selective (CM), and unclassified. Most of the neurons were unclassified (Fig. 4.4J-L, 67.26% for 60° plaid, 69.91% for 90° plaid, 76.99% for 120° plaid). We observed a comparable proportion of pattern selective (17.70%, 17.70%, 10.62% for 60°, 90°, 120°plaids, respectively) and component selective (15.04%, 12.39%, 12.39% for 60°, 90°, 120°plaids) neurons in all three cross angles tested (Fig. 4.4J-L). Hence, the pattern selectivity was less striking in the tree shrew SC neurons compared to the mouse SC (DePiero et al., 2024). However, the exhibited component-pattern selectivity balance resembled what was reported in primate and cat extrastriate visual cortical areas, as well as higher visual areas in mouse cortex (Smith et al., 2005; Juavinett and Callaway, 2015; Palagina et al., 2017).

4.3.4 Tree shrew SC neurons adopt vector sum to represent the direction of asymmetric plaids

The previous results indicate motion integration is already taking place in the tree shrew SC. Our recent study has shown that instead of representing a plaid pattern in the direction that are con-

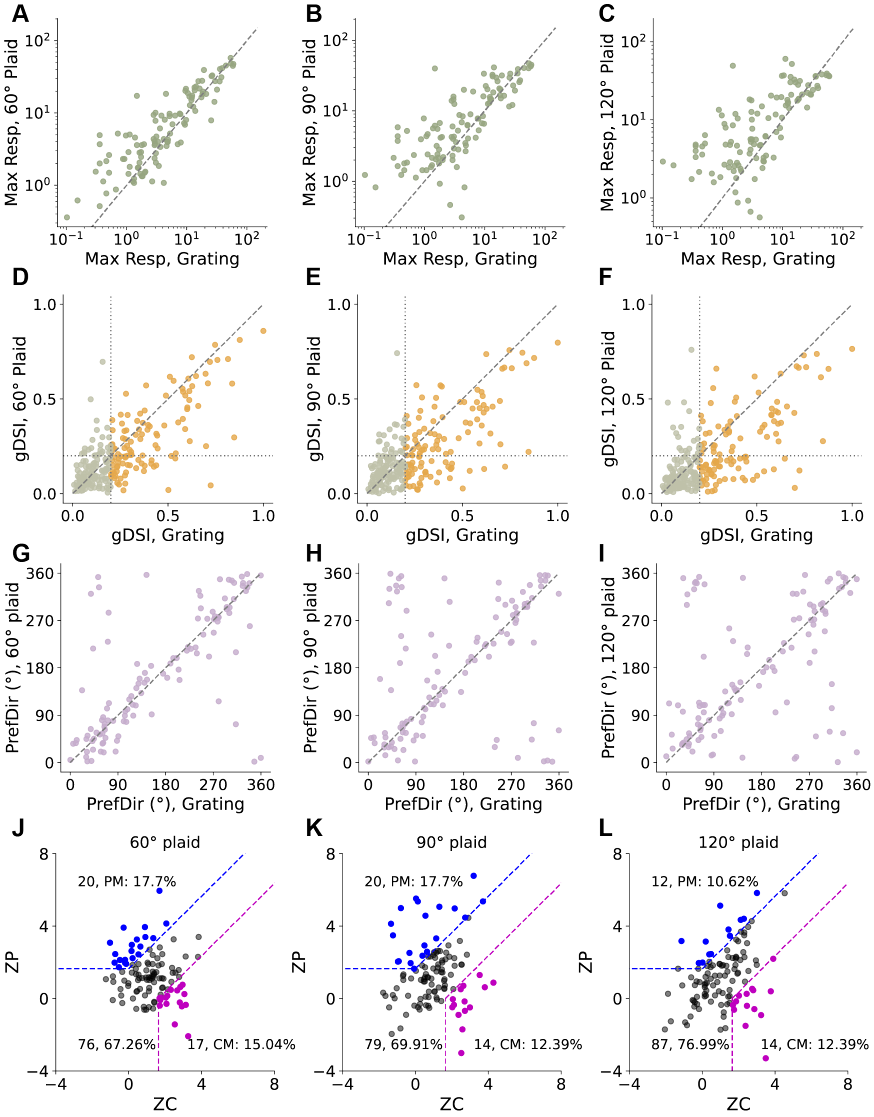

Figure 4.4: A mixture of pattern and component selectivity to symmetric plaids in the tree shrew SC. (A-C) The max response evoked by grating and plaids. Wilcoxon signed rank test, $W = 1910$, $p < 10^{-4}$ for 60° plaid (A), $W = 2019$, $p < .001$ for 90° plaid (B), $W = 1656$, $p < 10^{-5}$ for 120° plaid (C). Only single, responsive neurons that were highly DS for grating were included ($n = 113$). (D-F) gDSI for grating and plaids. Yellow dots: neurons highly DS for grating. Wilcoxon signed rank test, $W = 19071$, $p < 10^{-4}$ for 60° plaid (D), $W = 18872$, $p < 10^{-4}$ for 90° plaid (E), $W = 21570$, $p < 10^{-9}$ for 120° plaid (F). All single, responsive neurons were included in the statistical test ($n = 242$). (G-I) The preferred directions to grating and plaids. Circular correlation coefficient $\rho = 0.76$ for 60° plaid (G), $\rho = 0.51$ for 90° plaid (H), $\rho = 0.56$ for 120° plaid (I). Only single, responsive neurons that were highly DS for grating were included ($n = 113$). (J-L) ZP and ZC scores for 3 plaids tested ($n = 113$). Blue: pattern-motion (PM) selective neurons. Magenta: component-motion (CM) selective neurons. Black: unclassified neurons. We report the number of neurons in each category as well as their proportion.

sistent with human and non-human primate perception, the mouse SC follows a probabilistically constrained vector sum (VS) computation of the two grating component directions (Li et al., 2025). Thus, we next sought to determine what computational rule the tree shrew SC employs. In order to distinguish between possible computations, we used asymmetric plaids as used in the previous studies (Li et al., 2025; Wallisch and Movshon, 2019; Khawaja et al., 2013). Here, we generate the asymmetric plaids with two grating components of different TFs (Fig. 4.5A). We kept the SF = 0.1 cpd as in the symmetric plaid stimulus, but changed TFs so that TF_1 = 2 Hz, TF_2 = 8 Hz (i.e. $speed_1$= 20 deg/s, $speed_2$ = 80 deg/s, with a speed ratio of 1:4). Because it was unknown which direction of the plaid pattern would be represented by the SC neurons, the direction of component 1 (C1, the slower component) was used to define the direction of asymmetric plaids. We varied the cross angle between two grating components in 4 levels (20°, 45°, 135°, 160°). The motion direction consistent with primate perception and cortical neural representation can be calculated by intersection-of-constraint (IOC) method, in contrast to the VS method used by mouse SC and subcortical driven optokinetic reflex (OKR). In order to make direct comparison with the previous mouse study, we included both single units and multi-unit clusters in our analysis. We first extracted the direction tuning curves for grating stimulus for each neuron (Fig. 4.5B, example neuron, dark blue line). If a neuron follows VS rule, its tuning curve to plaids would shift to the VS prediction (Fig. 4.5B, purple dashed line), whereas if a neuron follows IOC rule, the plaid tuning curve would shift to the IOC prediction (Fig. 4.5B, yellow dashed line). In the example neuron, the plaid tuning curves were always centered around the VS direction of each cross angle condition. We calculated the difference between the preferred directions for grating and asymmetric plaids for each unit. For each plaid condition, we only include units that are highly DS for that condition and the grating stimulus in the following results. As it turned out, in all 4 cross angles tested, the preferred direction difference distributions were centered around the VS prediction rather than IOC (Fig. 4.5C). For 20°, 45°, 135°, and 160° plaids, the preferred direction differences were 12.66° ± 57.51°, 38.92° ± 58.32°, 124.30° ± 68.53°, and 152.95° ± 70.76° respectively. We next selected the responses of the same units that were highly DS in response to all 4 plaid conditions and the gratings. Their responses closely followed the VS prediction (Fig. 4.5D, n = 137). In addition, the number of highly DS units decreased with larger cross angles (Fig. 4.5C, n = 290, 278, 251, and 245 for 20°, 45°, 135°, and 160° plaids), suggesting a weaker representation of the stimulus direction for plaids with larger cross angles. This was further supported by lower gDSI values with increasing cross angles (Fig. 4.5E, n = 420, $gDSI > 0.2$ to gratings).

Previous study reported that the mouse optokinetic eye movement (i.e. OKR), although not directly driven by the SC, follows a very similar computation to integrate motion of asymmetric plaids as the SC neurons (Li et al., 2025). To determine whether VS computation found above also guided the OKR in tree shrews, we measured animals' eye movements when viewing full-field gratings and asymmetric plaids (see Methods). Right eye pupil was tracked with Facemap (Syeda et al., 2024) and converted to horizontal movement speed. We calculated the difference between the grating and plaid directions that elicited the largest horizontal eye movements. The OKR was overall close to the VS prediction, except for 45° plaids (Fig. 4.5F & 4.8B). Gratings elicited stronger OKR than all plaids (Fig. 4.8C). Taken together, the results suggest an overall consistency of using VS rule for motion integration in the SC as well as in the OKR behavior. However, details also indicate the computation underlying OKR is different from what was employed by the SC neurons, thus implicating a separate neural substrate driving OKR in tree shrews.

4.4 Discussion

In this study, we characterized the visual motion response properties of tree shrew superficial SC neurons with multiple motion stimuli. These motion stimuli are widely used in various contexts and probe different aspects of motion processing. With renewed interest in using tree shrews as an animal model for vision research, and evolving techniques of viral and genetic tools tailored to these animals (Savier et al., 2021; Yao et al., 2024; Liu et al., 2025), there is a growing need for more systematic functional characterization studies. Therefore, we for the first time performed in vivo electrophysiology in the SC of awake tree shrews to study its visual function.

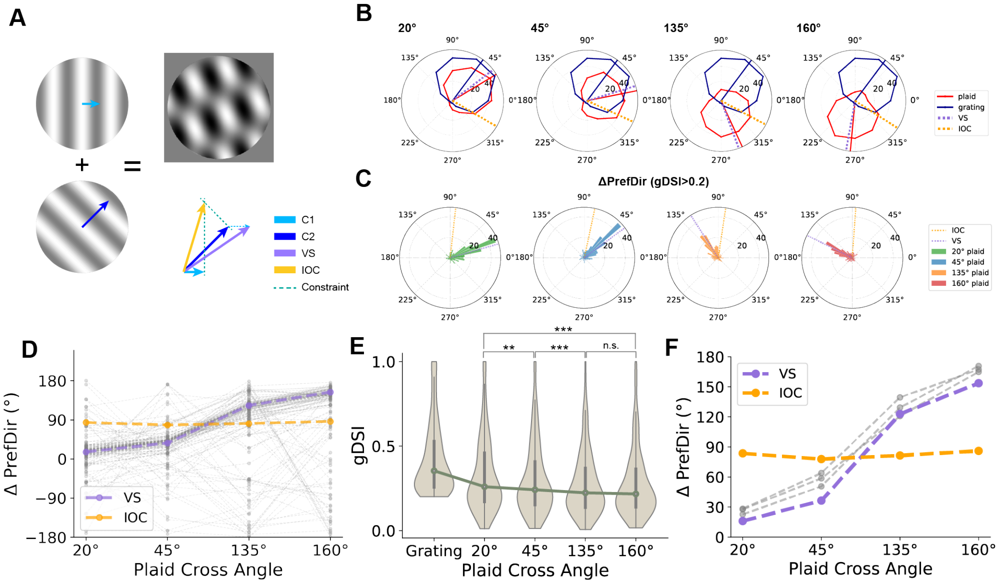

Figure 4.5: Tree shrew SC performs vector sum for asymmetric plaids. (A) We used asymmetric plaids comprising 2 gratings moving in different directions and temporal frequencies. The speed ratio of component 1 (C1, light blue) and component 2 (C2, dark blue) is 1:4. The vector sum (VS) of the two component motion vectors is indicated by purple arrow. Intersection-of-constraint (IOC, yellow arrow) is generated by the intersection of two constraint lines (green dashed lines). Schematic adapted from Li et al. (2025). (B) An example neuron's tuning curves to grating (dark blue) and plaids. Blue and red vertical lines: preferred direction calculated for grating and plaids. Purple and yellow dashed lines: VS and IOC prediction. This neuron preferred 53.30°, 31.12°, 11.43°, 294.67°, 264.59° for grating, 20°, 45°, 135°, and 160° plaids respectively. Thus, the preferred direction differences between grating and plaids were 22.18°, 41.87°, 118.63°, and 148.71° for 4 plaid cross angles. The VS predictions of the preferred direction difference are 16.04°, 36.46°, 122.88°, and 153.62°, while the IOC predictions are 83.62°, 77.88°, 81.46°, and 86.04°. (C) The distribution of the preferred direction difference between grating and plaids across the highly DS population. VS and IOC predictions were indicated by the purple and yellow dashed lines. For 20°, 45°, 135°, and 160° plaids, the preferred direction differences were 12.66° ± 57.51°, 38.92° ± 58.32°, 124.30° ± 68.53°, and 152.95° ± 70.76° respectively. (D) The preferred direction difference between grating and plaids of the neurons that were highly DS for all 4 plaid cross angles. VS and IOC predictions indicated by the purple and yellow dashed lines. Individual neurons were plotted in gray dotted lines. (E) The gDSI distribution of the neurons that were highly DS to grating. The distributions were significantly different among the 4 plaid cross angles (Friedman test, $\chi^2(3) = 90.70$, $p < 10^{-18}$. Post-hoc Wilcoxon singed rank test, $W = 35812$, $p = .005$ for 20° and 45° plaids, $W = 33105$, $p < 10^{-4}$ for 45° and 135° plaids, $W = 41209$, $p = .686$ for 135° and 160° plaids. (F) Optokinetic response of 3 animals also followed the VS prediction. Gray: OKR of individual animals. Purple and yellow: VS and IOC predictions.

Tree shrews are diurnal animals with high visual acuity. In both natural and laboratory environments, they exhibit agility to during navigation and appear to be very sensitive to fast moving objects. This is partly supported by the SC neurons' high temporal frequency tuning (8 Hz) and fast speed tuning ($\geq$ 160 deg/s). For reference, mouse SC neurons have a TF tuning around 2 Hz and speed tuning around 30 deg/s (Wang et al., 2010; De Franceschi and Solomon, 2018; Relota et al., 2025). The prevalence of high TF and high speed tuned neurons allows for capturing the rapid motion information in the visual stimulus for tree shrews, which better suits their ethological needs. In contrast, the tuned spatial frequency of tree shrew SC is comparable to, or even lower than, that of mice ($\sim$ 0.08 cpd, Wang et al. (2010)), suggesting a similar level of spatial resolution in the SC. This was at first surprising to us because tree shrews have much higher visual acuity than mice. However, high spatial resolution is generally advantageous for the representation of object details, but not necessarily for visual motion. Given the tuning to fast motion found in the neuron population, SC likely prioritizes motion processing, potentially trading off spatial details for processing efficiency.

In response to both drifting grating and RDK, we observed a population of highly DS neurons. The proportion of DS neurons to gratings was similar to what was reported in the mouse SC (Wang et al., 2010; Chen et al., 2021). Interestingly, when examining the z-score normalized tuning curves, even the weakly DS neurons showed clear tuned responses to motion directions, though with a more prominent two-peak shape. Additionally, highly OS neurons also exhibited response magnitude differences between the two directions corresponding to the same tuned orientation, suggesting they were also DS to some degrees. These results together indicate that direction selectivity is likely a fundamental response property in tree shrew SC neurons. Similarly, in a previous study characterizing mouse SC neuronal responses to plaids, researchers have found the preferred direction for gratings and plaids were highly correlated across the whole population, meaning even the 'non-DS' neurons (defined by the subthreshold gDSI values) retained some level of direction selectivity (Li et al., 2025). Our tree shrew data are thus consistent with the observations in mice.

The brain has been found to decompose moving plaids to its components and later integrate them into a single coherent motion (Adelson and Movshon, 1982; Movshon, 1985; Smith et al., 2005). In this study, we found tree shrew SC neurons exhibited a mixture of component and pattern selective responses when presented with symmetric plaids. This contrasts with the recent findings in the mouse SC, where pattern selective neurons predominate in the population (DePiero et al., 2024). In other species, brain areas known for being pattern selective, including MT and MST in monkeys, area 18 in cats, higher visual areas (and arguably V1) in mice, all contain a mix of component and pattern selective neurons (Smith et al., 2005; Juavinett and Callaway, 2015; Palagina et al., 2017; Khawaja et al., 2009). The overwhelming representation of pattern motion as observed in the mouse SC is very rare. Our data in the tree shrew SC therefore resembled more the cortical representations found in other species. The cross-species similarity, along with the contrast to the mouse SC, could suggest several possibilities. One of them is that the component and pattern representation within the same brain structure might have functional advantages. Instead of representing highly integrated motion information, the mixture could allow for flexible coding for different needs. For example, pattern selective neurons can be used to inform the global motion direction and energy, while the component selective neurons can further assist with object segmenting and local processing. Another possibility is that the high prevalence of pattern selectivity in mice correlates with strong component representation in the retina (DePiero et al., 2024). Mouse retina is known to have DS ganglion cells like rabbits (Weng et al., 2005; Barlow and Hill, 1963; Wei et al., 2011). However in primates, despite the recent discovery of DS ganglion cells and amacrine cells, the retinal direction selectivity is far less prominent compared to non-primate mammals (Kim et al., 2022). Given that the SC receives direct input from the retina and responds rapidly to visual stimuli, it is likely that the mouse SC is optimized for extracting global motion representation, potentially at the expense of the capability of component motion analysis. More studies on the direction selectivity and the complex motion pattern representation of tree shrew retina may offer insights about the source of species-specific differences in SC motion integration.

Here, using asymmetric plaids, we found the tree shrew SC neurons integrate plaid component motion in a way consistent with VS. One potential concern is whether this apparent VS could be a byproduct of linear summation by component-selective neurons, especially given a substantial amount of component cells in the tree shrew SC. We argue this is unlikely. If the observed VS direction tuning was due to linear summation by component cells, their responses to the individual component directions would need to scale proportionally with the TFs of those components (i.e. in a 1:4 ratio for the 2 and 8 Hz gratings in our plaids). However, based on the grating responses (Fig. 4.1B, right panel), the SC response magnitudes to 8 and 2 Hz differed by less than a factor of 2. Therefore, the VS computation we found arises from a non-linear integration of motion signals. It should be noted that the VS is inconsistent with human perception or primate cortical representation of asymmetric plaids (Movshon, 1985; Khawaja et al., 2013; Wallisch and Movshon, 2019). However, on both behavioral and neural level in primates, responses similar to VS have been reported to emerge during the ultra-fast processing stage (Barthélemy et al., 2010; Bowns, 1996; Yo and Wilson, 1992b; Ferrera and Wilson, 1990; Masson et al., 2000). Our observation is largely consistent with the recent mouse findings with minute distinction (Li et al., 2025). In the mouse SC, the visual neurons were found to follow the "probabilistically constrained VS" when representing the plaid stimulus. This additional probabilistic constraint on VS was thought to reflect two computations serving distinct purposes. VS itself is a simple and powerful linear operation, likely useful for indicating the visual space with dense motion information. The constraint, on the other hand, implements essential components of another computation - IOC, which is advantageous for tracking objects. The mouse SC likely balances both computations to maximize the efficiency of coarse motion direction encoding with IOC-like processing for speedy object tracking. In contrast, our data suggest tree shrew SC relies more purely on VS, with minimal evidence of a probabilistic constraint. Although the population responses for 135° plaids showed slight bimodal distribution with a peak near the theoretical constraint boundary, this effect was weak and resembled the mouse SC only marginally (Fig. 4.5C&D). This indicates that the tree shrew SC might be more specialized for the VS computation and its relevant function. The IOC-like computation, presumably supporting object tracking, could occur in separate brain areas (likely cortical structures). Surprisingly, the OKR to 45° plaids showed an unexpected shift of direction representation from VS to

IOC. This could suggest a different constraint on VS in the neural circuit driving the OKR.

Finally, in this study, we were not able to cover the whole SF range in gratings and speed range in RDK. The lower bound of the SF was limited by our selection of stimulus patch size, and the upper bound of the speed was selected to avoid potential motion streak effect. A more systematic measurement would be ideal in the future.

4.5 Methods

We used 3 adult tree shrews (*Tupaia Belangeri*, female=2, male=1, 5-8 months old) for electrophysiology recording and OKR behavior test. All experimental procedures in this and following sections were approved by the University of Virginia Institutional Animal Care and Use Committee and in conformance with the National Institutes of Health Guide for the Care and Use of Laboratory Animals and the Public Health Service Policy.

4.5.1 Surgery

Animals were first prepared for head plate implantation and craniotomy. A circular 4mm diameter cranial window was made 3mm lateral (right side) to the lambda point. A glass window, made of a stack of three 4mm and one 8mm thin cover glasses (0.2 mm thick), was used to cover and protect the brain. This glass window was secured within a circular titanium chamber with a retaining ring. The whole chamber was cemented with C&B Metabond onto the skull. Kwik-Cast sealant was applied over the window for additional coverage and sealing of the craniotomy. A titanium head plate was cemented with C&B Metabond onto the skull anterior to the craniotomy, with its front edge aligned with the midpoint between the two eyes. The exposed skull around was also covered with C&B Metabond.

The animal was fasted (with free access to water) for 3 hours prior to the surgery. We used 4-5% Isoflurane for anesthesia induction. Midazolam (5 mg/kg), Atropine (0.3 mg/kg), and Dexamethasone (1mg/kg) were then injected. The hair over the scalp was shaved, after which the animal was connected to EKG equipment to monitor the heart rate and was intubated. The endotracheal tube was connected to a CO_2 sensor. Isoflurane was delivered through intubation tubes for anesthesia during the surgery (1-4%, varied across animals). The animal was placed on the stereotaxic frame with earbar and toothbar fixing the head position. Skin flap resection was performed around the head plate and cranial chamber and secured with 3M Vetbond at the edge of the Metabond. Buprenorphine (0.05 mg/kg) was given as analgesic. Enrofloxacin (5 mg/kg) was given as antibiotic. Eye ointment was applied to the eyes for protection during surgery. Following recovery from anesthesia on a heating blanket under close monitoring, animals were monitored daily for 5 consecutive days.

4.5.2 Electrophysiology

5 days after the surgery, electrical signals from the SC of head-fixed awake tree shrews were recorded using 64 channel silicon microprobes (64ML) via a multichannel amplifier from Intan Technologies at 20 kHz. The tree shrews were restrained in a transparent acrylic box with their necks secured by a neckplate. In each recording, the retaining ring and the window were removed, and excessive tissue regrowth over the craniotomy was carefully cleaned. A small hole in the dura was made using a needle at the desired recording site. The probe was dropped through the hole to penetrate the cortex and reach the SC.

The location of the probe is estimated with full-screen luminance reversing checkerboard stimulus. We recorded mostly from the superficial layer of the SC, with part of the intermediate layer included. The receptive field location of each recording session was estimated using flashing dark squares ($5^\circ \times 5^\circ$) across the screen. The grating, random dot kinematogram (RDK), and plaid stimuli were then centered on the approximate receptive field location. Spikes were bandpass filtered with 300–6000 Hz range. Spike waveforms were sorted offline into single- and multi-units using MountainSort.

Visual stimuli were generated by customized script in MATLAB based on Psychtoolbox-3 and shown on an LCD monitor (59.7 × 33.6 cm, 60 Hz refresh rate, gamma corrected). Gratings, plaids, and RDK were shown within a 40° circular patch against a grey background. The screen was placed 25 cm away from the eye contralateral to the recording site. To get an estimation of the preferred spatial and temporal frequency (SF and TF) of the grating stimulus, we used 6 SFs (0.03-1 cpd, logarithmically spaced), 6 TFs (1-22 Hz, logarithmically spaced), and 4 motion directions (0°, 90°, 180°, 270°) (Fig. 4.1A). After this estimation, we fixed the TF to 8 Hz for the following grating and symmetric plaid stimulus presentation. To further characterize the SF tuning within the low SF range and the direction tuning responses of the SC neurons, we presented drifting gratings in 12 motion directions ($0-330^\circ$, linearly spaced) and 6 SFs (0.03-1 cpd, logarithmically spaced). All the gratings were presented for 2s with 0.5s inter-stimulus grey screen. Each condition was repeated for 8 times in a pseudorandom order. RDK (100% coherence, black and white dots, dot size = 2°, dot number = 80) was presented in 12 motion directions ($0-330^\circ$, linearly spaced) and 5 speeds (10-160 deg/s, logarithmically spaced). RDK stimuli were presented for 1.5s with 0.5s ISI. Each condition was repeated for 10 times in a pseudorandom order. Symmetric plaids comprised 2 grating components with 0.1 cpd SF and 8 Hz TF overlapped. Here, we chose an SF slightly higher than the population's preferred value because a 40° stimulus patch contained a more reasonable number of cycles (4 cycles) at 0.1 cpd compared to ultra-low SFs. We varied the cross angle between the directions of the two gratings (60°, 90°, 120°), as well as the direction of the first component (C1), which ranged from 0 to 330° in 12 linearly spaced steps, as comparable to previous mouse study (DePiero et al., 2024). The direction of the second component (C2) was always defined as C1 direction plus cross angle. Asymmetric plaids differed from the symmetric plaids in that C1 had a TF of 2 Hz, while C2 maintained a TF of 8 Hz. The cross angle between C1 and C2 varied across 4 levels: 20°, 45°, 135°, 180°, as comparable to previous mouse study (Li et al., 2025). Both Symmetric and asymmetric plaid blocks were mixed with 12-direction single grating conditions with SF = 0.1 cpd and TF = 8 Hz. The stimuli were presented for 2s with 0.5s ISI. Each condition was repeated for 10 times in a pseudorandom order. Room lights were turned off during the whole recording.

To control the length of the recording, we randomly chose a subset of stimuli to present in each recording session. Each animal was record for 20-30 days (one session per day).

4.5.3 Optokinetic reflex (OKR)

Animals used in the electrophysiology experiment underwent OKR test with their head fixed. Three computer screens (52.1 × 29.2 cm for each) were aligned vertically in portrait mode surrounding the animal. The angle between two neighboring screens was 120°. The distance between the eyes of the animal and the center of the screens was 25 cm. We recorded the tree shrews in the dark with an infrared light source. A dichroic mirror was placed in front of the right eye, and a video camera captured the eye from the back of the animal through the reflection in the mirror, thus minimizing visual occlusion. The camera was model FL3-U3-13Y3M-C (FLIR). Videos were recorded at 60Hz rate. We used Facemap (Syeda et al., 2024) to track the pupil location with the centroids coordinates. Only horizontal coordinates were used in our analysis to avoid the issue of direction-dependent gain difference in OKR behavior. Saccade-like eye movements were detected by the rapid coordinate change in eye movement trace and were removed so that only slow eye movements were used to quantify OKR. Eye movements towards the left of the animal were defined as having negative speeds, and rightward movements as positive.

Full field drifting gratings were shown on the 3-screen setup. To effectively elicit OKR in tree shrews, we increased the SF of grating and plaid components to 0.4 cpd. In addition, we used a slightly different set of TFs for gratings and plaids. Specifically, for gratings, we used TF = 8 Hz. For 45° and 20° plaids, we used TF1 = 1.5 Hz, TF2 = 6 Hz for component gratings. For 135° and 160° plaids, we used TF1 = 2.5 Hz, TF2 = 10 Hz for component gratings. These parameters made the VS motion speed for plaid and grating stimulus to be close, with 17, 17, 19, 19, 20 deg/s for 20°, 45°, 135°, 160° plaids and single gratings, respectively. Each stimulus was presented for 10 seconds with a 3s inter-stimulus-interval and repeated for 10 times in a pseudorandom order.

4.5.4 Quantification and statistical analysis

Responsiveness test

We consider a unit responsive to a stimulus when it fulfill 2 criteria: 1. its baseline subtracted response is larger than 2 spikes/s for at least one stimulus condition; 2. its response to at least one condition is significantly different from the blank condition tested by independent t-test with Benjamini-Hochberg FDR correction.

Direction selectivity

Direction selectivity were quantified with global direction selectivity index (gDSI) as $gDSI = |\frac{\Sigma R_\theta e^{i\theta}}{\Sigma R_\theta}|$, where R_θ is the response magnitude to stimulus direction θ in radians. If there were negative responses, the whole tuning curve was shifted so that the minimum response was 0. The preferred direction was calculated as the angle of the vector summation: $\theta_{pref} = arg(\Sigma R_\theta e^{i\theta})$. Orientation/axis selectivity were calculated similarly: $gOSI = |\frac{\Sigma R_\theta e^{2i\theta}}{\Sigma R_\theta}|$. The preferred orientation was defined as: $Ori_{pref} = \frac{1}{2}arg(\Sigma R_\theta e^{2i\theta}) + \frac{\pi}{2}$, while the preferred motion axis was: $Axis_{pref} = \frac{1}{2}arg(\Sigma R_\theta e^{2i\theta})$.

Component-pattern selectivity

We followed previous studies to quantify the component and pattern selectivity of neurons in response to symmetric plaids (DePiero et al., 2024; Smith et al., 2005; Palagina et al., 2017; Juavinett and Callaway, 2015). Briefly, based on each neuron's grating response, we generated the predicted component and pattern tuning curves to plaids. Pearson correlation coefficients were then calculated between the observed response and predicted pattern (P) and component (C) responses respectively, as well as between the predicted pattern and component responses themselves (PC).

Adjusted partial correlation coefficient for pattern (RP) and component (RC) were as follows:

$$RP = \frac{P - C \times PC}{\sqrt{(1 - C^2)(1 - PC^2)}}$$
$$RC = \frac{C - P \times PC}{\sqrt{(1 - P^2)(1 - PC^2)}}$$

Next, RP and RC were transformed into ZP and ZC with Fisher z-score transformation:

$$ZP = 1.5 \times ln(\frac{1 + RP}{1 - RP})$$
$$ZC = 1.5 \times ln(\frac{1 + RC}{1 - RC})$$

1.5 was the number of freedom calculated by $0.5 \times \sqrt{n - 3}$ where n is the number of stimulus directions ($n = 12$). A 95% confidence interval (z-score threshold = 1.645) was adopted to classify neurons into pattern, component, and unclassified.

OKR gain

We calculated the OKR gain as described in Li et al. (2025). In short, OKR gain is defined as the ratio of the eye movement speed and the stimulus speed in its vector sum direction: $OKRGain = \frac{speed_{eye}}{speed_{stim,VS}}$. The preferred direction of OKR was calculated as the angle of the vector summation of the OKR Gain tuning curve. OKR gain range was calculated by the maximum OKR gain minus the minimum.

4.6 Extended Data

4.6.1 Figure

4.7 Figure Legend

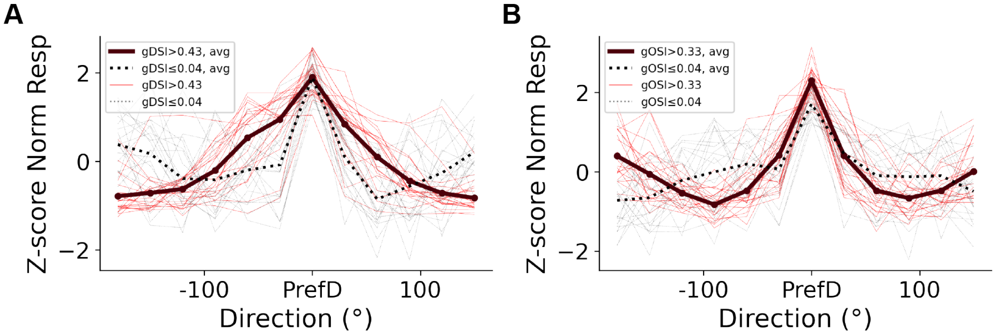

Figure 4.6: Aligned z-score normalized tuning curves with more strict cutoff. (A) We selected neurons with gDSI in the top and bottom 10% of the distribution and plotted their tuning curves aligned to their preferred directions. (B) Same as (A) but for gOSI.

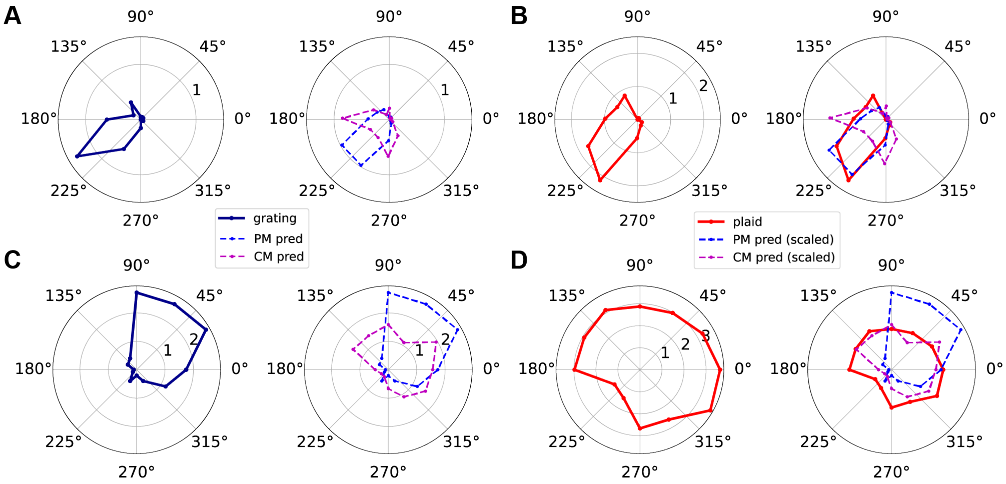

Figure 4.7: Example pattern and component neurons to symmetric plaids. (A-B) An example pattern neuron. (A) Left: its tuning curve to grating. Right: the component-selective (magenta) and pattern-selective (blue) response prediction to 90° plaid based on the grating tuning curve. (B) Left: the tuning curve to 90° plaid of this neuron. Right: prediction and observed tuning curves overlaid for comparison (the two predicted curves were scaled to match the observed response). (C-D) Same as (A-B) but for an example component neuron.

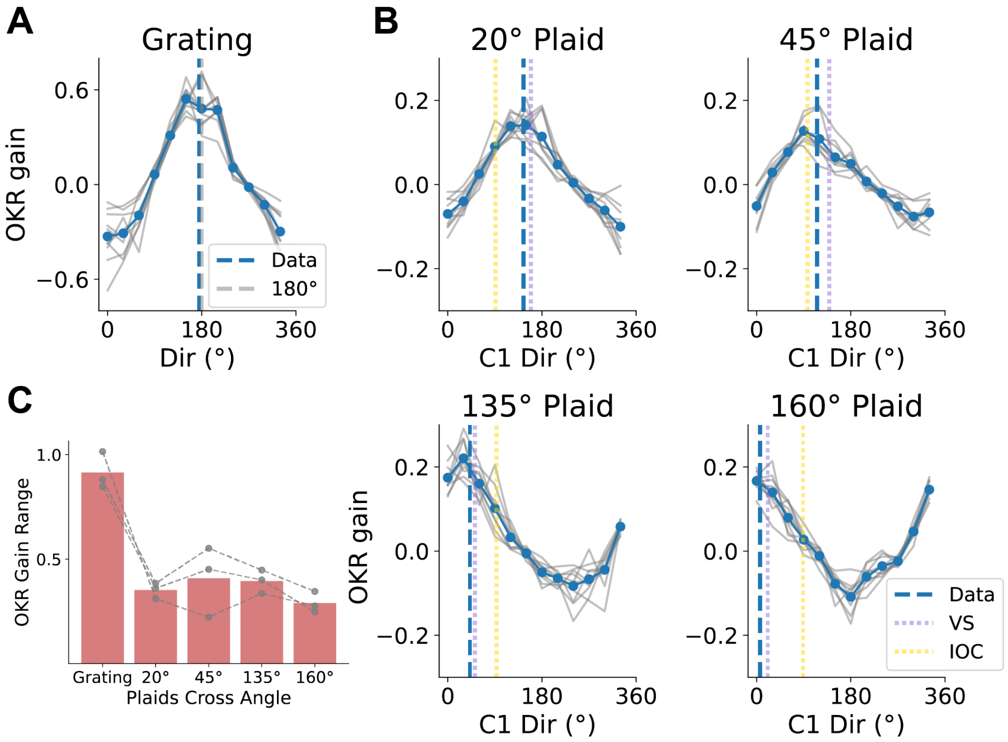

Figure 4.8: Tree shrew OKR. (A) The OKR gain to 12 directions of grating of an example tree shrew. Horizontal grating directions (blue vertical dashed line, close to 180°) elicited the largest horizontal eye movement. Blue solid line: trial-averaged response. Gray solid line: OKR responses of individual trials. (B) The OKR gain to 12 directions for 4 plaid cross angles tested. Data are from the same example tree shrew. VS and IOC predictions of the peak OKR response are indicated by purple and yellow vertical dashed lines. The peak OKR follows VS prediction except for 45° plaids. (C) The OKR strength for grating and plaids, quantified by OKR gain range - the difference between the peak and trough OKR gain in the tuning curves as in (A-B). OKR gain range is higher for grating than all the plaids, indicating a stronger OKR to grating. OKR gain range showed more variability to 45° plaid across animals, which is consistent with the preferred direction difference for 45° plaid being between VS and IOC predictions in Fig. 4.5F.

Chapter 5

Discussion

In the 3 chapters of studies I presented above, I explored the visual function of animals from visual behaviors such as decision-making and OKR to single neuron level representation of artificial visual stimuli in the SC. Using both tree shrews and mice as animal models allowed me to compare and find fundamental neural and behavioral principles across species, as well as to discover unique properties to species-specific ecological niche. Animals' neural activities and behaviors cannot be viewed as stand-alone functions, isolated from their "context". I will further discuss in the following content.

5.1 The "Impatient" Tree Shrews

In chapter 2, I showed an interesting speed and accuracy trade-off that naturally emerged in the tree shrew visual decision-making behaviors. In the training scheme, we rewarded the correct choices of the tree shrews with a constant amount of juice, and punished their incorrect choices with a constant timeout. We found that despite the best behavior to maximize the juice reward was to focus and increase the accuracy as much as possible (and most of the trials were not difficult at all for these animals), tree shrews still chose to respond prematurely in some trials, leading to a "lapse" in their psychometric curve, which corresponded to an imperfect plateau of the best accuracy that they can achieve. This lapse was seen in various animals (but mostly in mice) and tasks, and were viewed as a decision-independent property such as animals' inadequate ability to perform the sensory, motor, or cognitive aspects of the task, or viewed as an active task-irrelevant exploratory behavior (Ashwood et al., 2022). However, our study showed by simply changing the timeout function in relation to the animals' RT, the fast, low accuracy responses could be discouraged and eliminated almost completely. This new timeout scheme resulted in longer delays if the animals perform fast and incorrect choices, and shorter delays for slow, incorrect choices. Essentially, it discourages the impulsive guessing behaviors in the animals. The fact that tree shrews can have very low lapse rate under this new trial-delay scheme, when performing the same visual task with the same amount of training time as the "high lapse" group, ruled out the possibility of inadequate training or ability to distinguish the options. Rather, it suggested the animals' behaviors were optimized with additional factors taken into account.

The "low lapse" group's choice-RT behavior was captured with a Timed Racing Diffusion Model (TRDM), where an additional accumulator for time competed with the evidence accumulator. This model provides one of the potential mechanisms of a stimulus-independent process underlying tree shrew decision-making behavior. There are also other models such as Mixture model that can (Ratcliff and Kang, 2021) model the behavioral data in this study as well, but all of them require a mechanism that is independent of sensory evidence accumulation and dependent on the task structure in order to explain the tree shrew behaviors we saw in the study. This flexible mixture of multiple mechanisms we observed in the 2 groups of tree shrews likely stems from the physical properties of the animals. Tree shrews naturally move very fast. This is also true in the laboratory setup, which can be reflected by their fast RT for the contrast discrimination task. Their motor capabilities could promote a behavior pattern that uses high frequency sampling strategy to maximize the reward in natural environment with compromised accuracy. High accuracy can easily exhaust brain resources and energy in fast cognitive processing. The exhibited impulsive behaviors could indicate an intentional deployment of the most efficient strategy for the tree shrews. This deployment can be changed with specific trial delay schemes during learning, suggesting it is a flexible strategy that relies on the animals' understanding of the reward and cost function.

More specifically, our exponential-decay delay found and broke the balance between the effort they put in and the reward they got in the task, forcing the animals to find a new optimal strategy to re-gain the balance. In comparison, primates with well developed vision are relatively slow on similar visual decision tasks (Kirkpatrick et al., 2021; Jun et al., 2021). An advanced visual system arguably reflects an evolutionary emphasis on functions involving long-range exchange of information. Such organisms may prioritize high-precision information processing over frequent, close-range embodied interaction. Therefore, researchers usually observe high accuracy and low lapse rate in primates, but the reversal in mice and tree shrews. Interestingly, a study showed that the same neuron population in the monkey SC contains the information about whether the animal decides to make saccades, which emphasizes accuracy, or perform pursuit, which emphasizes speed (Krauzlis and Dill, 2002). This indicates that the speed-accuracy trade-off was adaptive to context, and such cognitive control could be implemented at least partly within subcortical circuits. More studies are needed to investigate the neural correlates of the stimulus-independent process. Further research on the interaction between the stimulus-independent process and evidence accumulation process, such as the attempt in the study of Ashwood et al. (2022), can shed light on the executive control and context representation during the decision-making behavior.

5.2 The Powerful Visual Subcortex

Our study on motion processing in mouse and tree shrew SC underscores the importance of subcortical visual functions. Traditionally, studies of visual functions have a predominant focus on cortical areas. There are good reasons for this emphasis. First, from an evolutionary standpoint, the primate cortex is well developed and constitutes the majority of the brain, with an expansion of visual functions compared to early mammals (Herculano-Houzel et al., 2007; Kaas, 2006). Second, our extensive, although still growing, understanding of V1, including basic response properties, anatomical organizations, and neural motifs, provides a strong foundation for vision research both within V1 and in its downstream areas (Hubel and Wiesel, 1962, 1998). Third, the visual cortex is relatively accessible surgically and experimentally in multiple species, allowing advanced recording techniques such as imaging and high-density linear probes, and neural manipulation to be carried out conveniently in the cortex. Fourth, the genetic and molecular tools are widely tested in the cortex, enabling precise cell-type-specific control over functions of interest. However, it is not negligible that many visual functions have been found to be related to the subcortical areas. One famous example is the Sprague effect (Sprague and Meikle, 1965; Sprague, 1966; Valero-Cabré et al., 2020). Unilateral lesion of the visual cortex can result in severe contralateral hemianopia, a blindness to half of the visual field, expressed by both visual neglect in contralateral fields and motor bias towards ipsilateral sides. Notably, a unilateral lesion of the superior colliculus also results in such deficits. However, if a unilateral cortical lesion is followed by a contralateral SC lesion, the hemianopia will be rescued. This surprising observation suggests a strong interaction between cortical and subcortical areas during visually guided behaviors. Another example is blindsight (also called residual vision). Unilateral V1 damage can lead to loss of visual awareness in contralateral visual field in primates. However, these patients/experimental monkeys can still respond to visual stimulus in various tasks requiring the processing of visual motion or even emotional face stimuli. Studies have shown that subcortical areas such as the SC and dLGN, is necessary for the blindsight phenomenon (Kinoshita et al., 2019; Schmid et al., 2010). The exact contributions of these subcortical structures depend on the task used to assess the residual vision. Similar observations have also been reported in rodent models. For example, a transgenic mouse line that is born without the majority of the cortex (including the entire visual cortex) can still perform visual behaviors such as Pavlovian fear conditioning and cued Morris water maze tasks (Shanks et al., 2016; Cang et al., 2018). Moreover, the SC was found to drive visually guided prey capture in mice (Hoy et al., 2016, 2019), as well as a series of other visual orienting behaviors (Hoy and Farrow, 2025; Cang et al., 2024). In tree shrews, studies also found they have the capacity to discriminate visual patterns in the absence of striate cortex (Ware et al., 1974, 1972).

Considering evolutionary history, vision is a function broadly found across a vast array of species, many of which lack a neocortex. Even within mammals, core visual functions such as motion processing, spatial navigation, and basic object recognition are shared across species with markedly different degrees of cortical development (Northcutt and Kaas, 1995). For most of the species, vision requires a non-cortical solution, either co-existing with the visual cortex or serving as the sole visual system. In zebrafish larvae, the optic tectum (homolog of the SC in mammals) mediates prey capture behaviors, just as in mammals (Gahtan et al., 2005). Ablation of the nucleus isthmi in frogs also stops their prey capture or threat avoidance behaviors (Caine and Gruberg, 1985). On the other hand, different species represent the visual information in similar ways, as many visual response properties are shared between mammals and non-mammals. For example, fish tectum prefers small spot of luminance change, has circular receptive fields, and shows direction selectivity, color related signals, binocular innervation, and pattern processing (Northmore, 2011). In addition, fish nucleus isthmi responds strongly to looming stimuli (Northmore, 2011). Furthermore, bird tectal neurons also prefer small spot with motion contrast to background, and center-surround RFs, and drive orienting movements (Wylie et al., 2009). Bird nucleus isthmi is involved in the orientation discrimination (Isa et al., 2021). Such conservation of structures and/or functions implies that these canonical computations arise early in evolution, and are implemented in similar ways neurally. Comparing and contrasting visual functions in different animals provides us insights on the relative importance of functions, as well as fundamental computational principles and species-specific adaptations.

5.2.1 Functional Implications of Plaid Motion Studies

In chapter 3 and 4, I showed the vector sum (VS) computation for plaid motion direction integration shared in mouse and tree shrew SC, as well as in their OKR behaviors. It is the first neural evidence of VS for plaid motion representation. Plaids are considered as 2 dimensional patterns containing two grating components. Gratings have been proven to effectively elicit stable responses in early visual areas such as SC and V1 (Wang et al., 2010; Relota et al., 2025; Liu et al., 2023b; DePiero et al., 2024; Ringach et al., 2002). Two gratings drifting towards different directions overlap to form a moving plaid pattern, which is usually perceived by humans as a rigid, coherent pattern in a certain direction instead of two gratings sliding through each other, except for special cases when the two component contrasts or spatial frequencies differ too much from each other (Adelson and Movshon, 1982). Moreover, the perceived pattern direction follows the mathematical prediction of the intersection-of-constraint (IOC). Such coherent motion perception was also found in non-human primates (Movshon, 1985; Kreyenmeier et al., 2024; Barthélemy et al., 2010; Pattadkal et al., 2023). However, both human and non-human primate studies have shown this perception is susceptible for distortion in various conditions using asymmetric plaids. For example, when the stimulus is presented for a very short duration (Bowns, 1996; Yo and Wilson, 1992b), or when type II plaids (a subset of asymmetric plaids) are used (Ferrera and Wilson, 1990), or when specific combinations of SF, TF, and contrast are used (Alais et al., 1997; Yo and Wilson, 1992a), the perceived motion direction deviates from the IOC prediction and towards the VS direction of the two components. Later, electrophysiological studies have found the neural correlates for an IOC-like perception in areas such as MT and MST (Khawaja et al., 2013; Wallisch and Movshon, 2019), but to date no neural substrate has been shown to implement the VS computation itself in any species. In our studies, we showed the first evidence that both mouse and tree shrew SC represent asymmetric plaids in their VS directions. Additionally, similar VS computations are used directly to guide reflexive OKR behavior. These findings suggest that a potential source of VS signal observed in primates might come from the subcortical visual structures. This is indirectly supported by previous studies in pigeons, who showed a perception of VS direction of plaids in a motion direction discrimination task (Hataji et al., 2020, 2019). Birds' visual processing depends majorly on optic tectum (Cook et al., 2015). For example, avian tectums are relatively larger and more complex compared to that in reptiles. Additionally, lesion of visual Wulst (a potential avian homolog of primary visual cortex in mammals) has very little impact on the visual behaviors. With a tectum dominated visual system, the perception of the pigeons becomes purely VS, which is very consistent with our findings in mouse and tree shrew SC and reflexive eye movements majorly driven by subcortical structures. These observations in different animal models suggest a possible evolutionary development of complex motion processing strategies: VS is a general, early rule to integrate motion, while IOC-like computation serves specific purposes.

Indeed, many studies have shown that the SC, even in primates, are involved in a VS computation during "saccade averaging" phenomenon. When facing two visual targets in the visual field, primate eye movement first follow a vector average of the stimuli before performing a winner-take-all saccade, and the SC contributes to both phases (Ottes et al., 1984; Nummela and Krauzlis, 2011; Glimcher and Sparks, 1993; van Opstal and van Gisbergen, 1990; Edelman and Keller, 1998). Vector averaging is simply a special form of weighted VS, presumably help to bring the eyes to the visual space with more information. Therefore, the subcortical VS computation likely serves a more general function of maximizing the information gain. This computation is largely linear and straightforward, facilitating a fast visual representation with the tolerance of low precision (another speed-accuracy trade-off phenomenon here), and benefiting animals in various survival-critical behaviors such as predation and predator avoidance.

However, we also observed that the mouse SC and OKR behavior clearly showed an IOC-like response pattern to 135° plaids. This can be explained by a probabilistically constrained VS model that is discussed in more details in Chapter 3. I want to emphasize again that the "probabilistic constraint" is independent of the VS computation, but share the same assumptions with the IOC or any computation that is underlying primates' coherent perception of plaid pattern motion. The two assumptions are 1. the grating patterns are parts of a larger moving pattern that exceeds the scope of the observing window; 2. the two overlapping gratings are from the same rigid, coherently moving pattern. This is very essential in understanding the function of this IOC-like computation. The first assumption is set to deal with the motion ambiguity brought by limited spatial receptive fields. Information outside the receptive fields is considered lost for individual processing units, no matter whether this unit is a single neuron, a brain structure, or an animal. To achieve a more accurate interpretation of the visual information, one approach is to sample larger visual fields, by pooling neurons together or by moving the "sensors" around. However, a far more efficient strategy is to program an internal "prior" on which stimuli and configurations are more likely to occur. Natural scenes contain highly correlated, and structured patterns, unlike noise stimuli. By exploiting this statistical regularity, a single processing unit can effectively "regularize" its inputs to produce a more accurate estimate despite the missing information. Given that all visual neurons have limited spatio-temporal RFs, I expect similar regularizations/priors are implemented along the visual pathway, but becoming most evident if the system is challenged with artificial stimuli that lack natural scene statistics. The second assumption highlights another important aspect of our perception of pattern motion - the brain prioritize the possibility that two gratings are from a single object. Object recognition and tracking demand precise, high-resolution processing, functions traditionally ascribed to the visual cortex (Serre et al., 2005). Therefore, the IOC-like motion representation, which precisely tracks the object motion under the two assumptions mentioned above, is more likely to be found in the cortex and expressed as stable perception. In contrast, subcortex is better suit for a coarse, speedy processing with a VS computation. In specific scenarios such as a very brief presentation of the stimulus, the brain may not have time for further processing, leading to a VS-like perception in primates extracted from subcortical circuits. Notably, the IOC-like perception was only observed for plaids consisting of 2 overlapping Fourier gratings. As long as a non-Fourier component is introduced, the perception becomes VS instead of IOC, even though the component motion is still considered 1-dimensional and ambiguous locally (Wilson and Kim, 1994). This suggests that the IOC-like computations only integrate first-order Fourier motion signals, whereas VS operates more broadly under a wide range of stimulus conditions.

Interestingly, we did not see a probabilistic constraint in tree shrew SC data. Rather, the tree shrew SC followed VS for all the plaid conditions tested. This likely points to a functional specialization between cortical and subcortical structures. In mice, the SC and other subcortical visual structures are highly involved in visual functions and process the majority of visual inputs. Therefore, a mixture of functional emphases might co-exist in the subcortex, allowing the animals to flexibly deal with different needs. The constraints we deduced from the data could reflect the boundary of a functional domain. In more visual animals like tree shrews, specialization might drive the subcortex to only perform the VS computation, and the cortex to perform other computations such as IOC. One hint from our data is that tree shrew OKR shows a IOC-like response to

45° plaids. This suggests two points: 1. the OKR-driving circuit does not use the same computation as the SC, and 2. a different motion integration rule similar to IOC exists in the brain and interact with the VS signals to drive OKR. Previous studies have suggested the cortex exerts more influence on the OKR behavior in highly visual animals (Harris et al., 1993; Cahill and Nathans, 2008; Ambrad Giovannetti and Rancz, 2024). Moreover, a study comparing human and cat OKR found a bias in humans towards the IOC direction but a bias in cats towards the component (likely a VS) direction (Harris et al., 1993). Taken together, the findings indicate the tree shrew OKR responses are potentially mediated by both subcortical and cortical pathways, placing tree shrews as an intermediate animal model on the continuum of subcortical-cortical contributions to OKR.

5.2.2 Rethinking Superior Colliculus Function

The SC's role in orienting behaviors is well established in various species (Hoy and Farrow, 2025). Because the SC is an integrative hub for rapid sensory-motor transformation such as saccades, head orienting, escape and predation, it is plausible that the SC is also involved in the execution of well-learned skills. Studies showed that the cortical areas such as posterior parietal cortex (PPC) and motor cortex are not required for task performance after learning (Kawai et al., 2015; Zhong et al., 2019). Reinhold et al. (2025) further studied a reward learning process with a focus on subcortical areas. They used optogenetic activation of striatum-projecting visual cortical neurons as a cue for mice to reach for a food pallet. They found that optogenetic inhibition of striatum prevented learning, but not improvement of skills already learned. However, muscimol inhibition of the SC disrupted the cued reaching behavior. Importantly, SC inhibition did not affect spontaneous reachings in those mice, suggesting a learned skill rather than motor capability was mediated by the SC. More studies are needed to examine the SC's contribution to the automatization of skilled actions.

In addition to orienting actions, accumulating evidence also implicates the SC's involvement in higher-order functions. For example, primate SC is found to encode visual saliency (White et al., 2021, 2017b,a; Heeman et al., 2025). Additionally, SC is involved in attention and decision-making

(Basso et al., 2021). Yet, it is worth noting that attention is closely related to orienting behaviors with blurred boundaries. Likewise, decision-related signals in the SC can also be correlated with the automatization of actions due to the extensive task training in laboratory settings. Strikingly, a recent human fMRI study showed that the SC orchestrates whole-brain dynamics during the unconscious sudden insight, the so called "eureka" moment (Murata et al., 2025), suggesting a role in large-scale, high-level cognitive processing. In summary, these findings point to a multi-functional SC that can benefit from further investigations for insights on its role in different stages and levels of functions, from the basic sensory representation and motor generation, ultimately to abstract cognition.

References

Bibliography

Adams, D. L. and Horton, J. C. (2003). A precise retinotopic map of primate striate cortex generated from the representation of angioscotomas. *Journal of Neuroscience*, 23(9):3771–3789.

Adelson, E. H. and Movshon, J. A. (1982). Phenomenal coherence of moving visual patterns. *Nature*, 300(5892):523–525.

Aglioti, S., DeSouza, J. F., and Goodale, M. A. (1995). Size-contrast illusions deceive the eye but not the hand. *Current Biology*, 5(6):679–685.

Aguillon-Rodriguez, V., Angelaki, D., Bayer, H., Bonacchi, N., Carandini, M., Cazettes, F., Chapuis, G., Churchland, A. K., Dan, Y., Dewitt, E., Faulkner, M., Forrest, H., Haetzel, L., Häusser, M., Hofer, S. B., Hu, F., Khanal, A., Krasniak, C., Laranjeira, I., Mainen, Z. F., Meijer, G., Miska, N. J., Mrsic-Flogel, T. D., Murakami, M., Noel, J. P., Pan-Vazquez, A., Rossant, C., Sanders, J., Socha, K., Terry, R., Urai, A. E., Vergara, H., Wells, M., Wilson, C. J., Witten, I. B., Wool, L. E., and Zador, A. M. (2021). Standardized and reproducible measurement of decision-making in mice. *eLife*, 10:e63711.

Alais, D., Wenderoth, P., and Burke, D. (1997). The size and number of plaid blobs mediate the misperception of Type-II plaid direction. *Vision Research*, 37(1):143–150.

Ambrad Giovannetti, E. and Rancz, E. (2024). Behind mouse eyes: The function and control of eye movements in mice. *Neuroscience & Biobehavioral Reviews*, 161:105671.

Aoki, R., Tsubota, T., Goya, Y., and Benucci, A. (2017). An automated platform for high-throughput mouse behavior and physiology with voluntary head-fixation. *Nature Communications*, 8(1):1–9.

Ashwood, Z. C., Roy, N. A., Stone, I. R., Urai, A. E., Churchland, A. K., Pouget, A., and Pillow, J. W. (2022). Mice alternate between discrete strategies during perceptual decision-making. *Nature Neuroscience*, 25(2):201–212. Publisher: Nature Publishing Group.

Barchini, J., Shi, X., Chen, H., and Cang, J. (2018). Bidirectional encoding of motion contrast in the mouse superior colliculus. *eLife*, 7:e35261. Publisher: eLife Sciences Publications, Ltd.

Barlow, H. B. and Hill, R. M. (1963). Selective sensitivity to direction of movement in ganglion cells of the rabbit retina. *Science*, 139(3553):412–414.

Barthélemy, F. V., Fleuriet, J., and Masson, G. S. (2010). Temporal dynamics of 2d motion integration for ocular following in macaque monkeys. *Journal of neurophysiology*, 103(3):1275–1282.

Basso, M. A., Bickford, M. E., and Cang, J. (2021). Unraveling circuits of visual perception and cognition through the superior colliculus. *Neuron*, 109(6):918–937.

Basso, M. A. and May, P. J. (2017). Circuits for action and cognition: a view from the superior colliculus. *Annual review of vision science*, 3(1):197–226.

Becker, W. and Jürgens, R. (1979). An analysis of the saccadic system by means of double step stimuli. *Vision Research*, 19(9):967–983.

Boehnke, S. E. and Munoz, D. P. (2008). On the importance of the transient visual response in the superior colliculus. *Current Opinion in Neurobiology*, 18(6):544–551.

Bogadhi, A. R. and Hafed, Z. M. (2023). Express detection of visual objects by primate superior colliculus neurons. *Scientific Reports*, 13(1):21730. Publisher: Nature Publishing Group.

Bonhoeffer, T. and Grinvald, A. (1991). Iso-orientation domains in cat visual cortex are arranged in pinwheel-like patterns. *Nature*, 353(6343):429–431. Publisher: Nature Publishing Group.

Bowns, L. (1996). Evidence for a feature tracking explanation of why type ii plaids move in the vector sum direction at short durations. *Vision research*, 36(22):3685–3694.

Brown, S. and Heathcote, A. (2005). A ballistic model of choice response time. *Psychological Review*, 112(1):117–128.

Buckingham, G. and Goodale, M. A. (2010). Lifting without Seeing: The Role of Vision in Perceiving and Acting upon the Size Weight Illusion. *PLOS ONE*, 5(3):e9709.

Cahill, H. and Nathans, J. (2008). The Optokinetic Reflex as a Tool for Quantitative Analyses of Nervous System Function in Mice: Application to Genetic and Drug-Induced Variation. *PLOS ONE*, 3(4):e2055.

Caine, H. S. and Gruberg, E. R. (1985). Ablation of nucleus isthmi leads to loss of specific visually elicited behaviors in the frog rana pipiens. *Neuroscience letters*, 54(2-3):307–312.

Callahan, T. L. and Petry, H. M. (2000). Psychophysical measurement of temporal modulation sensitivity in the tree shrew (tupaia belangeri). *Vision research*, 40(4):455–458.

Campagner, D., Vale, R., Tan, Y. L., Iordanidou, P., Pavón Arocas, O., Claudi, F., Stempel, A. V., Keshavarzi, S., Petersen, R. S., Margrie, T. W., et al. (2023). A cortico-collicular circuit for orienting to shelter during escape. *Nature*, 613(7942):111–119.

Cang, J., Chen, C., Li, C., and Liu, Y. (2024). Genetically defined neuron types underlying visuomotor transformation in the superior colliculus. *Nature Reviews Neuroscience*, 25(11):726–739.

Cang, J., Savier, E., Barchini, J., and Liu, X. (2018). Visual function, organization, and development of the mouse superior colliculus.

Casagrande, V. and Diamond, I. (1974). Ablation study of the superior colliculus in the tree shrew (tupaia glis). *Journal of Comparative Neurology*, 156(2):207–237.

Cavanaugh, J., Alvarez, B. D., and Wurtz, R. H. (2006). Enhanced Performance with Brain Stimulation: Attentional Shift or Visual Cue? *Journal of Neuroscience*, 26(44):11347–11358. Publisher: Society for Neuroscience Section: Articles.

Cavanaugh, J. and Wurtz, R. H. (2004). Subcortical Modulation of Attention Counters Change Blindness. *Journal of Neuroscience*, 24(50):11236–11243. Publisher: Society for Neuroscience Section: Behavioral/Systems/Cognitive.

Chandrasekaran, A. R., Plas, D. T., Gonzalez, E., and Crair, M. C. (2005). Evidence for an instructive role of retinal activity in retinotopic map refinement in the superior colliculus of the mouse. *Journal of Neuroscience*, 25(29):6929–6938.

Chaplin, T. A., Allitt, B. J., Hagan, M. A., Price, N. S., Rajan, R., Rosa, M. G., and Lui, L. L. (2017). Sensitivity of neurons in the middle temporal area of marmoset monkeys to random dot motion. *Journal of Neurophysiology*, 118(3):1567–1580.

Chapman, B., Stryker, M. P., and Bonhoeffer, T. (1996). Development of Orientation Preference Maps in Ferret Primary Visual Cortex. *Journal of Neuroscience*, 16(20):6443–6453. Publisher: Society for Neuroscience Section: Articles.

Chen, H., Savier, E. L., DePiero, V. J., and Cang, J. (2021). Lack of evidence for stereotypical direction columns in the mouse superior colliculus. *Journal of Neuroscience*, 41(3):461–473.

Cho, S.-H., Crapse, T., Grimaldi, P., Lau, H., and Basso, M. A. (2021). Variable Statistical Structure of Neuronal Spike Trains in Monkey Superior Colliculus. *The Journal of Neuroscience*, 41(14):3234–3253. Publisher: Society for Neuroscience.

Chou, I. h., Sommer, M. A., and Schiller, P. H. (1999). Express averaging saccades in monkeys. *Vision Research*, 39(25):4200–4216.

Chu, Y. W., Chinta, S., Keri, H. V. S., Beri, S., and Pluta, S. R. (2025). Stimulus selection enhances value-modulated somatosensory processing in the superior colliculus. *PLOS Biology*, 23(3):e3003057. Publisher: Public Library of Science.

Chung, J. E., Magland, J. F., Barnett, A. H., Tolosa, V. M., Tooker, A. C., Lee, K. Y., Shah, K. G., Felix, S. H., Frank, L. M., and Greengard, L. F. (2017). A fully automated approach to spike sorting. *Neuron*, 95(6):1381–1394.

Cisek, P., Puskas, G. A., and El-Murr, S. (2009). Decisions in changing conditions: The urgency-gating model. *Journal of Neuroscience*, 29(37):11560–11571.

Coëffé, C. and O'regan, J. K. (1987). Reducing the influence of non-target stimuli on saccade accuracy: Predictability and latency effects. *Vision Research*, 27(2):227–240.

Conway, J. L. and Schiller, P. H. (1983). Laminar organization of tree shrew dorsal lateral geniculate nucleus. *Journal of Neurophysiology*.

Cook, R. G., Qadri, M. A. J., and Keller, A. M. (2015). Chapter Six - The Analysis of Visual Cognition in Birds: Implications for Evolution, Mechanism, and Representation. In Ross, B. H., editor, *Psychology of Learning and Motivation*, volume 63, pages 173–210. Academic Press.

Coren, S. and Hoenig, P. (1972). Effect of non-target stimuli upon length of voluntary saccades. *Perceptual and motor skills*, 34(2):499–508.

Crapse, T. B., Lau, H., and Basso, M. A. (2018). A Role for the Superior Colliculus in Decision Criteria. *Neuron*, 97(1):181–194.e6. Publisher: Elsevier BV.

Cynader, M. and Berman, N. (1972). Receptive-field organization of monkey superior colliculus. *Journal of Neurophysiology*, 35(2):187–201.

Damjanović, I., Aliper, A., Maximov, P., Zaichikova, A., Gačić, Z., and Maximova, E. (2023). Direction selectivity of the retinotectal system of fish: findings based on microelectrode extracellular recordings of the tectum opticum. *Archives of Biological Sciences*, 75(1):27–45.

De Franceschi, G. and Solomon, S. G. (2018). Visual response properties of neurons in the superficial layers of the superior colliculus of awake mouse. *The Journal of physiology*, 596(24):6307–6332.

DePiero, V. J., Deng, Z., Chen, C., Savier, E. L., Chen, H., Wei, W., and Cang, J. (2024). Transformation of motion pattern selectivity from retina to superior colliculus. *Journal of Neuroscience*, 44(20).

Detwiler, P. B., Crook, J., Packer, O., Robinson, F., and Dacey, D. M. (2019). The recursive bistratified ganglion cell type of the macaque monkey retina is ON-OFF direction selective. *Investigative Ophthalmology & Visual Science*, 60(9):3884.

Dewar, M. T. and Carey, D. P. (2006). Visuomotor 'immunity' to perceptual illusion: A mismatch of attentional demands cannot explain the perception–action dissociation. *Neuropsychologia*, 44(8):1501–1508.

Ding, L. and Gold, J. I. (2010). Caudate Encodes Multiple Computations for Perceptual Decisions. *Journal of Neuroscience*, 30(47):15747–15759. Publisher: Society for Neuroscience Section: Articles.

Ding, W.-n., Sun, J.-h., Sun, Y.-w., Chen, X., Zhou, Y., Zhuang, Z.-g., Li, L., Zhang, Y., Xu, J.-r., and Du, Y.-s. (2014). Trait impulsivity and impaired prefrontal impulse inhibition function in adolescents with internet gaming addiction revealed by a Go/No-Go fMRI study. *Behavioral and Brain Functions*, 10(1):1–9.

Ditterich, J. (2006). Evidence for time-variant decision making. *European Journal of Neuroscience*, 24(12):3628–3641.

Dmochowski, J. P. and Norcia, A. M. (2015). Cortical components of reaction-time during perceptual decisions in humans. *PLoS ONE*, 10(11):e0143339.

Dong, G., Lu, Q., Zhou, H., and Zhao, X. (2010). Impulse inhibition in people with Internet addiction disorder: Electrophysiological evidence from a Go/NoGo study. *Neuroscience Letters*, 485(2):138–142.

Donner, T. H., Siegel, M., Fries, P., and Engel, A. K. (2009). Buildup of Choice-Predictive Activity in Human Motor Cortex during Perceptual Decision Making. *Current Biology*, 19(18):1581–1585.

Dorris, M. C., Paré, M., and Munoz, D. P. (1997). Neuronal Activity in Monkey Superior Colliculus Related to the Initiation of Saccadic Eye Movements. *Journal of Neuroscience*, 17(21):8566–8579.

Drager, U. C. and Hubel, D. H. (1976). Topography of visual and somatosensory projections to mouse superior colliculus. *Journal of Neurophysiology*, 39(1):91–101.

Drenhaus, U., Rager, G., Eggli, P., and Kretz, R. (2006). On the postnatal development of the striate cortex (V1) in the tree shrew (Tupaia belangeri). *European Journal of Neuroscience*, 24(2):479–490. _eprint: https://onlinelibrary.wiley.com/doi/pdf/10.1111/j.1460-9568.2006.04916.x.

Duan, C. A., Pan, Y., Ma, G., Zhou, T., Zhang, S., and Xu, N.-l. (2021). A cortico-collicular pathway for motor planning in a memory-dependent perceptual decision task. *Nature Communications*, 12(1):2727. Publisher: Nature Publishing Group.

Duchemin, A., Privat, M., and Sumbre, G. (2022). Fourier motion processing in the optic tectum and pretectum of the zebrafish larva. *Frontiers in Neural Circuits*, 15:814128.

Eagle, D. M., Bari, A., and Robbins, T. W. (2008). The neuropsychopharmacology of action inhibition: Cross-species translation of the stop-signal and go/no-go tasks. *Psychopharmacology*, 199(3):439–456.

Edelman, J. A. and Keller, E. L. (1998). Dependence on target configuration of express saccade-related activity in the primate superior colliculus. *Journal of Neurophysiology*, 80(3):1407–1426.

Essig, J., Hunt, J. B., and Felsen, G. (2021). Inhibitory neurons in the superior colliculus mediate selection of spatially-directed movements. *Communications Biology*, 4(1):1–14. Publisher: Nature Publishing Group.

Felsen, G. and Mainen, Z. F. (2008). Neural Substrates of Sensory-Guided Locomotor Decisions in the Rat Superior Colliculus. *Neuron*, 60(1):137–148. Publisher: Elsevier.

Ferrera, V. P. and Wilson, H. R. (1990). Perceived direction of moving two-dimensional patterns. *Vision research*, 30(2):273–287.

Findlay, J. M. (1982). Global visual processing for saccadic eye movements. *Vision Research*, 22(8):1033–1045.

Flanagan, J. R. and Beltzner, M. A. (2000). Independence of perceptual and sensorimotor predictions in the size–weight illusion. *Nature Neuroscience 2000 3:7*, 3(7):737–741.

Gahtan, E., Tanger, P., and Baier, H. (2005). Visual prey capture in larval zebrafish is controlled by identified reticulospinal neurons downstream of the tectum. *Journal of Neuroscience*, 25(40):9294–9303.

Gale, S. D. and Murphy, G. J. (2014). Distinct representation and distribution of visual information by specific cell types in mouse superficial superior colliculus. *Journal of Neuroscience*, 34(40):13458–13471.

Gale, S. D. and Murphy, G. J. (2016). Active Dendritic Properties and Local Inhibitory Input Enable Selectivity for Object Motion in Mouse Superior Colliculus Neurons. *Journal of Neuroscience*, 36(35):9111–9123. Publisher: Society for Neuroscience Section: Articles.

Ganel, T., Tanzer, M., and Goodale, M. A. (2008). A double dissociation between action and perception in the context of visual illusions: Opposite effects of real and illusory size: Research report. *Psychological Science*, 19(3):221–225.

Ghosh, S. and Maunsell, J. H. R. (2025). Neuronal modulation of the superior colliculus associated with visual spatial attention represents perceptual sensitivity, independent of perceptual decision and motor biases. Pages: 2025.04.01.646682 Section: New Results.

Glimcher, P. W. and Sparks, D. L. (1993). Representation of averaging saccades in the superior colliculus of the monkey. *Experimental Brain Research*, 95(3):429–435.

Goldberg, M. E. and Wurtz, R. H. (1972). Activity of superior colliculus in behaving monkey. i. visual receptive fields of single neurons. *Journal of neurophysiology*, 35(4):542–559.

Goodale, M. and Wolf, M. (2009). Vision for action.

Goodale, M. A. (2011). Transforming vision into action. *Vision Research*, 51(13):1567–1587.

Goodale, M. A. (2014). How (and why) the visual control of action differs from visual perception. *Proceedings of the Royal Society B: Biological Sciences*, 281(1785).

Goodale, M. A. and Milner, A. D. (1992). Separate visual pathways for perception and action. *Trends in neurosciences*, 15(1):20–25.

Goodale, M. A., Pelisson, D., and Prablanc, C. (1986). Large adjustments in visually guided reaching do not depend on vision of the hand or perception of target displacement. *Nature 1986 320:6064*, 320(6064):748–750.

Grandy, M. S. and Westwood, D. A. (2006). Opposite perceptual and sensorimotor responses to a size-weight illusion. *Journal of Neurophysiology*, 95(6):3887–3892.

Grimaldi, P., Cho, S. H., Lau, H., and Basso, M. A. (2018). Superior colliculus signals decisions rather than confidence: analysis of single neurons. *Journal of Neurophysiology*, 120(5):2614–2629. Publisher: American Physiological Society.

Grødem, S., Nymoen, I., Vatne, G. H., Rogge, F. S., Björnsdóttir, V., Lensjø, K. K., and Fyhn, M. (2023). An updated suite of viral vectors for in vivo calcium imaging using intracerebral and retro-orbital injections in male mice. *Nature Communications 2023 14:1*, 14(1):1–13.

Guillamón-Vivancos, T., Aníbal-Martínez, M., Puche-Aroca, L., Moreno-Bravo, J. A., Valdeolmillos, M., Martini, F. J., and López-Bendito, G. (2022). Input-dependent segregation of visual and somatosensory circuits in the mouse superior colliculus. *Science*, 377(6608):845–850. Publisher: American Association for the Advancement of Science.

Guo, L., Frost, M. R., He, L., Siegwart, J. T., and Norton, T. T. (2013). Gene Expression Signatures in Tree Shrew Sclera in Response to Three Myopiagenic Conditions. *Investigative Ophthalmology & Visual Science*, 54(10):6806–6819.

Hafed, Z. M. and Chen, C.-Y. (2016). Sharper, Stronger, Faster Upper Visual Field Representation in Primate Superior Colliculus. *Current Biology*, 26(13):1647–1658. Publisher: Elsevier.

Hafed, Z. M., Hoffmann, K.-P., Chen, C.-Y., and Bogadhi, A. R. (2023). Visual functions of the primate superior colliculus. *Annual review of vision science*, 9(1):361–383.

Harris, L. R., Lewis, T. L., and Maurer, D. (1993). Brain stem and cortical contributions to the generation of horizontal optokinetic eye movements in humans. *Visual Neuroscience*, 10(2):247–259.

Hartline, P. H., Kass, L., and Loop, M. S. (1978). Merging of modalities in the optic tectum: infrared and visual integration in rattlesnakes. *Science*, 199(4334):1225–1229.

Hataji, Y., Fujita, K., and Kuroshima, H. (2020). Pigeons (Columba livia) integrate visual motion using the vector average rule: effect of viewing distance. *Animal Cognition*, 23(4):819–825.

Hataji, Y., Kuroshima, H., and Fujita, K. (2019). Pigeons integrate visual motion signals differently than humans. *Scientific Reports*, 9(1):13411. Publisher: Nature Publishing Group.

Hawkins, G. E. and Heathcote, A. (2021). Racing against the clock: Evidence-based versus time-based decisions. *Psychological review*, 128(2):222–263.

Heathcote, A. (2004). Fitting Wald and ex-Wald distributions to response time data: An example using functions for the S-PLUS package. *Behavior Research Methods, Instruments, and Computers*, 36(4):678–694.

Heeman, J., White, B. J., Stigchel, S. V. d., Theeuwes, J., Itti, L., and Munoz, D. P. (2025). Saliency Response in Superior Colliculus at the Future Saccade Goal Predicts Fixation Duration during Free Viewing of Dynamic Scenes. *Journal of Neuroscience*, 45(3). Publisher: Society for Neuroscience Section: Research Articles.

Herculano-Houzel, S., Collins, C. E., Wong, P., and Kaas, J. H. (2007). Cellular scaling rules for primate brains. *Proceedings of the National Academy of Sciences*, 104(9):3562–3567. Publisher: Proceedings of the National Academy of Sciences.

Hjorth, J. J. J., Sterratt, D. C., Cutts, C. S., Willshaw, D. J., and Eglen, S. J. (2015). Quantitative assessment of computational models for retinotopic map formation. *Developmental Neurobiology*, 75(6):641–666. _eprint: https://onlinelibrary.wiley.com/doi/pdf/10.1002/dneu.22241.

Ho, C. L. A., Zimmermann, R., Weidinger, J. D. F., Prsa, M., Schottdorf, M., Merlin, S., Okamoto, T., Ikezoe, K., Pifferi, F., Aujard, F., Angelucci, A., Wolf, F., and Huber, D. (2021). Orientation Preference Maps in Microcebus murinus Reveal Size-Invariant Design Principles in Primate Visual Cortex. *Current Biology*, 31(4):733–741.e7. Publisher: Elsevier.

Horwitz, G. D., Batista, A. P., and Newsome, W. T. (2004). Representation of an Abstract Perceptual Decision in Macaque Superior Colliculus. *Journal of Neurophysiology*, 91(5):2281–2296. Publisher: American Physiological Society.

Horwitz, G. D. and Newsome, W. T. (1999). Separate Signals for Target Selection and Movement Specification in the Superior Colliculus. *Science*, 284(5417):1158–1161. Publisher: American Association for the Advancement of Science.

Horwitz, G. D. and Newsome, W. T. (2001). Target selection for saccadic eye movements: direction-selective visual responses in the superior colliculus. *Journal of Neurophysiology*, 86(5):2527–2542.

Hoy, J. L., Bishop, H. I., and Niell, C. M. (2019). Defined cell types in superior colliculus make distinct contributions to prey capture behavior in the mouse. *Current Biology*, 29(23):4130–4138.

Hoy, J. L. and Farrow, K. (2025). The superior colliculus. *Current Biology*, 35(5):R164–R168.

Hoy, J. L., Yavorska, I., Wehr, M., and Niell, C. M. (2016). Vision drives accurate approach behavior during prey capture in laboratory mice. *Current Biology*, 26(22):3046–3052.

Huang, M., Li, D., Cheng, X., Pei, Q., Xie, Z., Gu, H., Zhang, X., Chen, Z., Liu, A., Wang, Y., et al. (2021). The tectonigral pathway regulates appetitive locomotion in predatory hunting in mice. *Nature communications*, 12(1):4409.

Huang, S., Niu, X., Wang, J., Wang, Z., Xu, H., and Shi, L. (2022). Visual responses to moving and flashed stimuli of neurons in domestic pigeon (columba livia domestica) optic tectum. *Animals*, 12(14):1798.

Hubel, D. H. and Wiesel, T. N. (1962). Receptive fields, binocular interaction and functional architecture in the cat's visual cortex. *The Journal of Physiology*, 160(1):106.

Hubel, D. H. and Wiesel, T. N. (1998). Early Exploration of the Visual Cortex. *Neuron*, 20(3):401–412. Publisher: Elsevier.

Hubel, D. H., Wiesel, T. N., and Stryker, M. P. (1977). Orientation columns in macaque monkey visual cortex demonstrated by the 2-deoxyglucose autoradiographic technique. *Nature*, 269(5626):328–330. Publisher: Nature Publishing Group.

Humphrey, A. L. and Norton, T. T. (1980). Topographic organization of the orientation column system in the striate cortex of the tree shrew (Tupaia glis). I. Microelectrode recording. *Journal of Comparative Neurology*, 192(3):531–547. _eprint: https://onlinelibrary.wiley.com/doi/pdf/10.1002/cne.901920311.

Ignashchenkova, A., Dicke, P. W., Haarmeier, T., and Thier, P. (2004). Neuron-specific contribution of the superior colliculus to overt and covert shifts of attention. *Nature Neuroscience*, 7(1):56–64. Publisher: Nature Publishing Group.

Inayat, S., Barchini, J., Chen, H., Feng, L., Liu, X., and Cang, J. (2015). Neurons in the most superficial lamina of the mouse superior colliculus are highly selective for stimulus direction. *Journal of Neuroscience*, 35(20):7992–8003.

Isa, K., Sooksawate, T., Kobayashi, K., Kobayashi, K., Redgrave, P., and Isa, T. (2020). Dissecting the Tectal Output Channels for Orienting and Defense Responses. *eNeuro*, 7(5):1–18.

Isa, T., Marquez-Legorreta, E., Grillner, S., and Scott, E. K. (2021). The tectum/superior colliculus as the vertebrate solution for spatial sensory integration and action. *Current Biology*, 31(11):R741–R762.

Ito, S., Si, Y., Litke, A. M., and Feldheim, D. A. (2021). Nonlinear visuoauditory integration in the mouse superior colliculus. *PLOS Computational Biology*, 17(11):e1009181. Publisher: Public Library of Science.

Jacobs, G. H. and Neitz, J. (1986). Spectral mechanisms and color vision in the tree shrew (*Tupaia belangeri*). *Vision Research*, 26(2):291–298.

Jay, M. F. and Sparks, D. L. (1984). Auditory receptive fields in primate superior colliculus shift with changes in eye position. *Nature*, 309(5966):345–347. Publisher: Nature Publishing Group.

Juavinett, A. L. and Callaway, E. M. (2015). Pattern and component motion responses in mouse visual cortical areas. *Current Biology*, 25(13):1759–1764.

Jun, E. J., Bautista, A. R., Nunez, M. D., Allen, D. C., Tak, J. H., Alvarez, E., and Basso, M. A.

(2021). Causal role for the primate superior colliculus in the computation of evidence for perceptual decisions. *Nature Neuroscience*, 24(8):1121–1131. Publisher: Nature Publishing Group.

Kaas, J. H. (2006). Evolution of the neocortex. *Current Biology*, 16(21):R910–R914. Publisher: Elsevier.

Kardamakis, A. A., Perez-Fernandez, J., and Grillner, S. (2016). Spatiotemporal interplay between multisensory excitation and recruited inhibition in the lamprey optic tectum. *Elife*, 5:e16472.

Kaschube, M., Schnabel, M., Löwel, S., Coppola, D. M., White, L. E., and Wolf, F. (2010). Universality in the Evolution of Orientation Columns in the Visual Cortex. *Science*, 330(6007):1113–1116. Publisher: American Association for the Advancement of Science.

Kass, R. E. and Raftery, A. E. (1995). Bayes factors. *Journal of the American Statistical Association*, 90(430):773–795.

Kawai, R., Markman, T., Poddar, R., Ko, R., Fantana, A. L., Dhawale, A. K., Kampff, A. R., and Ölveczky, B. P. (2015). Motor Cortex Is Required for Learning but Not for Executing a Motor Skill. *Neuron*, 86(3):800–812. Publisher: Elsevier.

Khawaja, F. A., Liu, L. D., and Pack, C. C. (2013). Responses of mst neurons to plaid stimuli. *Journal of neurophysiology*, 110(1):63–74.

Khawaja, F. A., Tsui, J. M., and Pack, C. C. (2009). Pattern motion selectivity of spiking outputs and local field potentials in macaque visual cortex. *Journal of Neuroscience*, 29(43):13702–13709.

Kiani, R. and Shadlen, M. N. (2009). Representation of Confidence Associated with a Decision by Neurons in the Parietal Cortex. *Science*, 324(5928):759–764. Publisher: American Association for the Advancement of Science.

Kim, Y. J., Peterson, B. B., Crook, J. D., Joo, H. R., Wu, J., Puller, C., Robinson, F. R., Gamlin,

P. D., Yau, K.-W., Viana, F., et al. (2022). Origins of direction selectivity in the primate retina. *Nature communications*, 13(1):2862.

Kinoshita, M., Kato, R., Isa, K., Kobayashi, K., Kobayashi, K., Onoe, H., and Isa, T. (2019). Dissecting the circuit for blindsight to reveal the critical role of pulvinar and superior colliculus. *Nature Communications*, 10(1):135. Publisher: Nature Publishing Group.

Kirkpatrick, R. P., Turner, B. M., and Sederberg, P. B. (2021). Equal evidence perceptual tasks suggest a key role for interactive competition in decision-making. *Psychological review*, 128(6):1051.

Knudsen, E. I. (1982). Auditory and visual maps of space in the optic tectum of the owl. *Journal of Neuroscience*, 2(9):1177–1194.

Krauzlis, R. J. and Dill, N. (2002). Neural Correlates of Target Choice for Pursuit and Saccades in the Primate Superior Colliculus. *Neuron*, 35(2):355–363. Publisher: Elsevier.

Krauzlis, R. J., Lovejoy, L. P., and Z\' enon, A. (2013). Superior Colliculus and Visual Spatial Attention. *Annual Review of Neuroscience*, 36(1):165–182. Publisher: Annual Reviews.

Kreyenmeier, P., Kumbhani, R., Movshon, J. A., and Spering, M. (2024). Shared Mechanisms Drive Ocular Following and Motion Perception. *eNeuro*, 11(6).

Krizan, J., Song, X., Fitzpatrick, M. J., Shen, N., Soto, F., and Kerschensteiner, D. (2024). Predation without direction selectivity. *Proceedings of the National Academy of Sciences*, 121(12):e2317218121. Publisher: Proceedings of the National Academy of Sciences.

Lam, N. H., Mukherjee, A., Wimmer, R. D., Nassar, M. R., Chen, Z. S., and Halassa, M. M. (2025). Prefrontal transthalamic uncertainty processing drives flexible switching. *Nature*, 637(8044):127–136.

Lee, K. H., Tran, A., Turan, Z., and Meister, M. (2020). The sifting of visual information in the superior colliculus. *eLife*, 9:e50678. Publisher: eLife Sciences Publications, Ltd.

Lee, K. S., Huang, X., and Fitzpatrick, D. (2016). Topology of on and off inputs in visual cortex enables an invariant columnar architecture. *Nature*, 533(7601):90–94.

Li, C., DePiero, V. J., Chen, H., Tanabe, S., and Cang, J. (2025). Probabilistically constrained vector summation of motion direction in the mouse superior colliculus. *Current Biology*.

Li, C., McHaney, K. M., Sederberg, P. B., and Cang, J. (2022a). Tree shrews as an animal model for studying perceptual decision-making reveal a critical role of stimulus-independent processes in guiding behavior. *Eneuro*, 9(6).

Li, C. H., Yan, L. Z., Ban, W. Z., Tu, Q., Wu, Y., Wang, L., Bi, R., Ji, S., Ma, Y. H., Nie, W. H., Lv, L. B., Yao, Y. G., Zhao, X. D., and Zheng, P. (2017). Long-term propagation of tree shrew spermatogonial stem cells in culture and successful generation of transgenic offspring. *Cell Research*, 27(2):241–252.

Li, C.-J., Hui, Y.-Q., Zhang, R., Zhou, H.-Y., Cai, X., and Lu, L. (2023). A comparison of behavioral paradigms assessing spatial memory in tree shrews. *Cerebral Cortex*, 33(19):10303–10321.

Li, V. J., Schohl, A., and Ruthazer, E. S. (2022b). Topographic map formation and the effects of nmda receptor blockade in the developing visual system. *Proceedings of the National Academy of Sciences*, 119(8):e2107899119.

Li, X. and Basso, M. A. (2008). Preparing to Move Increases the Sensitivity of Superior Colliculus Neurons. *Journal of Neuroscience*, 28(17):4561–4577. Publisher: Society for Neuroscience Section: Articles.

Li, Y.-t. and Meister, M. (2023). Functional cell types in the mouse superior colliculus. *eLife*, 12:e82367. Publisher: eLife Sciences Publications, Ltd.

Liu, J., He, Y., Lavoie, A., Bouvier, G., and Liu, B.-h. (2023a). A direction-selective cortico-brainstem pathway adaptively modulates innate behaviors. *Nature Communications*, 14(1):8467.

Liu, Y., McDaniel, J. A., Chen, C., Yang, L., Kipcak, A., Savier, E. L., Erisir, A., Cang, J., and Campbell, J. N. (2025). Co-conservation of synaptic gene expression and circuitry in collicular neurons. *bioRxiv*.

Liu, Y., Savier, E. L., DePiero, V. J., Chen, C., Schwalbe, D. C., Abraham-Fan, R.-J., Chen, H., Campbell, J. N., and Cang, J. (2023b). Mapping visual functions onto molecular cell types in the mouse superior colliculus. *Neuron*, 111(12):1876–1886.

Lodewyckx, T., Kim, W., Lee, M. D., Tuerlinckx, F., Kuppens, P., and Wagenmakers, E. J. (2011). A tutorial on Bayes factor estimation with the product space method. *Journal of Mathematical Psychology*, 55(5):331–347.

Lovejoy, L. P. and Krauzlis, R. J. (2010). Inactivation of primate superior colliculus impairs covert selection of signals for perceptual judgments. *Nature Neuroscience*, 13(2):261–266. Publisher: Nature Publishing Group.

Lu, X., Hu, Z., Xin, Y., Yang, T., Wang, Y., Zhang, P., Liu, N., and Jiang, Y. (2024). Detecting biological motion signals in human and monkey superior colliculus: a subcortical-cortical pathway for biological motion perception. *Nature Communications*, 15(1):9606.

Mante, V., Sussillo, D., Shenoy, K. V., and Newsome, W. T. (2013). Context-dependent computation by recurrent dynamics in prefrontal cortex. *Nature*, 503(7474):78–84. Publisher: Nature Publishing Group.

Marbach, F. and Zador, A. (2017). A self-initiated two-alternative forced choice paradigm for head-fixed mice. *bioRxiv*, page 073783.

Masseck, O. A. and Hoffmann, K. (2009). Comparative Neurobiology of the Optokinetic Reflex. *Annals of the New York Academy of Sciences*, 1164(1):430–439.

Masson, G. S. and Castet, E. (2002). Parallel Motion Processing for the Initiation of Short-Latency Ocular Following in Humans. *Journal of Neuroscience*, 22(12):5149–5163.

Masson, G. S., Rybarczyk, Y., Castet, E., and Mestre, D. R. (2000). Temporal dynamics of motion integration for the initiation of tracking eye movements at ultra-short latencies. *Visual neuroscience*, 17(5):753–767.

Masullo, L., Mariotti, L., Alexandre, N., Freire-Pritchett, P., Boulanger, J., and Tripodi, M. (2019). Genetically Defined Functional Modules for Spatial Orienting in the Mouse Superior Colliculus. *Current Biology*, 29(17):2892–2904.e8. Publisher: Elsevier.

Mekhaiel, D. Y., Goodale, M. A., and Corneil, B. D. (2024). Rapid integration of face detection and task set in visually guided reaching. *European Journal of Neuroscience*, 60(6):5328–5347. _eprint: https://onlinelibrary.wiley.com/doi/pdf/10.1111/ejn.16497.

Meredith, M. A. and Stein, B. E. (1986). Visual, auditory, and somatosensory convergence on cells in superior colliculus results in multisensory integration. *Journal of Neurophysiology*, 56(3):640–662. Publisher: American Physiological Society.

Milner, A. D. and Goodale, M. A. (2008). Two visual systems re-viewed. *Neuropsychologia*, 46(3):774–785.

Mooney, R. D., Klein, B. G., and Rhoades, R. W. (1985). Correlations between the structural and functional characteristics of neurons in the superficial laminae and the hamster's superior colliculus. *Journal of Neuroscience*, 5(11):2989–3009.

Movshon, J. A. (1985). The analysis of moving visual patterns. *Experimental Brain Research*, pages 117–151.

Muir, D. R., Roth, M. M., Helmchen, F., and Kampa, B. M. (2015). Model-based analysis of pattern motion processing in mouse primary visual cortex. *Frontiers in neural circuits*, 9:38.

Munoz, D. P. and Wurtz, R. H. (1995). Saccade-related activity in monkey superior colliculus. II. Spread of activity during saccades. *https://doi.org/10.1152/jn.1995.73.6.2334*, 73(6):2334–2348.

Murata, T., Kunishige, K., Seno, S., Ohzawa, I., Kaneko, K., Yanagida, T., Haruno, M., and Hosoda, K. (2025). The superior colliculus arbitrates whole-brain dynamics for unconscious visual insight. Pages: 2025.04.09.648050 Section: New Results.

Mustafar, F., Harvey, M. A., Khani, A., Arató, J., and Rainer, G. (2018). Divergent solutions to visual problem solving across mammalian species. *ENeuro*, 5(4).

Müller, B. and Peichl, L. (1989). Topography of cones and rods in the tree shrew retina. *Journal of Comparative Neurology*, 282(4):581–594. _eprint: https://onlinelibrary.wiley.com/doi/pdf/10.1002/cne.902820409.

Müller, J. R., Philiastides, M. G., and Newsome, W. T. (2004). Microstimulation of the superior colliculus focuses attention without moving the eyes. *Proceedings of the National Academy of Sciences*, 102(3):524–529. Publisher: Proceedings of the National Academy of Sciences.

Newman, E. A. and Hartline, P. H. (1981). Integration of visual and infrared information in bimodal neurons in the rattlesnake optic tectum. *Science*, 213(4509):789–791.

Newsome, W. T., Britten, K. H., and Movshon, J. A. (1989). Neuronal correlates of a perceptual decision. *Nature*, 341(6237):52–54.

Nguyen, M. N., Matsumoto, J., Hori, E., Maior, R. S., Tomaz, C., Tran, A. H., Ono, T., and Nishijo, H. (2014). Neuronal responses to face-like and facial stimuli in the monkey superior colliculus. *Frontiers in Behavioral Neuroscience*, 8. Publisher: Frontiers.

Northcutt, R. G. and Kaas, J. H. (1995). The emergence and evolution of mammalian neocortex. *Trends in neurosciences*, 18(9):373–379.

Northmore, D. (2011). The optic tectum. *Encyclopedia of fish physiology: from genome to environment*, 1:131–142.

Nummela, S. U. and Krauzlis, R. J. (2011). Superior Colliculus Inactivation Alters the Weighted Integration of Visual Stimuli. *Journal of Neuroscience*, 31(22):8059–8066.

Odegaard, B., Grimaldi, P., Cho, S. H., Peters, M. A., Lau, H., and Basso, M. A. (2018). Superior colliculus neuronal ensemble activity signals optimal rather than subjective confidence. *Proceedings of the National Academy of Sciences*, 115(7):E1588–E1597.

Odoemene, O., Pisupati, S., Nguyen, H., and Churchland, A. K. (2018). Visual evidence accumulation guides decision-making in unrestrained mice. *Journal of Neuroscience*, 38(47):10143–10155.

Ohl, F., Oitzl, M. S., and Fuchs, E. (1998). Assessing cognitive functions in tree shrews: visuo-spatial and spatial learning in the home cage. *Journal of Neuroscience Methods*, 81(1-2):35–40.

Orsolic, I., Rio, M., Mrsic-Flogel, T. D., and Znamenskiy, P. (2021). Mesoscale cortical dynamics reflect the interaction of sensory evidence and temporal expectation during perceptual decision-making. *Neuron*, 109(11):1861–1875.e10.

Ottes, F. P., Van Gisbergen, J. A., and Eggermont, J. J. (1984). Metrics of saccade responses to visual double stimuli: Two different modes. *Vision Research*, 24(10):1169–1179.

Palagina, G., Meyer, J. F., and Smirnakis, S. M. (2017). Complex visual motion representation in mouse area v1. *Journal of Neuroscience*, 37(1):164–183.

Palmer, J., Huk, A. C., and Shadlen, M. N. (2005). The effect of stimulus strength on the speed and accuracy of a perceptual decision. *Journal of Vision*, 5(5):376–404.

Pan, T.-T., Liu, C., Li, D.-M., Nie, B.-B., Zhang, T.-H., Zhang, W., Zhao, S.-L., Zhou, Q.-X., Liu, H., Zhu, G.-H., et al. (2022). Nucleus accumbens-linked executive control networks mediating reversal learning in tree shrew brain. *Zoological Research*, 43(4):528.

Pattadkal, J. J., Barr, C., and Priebe, N. J. (2023). Ocular following Eye Movements in Marmosets Follow Complex Motion Trajectories. *eNeuro*, 10(6).

Perry, V. H. and Cowey, A. (1984). Retinal ganglion cells that project to the superior colliculus and pretectum in the macaque monkey. *Neuroscience*, 12(4):1125–1137.

Petry, H. M. and Bickford, M. E. (2019). The second visual system of the tree shrew. *Journal of Comparative Neurology*, 527(3):679–693.

Petry, H. M., Fox, R., and Casagrande, V. A. (1984). Spatial contrast sensitivity of the tree shrew. *Vision research*, 24(9):1037–1042.

Petry, H. M. and Kelly, J. P. (1991). Psychophysical measurement of spectral sensitivity and color vision in red-light-reared tree shrews (tupaia belangeri). *Vision research*, 31(10):1749–1757.

Peysakhovich, B., Zhu, O., Tetrick, S. M., Shirhatti, V., Silva, A. A., Li, S., Ibos, G., Rosen, M. C., Johnston, W. J., and Freedman, D. J. (2024). Primate superior colliculus is causally engaged in abstract higher-order cognition. *Nature Neuroscience*, 27(10):1999–2008. Publisher: Nature Publishing Group.

Philiastides, M. G., Auksztulewicz, R., Heekeren, H. R., and Blankenburg, F. (2011). Causal role of dorsolateral prefrontal cortex in human perceptual decision making. *Current Biology*, 21(11):980–983.

Platkiewicz, J. and Hayward, V. (2014). Perception-action dissociation generalizes to the size-inertia illusion. *Journal of Neurophysiology*, 111(7):1409–1416.

Prins, N. (2012). The psychometric function: The lapse rate revisited. *Journal of Vision*, 12(6):25.

Prusky, G. T., West, P. W. R., and Douglas, R. M. (2000). Behavioral assessment of visual acuity in mice and rats. *Vision Research*, 40(16):2201–2209.

Ratcliff, R. (1978). A theory of memory retrieval. *Psychological Review*, 85(2):59–108.

Ratcliff, R., Cherian, A., and Segraves, M. (2003). A Comparison of Macaque Behavior and Superior Colliculus Neuronal Activity to Predictions From Models of Two-Choice Decisions. *Journal of Neurophysiology*, 90(3):1392–1407. Publisher: American Physiological Society.

Ratcliff, R., Hasegawa, Y. T., Hasegawa, R. P., Smith, P. L., and Segraves, M. A. (2007). Dual Diffusion Model for Single-Cell Recording Data From the Superior Colliculus in a Brightness-Discrimination Task. *Journal of Neurophysiology*, 97(2):1756–1774. Publisher: American Physiological Society.

Ratcliff, R. and Kang, I. (2021). Qualitative speed-accuracy tradeoff effects can be explained by a diffusion/fast-guess mixture model. *Scientific Reports*, 11(1):15169.

Reinhold, K., Iadarola, M., Tang, S., Chang, A., Kuwamoto, W., Albanese, M. A., Sun, S., Hakim, R., Zimmer, J., Wang, W., and Sabatini, B. L. (2025). Striatum supports fast learning but not memory recall. *Nature*, pages 1–10. Publisher: Nature Publishing Group.

Relota, X. J., Ford, A., and Savier, E. L. (2025). Behavioral modulation and molecular definition of wide-field vertical cells in the mouse superior colliculus. *Journal of Neuroscience*, 45(16).

Resulaj, A., Kiani, R., Wolpert, D. M., and Shadlen, M. N. (2009). Changes of mind in decision-making. *Nature*, 461(7261):263–266.

Ridder III, W. H., Zhang, K. M., Karsolia, A., Engles, M., and Burke, J. (2019). Comparison of contrast sensitivity in macaque monkeys and humans. *Visual Neuroscience*, 36:E008.

Ringach, D. L., Shapley, R. M., and Hawken, M. J. (2002). Orientation selectivity in macaque v1: diversity and laminar dependence. *Journal of neuroscience*, 22(13):5639–5651.

Roitman, J. D. and Shadlen, M. N. (2002). Response of Neurons in the Lateral Intraparietal Area during a Combined Visual Discrimination Reaction Time Task. *Journal of Neuroscience*, 22(21):9475–9489.

Roy, S., Bohlen, M. O., Cruger, J., Kuczewski, G., Freling, S., Shultz, N., Sommer, M., Fitzpatrick, D., and Field, G. D. (2024). Retinal ganglion cell diversity and projection patterns to the superior colliculus in tree shrew. *Investigative Ophthalmology & Visual Science*, 65(7):2477.

Sanes, J. R. and Zipursky, S. L. (2010). Design Principles of Insect and Vertebrate Visual Systems. *Neuron*, 66(1):15–36. Publisher: Elsevier.

Savier, E., Sedigh-Sarvestani, M., Wimmer, R., and Fitzpatrick, D. (2021). A bright future for the tree shrew in neuroscience research: summary from the inaugural tree shrew users meeting. *Zoological Research*, 42(4):478.

Savier, E. L., Chen, H., and Cang, J. (2019). Effects of Locomotion on Visual Responses in the Mouse Superior Colliculus. *Journal of Neuroscience*, 39(47):9360–9368.

Schenk, T. (2006). An allocentric rather than perceptual deficit in patient D.F. *Nature Neuroscience 2006 9:11*, 9(11):1369–1370.

Schmid, M. C., Mrowka, S. W., Turchi, J., Saunders, R. C., Wilke, M., Peters, A. J., Ye, F. Q., and Leopold, D. A. (2010). Blindsight depends on the lateral geniculate nucleus. *Nature*, 466(7304):373–377. Publisher: Nature Publishing Group.

Sedigh-Sarvestani, M., Lee, K.-S., Jaepel, J., Satterfield, R., Shultz, N., and Fitzpatrick, D. (2021). A sinusoidal transformation of the visual field is the basis for periodic maps in area v2. *Neuron*, 109(24):4068–4079.

Serre, T., Kouh, M., Cadieu, C., Knoblich, U., Kreiman, G., and Poggio, T. (2005). A theory of object recognition: computations and circuits in the feedforward path of the ventral stream in primate visual cortex. *CSAIL Technical Reports*.

Shang, C., Liu, A., Li, D., Xie, Z., Chen, Z., Huang, M., Li, Y., Wang, Y., Shen, W. L., and Cao, P. (2019). A subcortical excitatory circuit for sensory-triggered predatory hunting in mice. *Nature neuroscience*, 22(6):909–920.

Shanks, J. A., Ito, S., Schaevitz, L., Yamada, J., Chen, B., Litke, A., and Feldheim, D. A. (2016). Corticothalamic Axons Are Essential for Retinal Ganglion Cell Axon Targeting to the Mouse

Dorsal Lateral Geniculate Nucleus. *Journal of Neuroscience*, 36(19):5252–5263. Publisher: Society for Neuroscience Section: Articles.

Shi, X., Barchini, J., Ledesma, H. A., Koren, D., Jin, Y., Liu, X., Wei, W., and Cang, J. (2017). Retinal origin of direction selectivity in the superior colliculus. *Nature Neuroscience*, 20(4):550–558. Publisher: Nature Publishing Group.

Shriver, J. and Noback, C. (2008). COLOR VISION IN THE TREE SHREW (TUPAIA GLIS). *Folia Primatologica*, 6(3-4):161–169.

Smith, M. A., Majaj, N. J., and Movshon, J. A. (2005). Dynamics of motion signaling by neurons in macaque area mt. *Nature neuroscience*, 8(2):220–228.

Smith, P. L. and Ratcliff, R. (2004). Psychology and neurobiology of simple decisions. *Trends in Neurosciences*, 27(3):161–168.

Snowden, R. J., Treue, S., and Andersen, R. A. (1992). The response of neurons in areas v1 and mt of the alert rhesus monkey to moving random dot patterns. *Experimental Brain Research*, 88:389–400.

Spead, O., Weaver, C. J., Moreland, T., and Poulain, F. E. (2021). Live imaging of retinotectal mapping reveals topographic map dynamics and a previously undescribed role for contactin 2 in map sharpening. *Development*, 148(22):dev199584.

Sprague, J. M. (1966). Interaction of Cortex and Superior Colliculus in Mediation of Visually Guided Behavior in the Cat. *Science*, 153(3743):1544–1547. Publisher: American Association for the Advancement of Science (AAAS).

Sprague, J. M. and Meikle, T. H. (1965). The role of the superior colliculus in visually guided behavior. *Experimental Neurology*, 11(1):115–146.

Sridharan, D., Steinmetz, N. A., Moore, T., and Knudsen, E. I. (2017). Does the Superior Colliculus Control Perceptual Sensitivity or Choice Bias during Attention? Evidence from a Multialternative Decision Framework. *The Journal of Neuroscience*, 37(3):480–511. Publisher: Society for Neuroscience.

Stine, G. M., Trautmann, E. M., Jeurissen, D., and Shadlen, M. N. (2023). A neural mechanism for terminating decisions. *Neuron*, 111(16):2601–2613.e5. Publisher: Elsevier.

Summers, M. T. and Feller, M. B. (2022). Distinct inhibitory pathways control velocity and directional tuning in the mouse retina. *Current Biology*, 32(10):2130–2143.e3.

Suzuki, D. G., Pérez-Fernández, J., Wibble, T., Kardamakis, A. A., and Grillner, S. (2019). The role of the optic tectum for visually evoked orienting and evasive movements. *Proceedings of the National Academy of Sciences*, 116(30):15272–15281. Publisher: Proceedings of the National Academy of Sciences.

Syeda, A., Zhong, L., Tung, R., Long, W., Pachitariu, M., and Stringer, C. (2024). Facemap: a framework for modeling neural activity based on orofacial tracking. *Nature neuroscience*, 27(1):187–195.

Tanabe, S., Fu, J., and Cang, J. (2022). Strong tuning for stereoscopic depth indicates orientation-specific recurrent circuitry in tree shrew V1. *Current Biology*, 32(24):5274–5284.e6. Publisher: Elsevier.

Ter Braak, C. J. (2006). A Markov Chain Monte Carlo version of the genetic algorithm Differential Evolution: Easy Bayesian computing for real parameter spaces. *Statistics and Computing*, 16(3):239–249.

Thevarajah, D., Mikulić, A., and Dorris, M. C. (2009). Role of the Superior Colliculus in Choosing Mixed-Strategy Saccades. *Journal of Neuroscience*, 29(7):1998–2008. Publisher: Society for Neuroscience Section: Articles.

Thomas, A., Yang, W., Wang, C., Tipparaju, S. L., Chen, G., Sullivan, B., Swiekatowski, K., Tatam, M., Gerfen, C., and Li, N. (2023). Superior colliculus bidirectionally modulates choice activity in frontal cortex. *Nature Communications*, 14(1):7358. Publisher: Nature Publishing Group.

Turner, B. M. and Sederberg, P. B. (2012). Approximate Bayesian computation with differential evolution. *Journal of Mathematical Psychology*, 56(5):375–385.

Turner, B. M., Sederberg, P. B., Brown, S. D., and Steyvers, M. (2013). A Method for efficiently sampling from distributions with correlated dimensions. *Psychological Methods*, 18(3):368–384.

Ulinski, P. S., Dacey, D. M., and Sereno, M. I. (1992). Optic tectum. *Biology of the Reptilia*, 17:241–366.

Urai, A. E., Aguillon-Rodriguez, V., Laranjeira, I. C., Cazettes, F., Mainen, Z. F., and Churchland, A. K. (2021). Citric acid water as an alternative to water restriction for high-yield mouse behavior. *eNeuro*, 8(1):1–8.

Usher, M. and McClelland, J. L. (2001). The time course of perceptual choice: The leaky, competing accumulator model. *Psychological Review*, 108(3):550–592.

Valero-Cabré, A., Toba, M. N., Hilgetag, C. C., and Rushmore, R. J. (2020). Perturbation-driven paradoxical facilitation of visuo-spatial function: Revisiting the ‘Sprague effect’. *Cortex*, 122:10–39.

van Opstal, A. J. and van Gisbergen, J. A. (1990). Role of monkey superior colliculus in saccade averaging. *Experimental Brain Research*, 79(1):143–149.

van Ravenzwaaij, D., Brown, S. D., Marley, A. A., and Heathcote, A. (2020). Accumulating Advantages: A New Conceptualization of Rapid Multiple Choice. *Psychological Review*.

Vokoun, C. R., Huang, X., Jackson, M. B., and Basso, M. A. (2014). Response Normalization in the Superficial Layers of the Superior Colliculus as a Possible Mechanism for Saccadic Averaging. *The Journal of Neuroscience*, 34(23):7976.

Wallace, M. T., Wilkinson, L. K., and Stein, B. E. (1996). Representation and integration of multiple sensory inputs in primate superior colliculus. *Journal of Neurophysiology*, 76(2):1246–1266. Publisher: American Physiological Society.

Wallisch, P. and Movshon, J. A. (2019). Responses of neurons in macaque mt to unikinetic plaids. *Journal of neurophysiology*, 122(5):1937–1945.

Wandell, B. A. and Winawer, J. (2011). Imaging retinotopic maps in the human brain. *Vision research*, 51(7):718–737.

Wang, L., Herman, J. P., and Krauzlis, R. J. (2022). Neuronal modulation in the mouse superior colliculus during covert visual selective attention. *Scientific Reports 2022 12:1*, 12(1):1–16.

Wang, L., McAlonan, K., Goldstein, S., Gerfen, C. R., and Krauzlis, R. J. (2020a). A causal role for mouse superior colliculus in visual perceptual decision-making. *Journal of Neuroscience*, 40(19):3768–3782.

Wang, L., McAlonan, K., Goldstein, S., Gerfen, C. R., and Krauzlis, R. J. (2020b). A Causal Role for Mouse Superior Colliculus in Visual Perceptual Decision-Making. *The Journal of Neuroscience*, 40(19):3768–3782. Publisher: Society for Neuroscience.

Wang, L., Sarnaik, R., Rangarajan, K., Liu, X., and Cang, J. (2010). Visual receptive field properties of neurons in the superficial superior colliculus of the mouse. *Journal of Neuroscience*, 30(49):16573–16584.

Ware, C., Diamond, I., and Casagrande, V. (1974). Effects of Ablating the Striate Cortex on a Successive Pattern Discrimination: Further Study of the Visual System in the Tree Shrew (Tupaia glis). *Brain, Behavior and Evolution*, 9(4):264–279.

Ware, C. B., Casagrande, V. A., and Diamond, I. (1972). Does the Acuity of the Tree Shrew Suffer from Removal of Striate Cortex? | Brain Behavior and Evolution | Karger Publishers.

Wei, W., Hamby, A. M., Zhou, K., and Feller, M. B. (2011). Development of asymmetric inhibition underlying direction selectivity in the retina. *Nature*, 469(7330):402–406.

Weiß, C. H. (2024). The Mollified (Discrete) Uniform Distribution and its Applications.

Weng, S., Sun, W., and He, S. (2005). Identification of on–off direction-selective ganglion cells in the mouse retina. *The Journal of physiology*, 562(3):915–923.

Wentura, D. (2000). Dissociative Affective and Associative Priming Effects in the Lexical Decision Task: Yes Versus No Responses to Word Targets Reveal Evaluative Judgment Tendencies. *Journal of Experimental Psychology: Learning Memory and Cognition*, 26(2):456–469.

White, B. J., Berg, D. J., Kan, J. Y., Marino, R. A., Itti, L., and Munoz, D. P. (2017a). Superior colliculus neurons encode a visual saliency map during free viewing of natural dynamic video. *Nature communications*, 8(1):14263.

White, B. J., Itti, L., and Munoz, D. P. (2021). Superior colliculus encodes visual saliency during smooth pursuit eye movements. *European Journal of Neuroscience*, 54(1):4258–4268. _eprint: https://onlinelibrary.wiley.com/doi/pdf/10.1111/ejn.14432.

White, B. J., Kan, J. Y., Levy, R., Itti, L., and Munoz, D. P. (2017b). Superior colliculus encodes visual saliency before the primary visual cortex. *Proceedings of the National Academy of Sciences*, 114(35):9451–9456.

Wichmann, F. A. and Hill, N. J. (2001). The psychometric function: I. Fitting, sampling, and goodness of fit. *Perception and Psychophysics*, 63(8):1293–1313.

Wilson, H. R. and Kim, J. (1994). Perceived motion in the vector sum direction. *Vision Research*, 34(14):1835–1842.

Wurtz, R. H. and Goldberg, M. E. (1972). The primate superior colliculus and the shift of visual attention. *Investigative Ophthalmology & Visual Science*, 11(6):441–450.

Wurtz, R. H. and Mohler, C. W. (1976). Organization of monkey superior colliculus: enhanced visual response of superficial layer cells. *Journal of Neurophysiology*, 39(4):745–765. Publisher: American Physiological Society.

Wylie, D. R., Gutierrez-Ibanez, C., Pakan, J. M., and Iwaniuk, A. N. (2009). The optic tectum of birds: mapping our way to understanding visual processing. *Canadian Journal of Experimental Psychology/Revue canadienne de psychologie expérimentale*, 63(4):328.

Yang, L., Lee, K., Villagracia, J., and Masmanidis, S. C. (2020). Open source silicon microprobes for high throughput neural recording. *Journal of Neural Engineering*, 17(1):016036.

Yao, Y. G. (2017). Creating animal models, why not use the Chinese tree shrew (Tupaia belangeri chinensis)? *Zoological research*, 38(3):118–126.

Yao, Y.-G., Lu, L., Ni, R.-J., Bi, R., Chen, C., Chen, J.-Q., Fuchs, E., Gorbatyuk, M., Lei, H., Li, H., et al. (2024). Study of tree shrew biology and models: A booming and prosperous field for biomedical research. *Zoological Research*, 45(4):877.

Yilmaz, M. and Meister, M. (2013). Rapid innate defensive responses of mice to looming visual stimuli. *Current Biology*, 23(20):2011–2015.

Yo, C. and Wilson, H. R. (1992a). Moving two-dimensional patterns can capture the perceived directions of lower or higher spatial frequency gratings. *Vision Research*, 32(7):1263–1269.

Yo, C. and Wilson, H. R. (1992b). Perceived direction of moving two-dimensional patterns depends on duration, contrast and eccentricity. *Vision research*, 32(1):135–147.

Yu, G., Katz, L. N., Quaia, C., Messinger, A., and Krauzlis, R. J. (2024). Short-latency preference for faces in primate superior colliculus depends on visual cortex. *Neuron*, 112(16):2814–2822.e4. Publisher: Elsevier.

Zahler, S. H., Taylor, D. E., Wong, J. Y., Adams, J. M., and Feinberg, E. H. (2021). Superior colliculus drives stimulus-evoked directionally biased saccades and attempted head movements in head-fixed mice. *eLife*, 10:73081.

Zahler, S. H., Taylor, D. E., Wright, B. S., Wong, J. Y., Shvareva, V. A., Park, Y. A., and Feinberg, E. H. (2023). Hindbrain modules differentially transform activity of single collicular neurons to coordinate movements. *Cell*, 186(14):3062–3078.e20. Publisher: Elsevier.

Zhang, B., Kan, J. Y. Y., Yang, M., Wang, X., Tu, J., and Dorris, M. C. (2021). Transforming absolute value to categorical choice in primate superior colliculus during value-based decision making. *Nature Communications*, 12(1):3410. Publisher: Nature Publishing Group.

Zhong, L., Zhang, Y., Duan, C. A., Deng, J., Pan, J., and Xu, N.-l. (2019). Causal contributions of parietal cortex to perceptual decision-making during stimulus categorization. *Nature Neuroscience*, 22(6):963–973. Publisher: Nature Publishing Group.

Zivotofsky, A. Z. (2005). A dissociation between perception and action in open-loop smooth-pursuit ocular tracking of the Duncker Illusion. *Neuroscience Letters*, 376(2):81–86.

Zénon, A. and Krauzlis, R. J. (2012). Attention deficits without cortical neuronal deficits. *Nature*, 489(7416):434–437. Publisher: Nature Publishing Group.